Channel-forming activity of syringopeptin 25 A in mercury-supported phospholipid monolayers and negatively charged bilayers

Becucci, Lucia
Toppi, Arianna
Fiore, Alberto
Scaloni, Andrea
Guidelli, Rolando

The published article is available from doi: https://dx.doi.org/10.1016/j.bioelechem.2016.06.004

Channel-forming activity of syringopeptin 25A in mercury-supported phospholipid monolayers and negatively charged bilayers

Lucia Becucci[#†,&], Arianna Toppi[†], Alberto Fiore [‡≠], Andrea Scaloni [¥], and Rolando Guidelli[1]

[†] *Department of Chemistry, Florence University, via della Lastruccia 3, 50019 Sesto Fiorentino (Firenze), Italy*

[&] *Department of Chemistry, University of Padova, Via Marzolo 1, 35131 Padova, Italy*

[‡] *Department of Agricultural and Food Science, University of Naples "Federico II", 80055 Portici, Italy*

[¥] *Proteomics & Mass Spectrometry Laboratory, ISPAAM-National Research Council, 80147 Naples, Italy*

[≠] *School of Science, Engineering & Technology, Division of Food & Life Sciences, Abertay University, Kydd Building, Dundee, DD1 1HG, UK*

Abstract

Interactions of the cationic lipodepsipeptide syringopeptin 25A (SP25A) with mercury-supported dioleoylphosphatidylcholine (DOPC), dioleoylphosphatidylserine (DOPS) and dioeleoylphosphatidic acid (DOPA) self-assembled monolayers (SAMs) were investigated by AC voltammetry in 0.1 M KCl at pH 3, 5.4 and 6.8. SP25A targets and penetrates the DOPS SAM much more effectively than the other SAMs not only at pH 6.8, where the DOPS SAM is negatively charged, but also at pH 3, where it is positively charged just as SP25A. Similar investigations at tethered bilayer lipid membranes (tBLMs) consisting of a thiolipid called DPTL anchored to mercury, with a DOPS, DOPA or DOPC distal monolayer on top of it, showed that, at physiological transmembrane potentials, SP25A forms ion channels spanning the tBLM only if DOPS is the distal monolayer. The distinguishing chemical feature of the DOPS SAM is the ionic interaction between the protonated amino group of a DOPS molecule and the carboxylate group of an adjacent phospholipid molecule. Under the reasonable assumption that SP25A preferentially interacts with this ion pair, the selective lipodepsipeptide antimicrobial activity against Gram-positive bacteria may be tentatively explained by its affinity for similar protonated amino-carboxylate pairs, which are expected to be present in the peptide moieties of peptidoglycan strands.

Keywords: Antimicrobial peptides; lipodepsipeptides; ion channels; lipid monolayers self-assembled on mercury; tethered bilayer lipid membranes; cyclic voltammetry

[#] Corresponding author. Telephone: (+39) 055-457-3095. Fax: (+39) 055-457-3385

E-mail: luci_be@tiscali.it; lucia.becucci@unifi.it

[1] Former Professor at Florence University

1. Introduction

In addition to the lipodepsinonapeptides syringomycin (SR) and syringotoxin, the plant pathogenic bacterium *Pseudomonas syringae* pv. *syringae* produces syringopeptins SP22 and SP25, which contain 22 and 25 amino acids, respectively. Combined biochemical approaches demonstrated that the latter lipodepsipeptides have common structural characteristics, e.g. a similar peptide chain preferentially made of hydrophobic D-amino acids, a similar C-terminal octadepsipeptide ring containing 2,4-diaminobutanoic acid, and N-terminal 3-hydroxy-decanoic or 3-hydroxy-dodecanoic acid moieties generating A or B molecular isoforms, respectively [1,2]. NMR investigations in aqueous solution showed that SP25A assumes a conformation having distinct structural portions, e.g. a loop region (amino acids 2-6), a left-handed helical region (amino acids 8-15), and an octadepsipeptide moiety (amino acids 18-25) that resembles the seam of a tennis ball [3,4]. Syringopeptins have phytotoxic, antifungal and antibacterial properties. The latter action seems mainly directed against Gram-positive (G+) organisms, seemingly toward their teichoic acid-containing peptidoglycan layer [5,6]. It was demonstrated that syringopeptins have a stronger phytotoxic activity than SR [7,8], and disrupt erythrocytes and tobacco protoplasts below their critical micellar concentration [9]. Even though the main plant target is the cellular plasma membrane, these lipodepsipeptides may also lyse intracellular membranes [10].

When assayed for the induction of macroscopic conductance on neutral dioleoylphosphatidylcholine (DOPC) bilayers, syringopeptins were found to be more effective than SR [10]. This property was associated with their long hydrophobic peptide chain, which may strongly interact with lipids. Differently from SR, which presents an increased activity on phospholipid vesicles in the presence of sterols, syringopeptins do not require the latter molecules to elicit their potential. Measurements of single- and multi-channel currents induced by syringopeptins at conventional bilayer lipid membranes (BLMs) have been performed by different groups [11-14]. Both small and large single-channel conductance fluctuations were observed, which present a 4-6 fold difference in their level of conductance and in the corresponding open state lifetime [11,13,14]. The latter parameter ranges from several sec (for the higher conductance levels) to a few tens of msec (for the lower ones). When SP25A was added to the *cis* side of a BLM consisting of 2:2:1 phosphatidylcholine (PC), phosphatidylethanolamine (PE) and phosphatidylserine (PS) mixture, bathed by an electrolyte solution, lipodepsipeptide incorporation induced a multichannel current upon applying a positive transmembrane potential ($\Delta\phi$) at the *trans* side [13], which tended exponentially to a constant limiting value. A symmetrically opposite behavior was observed when a negative potential of the same magnitude was quickly applied. On this basis, the SP25A channel seems to open at positive $\Delta\phi$ values, whereas a step-like voltage sign reversal induces its closure in about 10 sec. Single channel currents obtained from voltage sign reversal measurements at the same BLM, once reported against $\Delta\phi$, yielded a plot exhibiting a higher slope at positive $\Delta\phi$ values than at negative ones [13]. Therefore, the corresponding estimated single channel conductance was higher at positive $\Delta\phi$ values. This behavior was associated with the positive charge of the cyclic moieties present at the mouth of the lipodepsipeptide channel. This positive charge attracts anions, increasing their local concentration at this site, while decreasing that of cations. Thus, anions are moved by a positive $\Delta\phi$ value along the SP25A channel more favorably than cations by the negative $\Delta\phi$ counterpart. A similar phenomenon was observed with a DOPC-containing BLM incorporating SP25A, when the peptide was dissolved in an electrolyte solution, pH 6 [11]. Measurements performed with reversed $\Delta\phi$ values pointed to a modest anion selectivity [13].

We have recently evaluated some aspects of the SP25A ion-channel activity at a biomimetic membrane in relation to transmembrane potential and pH values [15]. To this purpose, use was made of a Hg-supported biomimetic membrane consisting of a monolayer of a thiolipid, called DPTL, with a DOPC monolayer on top of it. DPTL is made of a tetraethyleneoxy hydrophilic chain, called spacer, ending at one side with a lipoic acid residue (for anchoring to the mercury surface). At the other side, it is covalently linked to two phytanyl chains that mimic the hydrocarbon tails of a lipid [16]. The hydrophobic interactions between the phytanyl chains and the overlying phospholipid monolayer give rise to a lipid bilayer interposed between the tetraethyleneoxy chain and the bulk aqueous solution. The spacer may accommodate a number of water molecules and ions, thus acting as an ionic reservoir. The incorporation of SP25A in the DPTL/DOPC tBLM required the application of non-physiological $\Delta\phi$ values. Nonetheless, once incorporated, SP25A formed stable ion channels over the narrower range of physiological $\Delta\phi$ values. Ion flow into and out of the spacer through the lipid bilayer moiety of the tBLM was monitored by potential step chronocoulometry and cyclic voltammetry, at different pH values. Potassium ion flow into the hydrophilic spacer along the SP25A channels during the negative potential scan was found to proceed in two stages.

The present work aims at investigating the behavior of SP25A in Hg-supported lipid mono- and bi-layers composed of DOPC, dioleoylphosphatidylserine (DOPS) or dioleoylphosphatidic acid (DOPA). The variation of the lipid composition intends to simulate the different lipid films that SP25A may encounter *in vivo*, in order to verify the possible effect of their nature on its activity. The effect of a change of pH in aqueous 0.1 M KCl was also evaluated. In addition to Hg-supported DPTL/DOPS and DPTL/DOPA tBLMs, self-assembled monolayers (SAMs) of DOPC, DOPS and DOPA were used. Mercury provides a defect free, fluid and readily renewable surface to both SAMs and tBLMs. Moreover, it imparts to the lipid molecules of the whole film a lateral mobility comparable with that of biomembranes. Hg-supported tBLMs have been extensively used in our laboratory for the investigation of ion channels [17-25]. Thanks to its partially hydrophobic nature, mercury is also an excellent substrate for phospholipid monolayers. Phospholipid molecules self-assemble onto the mercury surface with the hydrocarbon tails directed toward the metal and the polar heads facing the bathing solution. Lacking a hydrophilic spacer and one of the two lipid leaflets, Hg-supported lipid SAMs represent a poorer biomimetic membrane with respect to tBLMs. Nonetheless, their dielectric properties are extremely sensitive to the presence of exogenous molecules. This has stimulated the use of SAMs to investigate the effect of the interaction of peptides and small proteins with the outer leaflet of biological membranes [20,22-25]. Combining the features of this interaction with those of SP25A penetration into tBLMs may reveal novel insights into the mechanism of action of this lipodepsipeptide on biomembranes.

2. Material and methods

Water was obtained by an inverted osmosis unit; it was then distilled once and redistilled from alkaline permanganate. Suprapur® KCl (Merck, Darmstadt, Germany) was baked at 500 °C before use to remove any organic impurities. Adenosine-5'-triphosphate disodium salt (Na_2H_2ATP) from Fluka (Milwaukee, WI, USA), dimethylsulfoxide (DMSO), HCl and $TlNO_3$ from Sigma-Aldrich (St. Louis, MO, USA) and KH_2PO_4 and K_2HPO_4 from Merck were used without further purification. DOPC, DOPS and DOPA were purchased in chloroform solution from Avanti Polar Lipids (Birmingham, AL, USA). 2,3,di-O-phytanyl-*sn*-glycerol-1-tetraethylene-glycol-D,L-α lipoic acid ester thiolipid (DPTL) was provided by Prof. Adrian Schwan (Department of Chemistry, University of Guelph, Canada). Solutions of 0.2 mg/mL

DPTL in ethanol were prepared from a 2 mg/mL solution of DPTL in ethanol. Stock solutions of this thiolipid were stored at –18 °C. SP25A was obtained from *P. syringae* pv. *syringae* culture broths and purified as already reported [1]. SP25A stock solutions (1 mg/mL) in DMSO were stored at 4 °C.

All measurements were carried out with a homemade hanging mercury drop electrode (HMDE) described elsewhere [26]. A homemade glass capillary with a finely tapered tip (about 1 mm in outer diameter) was employed. Capillary and mercury reservoir were thermostated at 25 ± 0.1 °C in a water-jacketed box to avoid any changes in drop area due to temperature changes. The HMDE acted as the working electrode in a three-electrode system, with an Ag/AgCl (0.1 M KCl) reference electrode and a platinum coil counter electrode.

Phospholipid monolayers were obtained by first spreading a DOPC, DOPS or DOPA solution in pentane on the surface of a buffered or unbuffered 0.1 M KCl aqueous solution, in an amount corresponding to about five phospholipid monolayers, and allowing the solvent to evaporate. The lipid film so formed was a monolayer at its equilibrium spreading pressure (about 45 mN m^{-1}), in equilibrium with the bulk phase of the surfactant, which consisted of floating 'icebergs' [27]. A HMDE was then immersed into the solution across the formed lipid film, at a controlled rate. Preparation of these lipid SAMs did not require any electrochemical stabilization. Hg-supported tBLMs were obtained by tethering a DPTL monolayer to a HMDE upon keeping the mercury drop immersed in a 0.2 mg/mL DPTL solution in ethanol, for about 20 min [18]. The mercury drop was then extracted from the solution, and ethanol was allowed to evaporate under N_2 atmosphere. A lipid monolayer was subsequently self-assembled on top of the DPTL monolayer by the same procedure adopted to form it on a bare mercury drop. The tBLM was subjected to repeated potential scans over a potential range from –0.20 to –1.20 V, while continuously monitoring the curve of the quadrature component of the current at 75 Hz against the applied potential (*E*) using AC voltammetry, until a stable curve was attained.

Electrochemical impedance spectroscopy (EIS), potential-step chronocoulometry, phase-sensitive AC voltammetry and cyclic voltammetry measurements were carried out with an Autolab instrument PGSTAT12 (Echo Chemie, Utrecht, The Netherlands) supplied with FRA2 module for impedance measurements, SCAN-GEN scan generator and GPES 4.9007 software. All AC voltammetry and EIS measurements were carried out by superimposing an AC voltage of 10 mV peak-to-peak amplitude to the bias potential *E*. In EIS measurements the frequency was varied between 10^{-1} and 10^{5} Hz. Potentials were measured *vs*. a Ag/AgCl electrode immersed in the 0.1 M KCl working solution, and are referred to this reference electrode.

3. Results and discussion

3.1. Lipid SAMs

A self-assembled lipid monolayer can be regarded as the first barrier that a peptide encounters in its attempt to penetrate a membrane. Nonetheless, the interactions of the peptide with the hydrocarbon tail region of a SAM are generally different from those occurring with a lipid bilayer, especially if its length is appreciably greater than the SAM thickness, as is often the case. In fact, the peptide can only intercalate partially between the hydrocarbon tails, without being capable of assuming the conformation otherwise present in a biomembrane. Conversely, its interactions with the polar heads of a SAM may realistically reproduce those with the outer leaflet of a biomembrane. AC voltammograms are plots of the quadrature component of the current against the applied potential (*E*) at constant frequency (*f*); the current is converted into a capacitance (*C*) by calibrating the instrument with a high precision capacitor in place of the electrochemical cell. All lipid SAMs are characterized by a potential region of low and almost

constant capacitance, followed by two or more pseudo-capacitance peaks at more negative potentials. The less negative peak is ascribed to a cooperative reorientation of the lipid molecules, whereas the most negative one is due to their partial desorption [27]. As a rule, molecules capable of penetrating the hydrocarbon tail region of the phospholipid monolayer increase its capacitance over the potential range of the flat capacitance minimum, with respect to its value in the absence of foreign species, provided that their polarizability is appreciably higher than that of the lipid molecules. Conversely, they affect the monolayer capacitance only slightly if they have a low polarizability [28]. In both cases, whenever their concentration in the lipid monolayer is sufficiently high, their intercalation with the lipid molecules prevents the latter molecules from undergoing a sufficiently sharp cooperative reorientation, thus broadening and depressing the pseudo-capacitance peaks. Molecules adsorbed on top of the lipid monolayer, but unable to penetrate it, alter and depress the pseudo-capacitance peaks by interacting with the polar heads [29,30]; they may also decrease the capacitance over the potential range of the flat capacitance minimum, whenever they form a sufficiently compact layer, thus increasing the thickness of the whole adsorbed material [28].

Scanning the potential from –0.20 V to potentials negative with respect to one or two peaks may allow the penetration of exogenous molecules present in the solution into the SAM or, at least, into its polar head region, provided they have some affinity for it. Another procedure adopted to favor the possible penetration of an exogenous molecule consists in carrying out a series of electrochemical impedance spectra, at regular intervals of the bias potential, over the potential range of stability of the SAM; this procedure will be briefly referred to as an 'EIS scan'. In this case, incorporation may be favored by the relatively long time during which the SAM is maintained at each of the stepwise varied potentials over its stability range, and/or by some effect of the small AC signals covering the frequency range from 10^{-1} to 10^{5} Hz. The AC voltammetry profile of a lipid SAM is its outright fingerprint, just as its alteration upon addition of an exogenous species is a measure of the nature and extent of its interaction with the SAM. In the absence of interacting species, Hg-supported lipid SAMs constitute an impenetrable barrier to inorganic ions. If a peptide alters the compact and well-organized structure of the SAM, it may induce defects and/or pores (not ion channels) allowing the penetration of ions. These structural changes affect both the capacitance and, to a lesser extent, the resistance, in a frequency dependent manner. Thus, the effect of SP25A was investigated at DOPC and DOPS SAMs in unbuffered solutions, pH 3 and 5.4, and in a phosphate buffer solution, pH 6.8, as well as at a DOPA SAM in an unbuffered solution, pH 5.4.

Fig. 1 shows the AC voltammograms at a Hg-supported DOPC SAM in an unbuffered solution of 0.1 M KCl, pH 5.4, as obtained in the absence of SP25A (solid curve), immediately after the addition of 0.2 μg/mL SP25A (dashed curve) and after a complete EIS scan from –0.30 to –0.80 V (dash-dotted curve). In the absence of SP25A, the DOPC SAM was characterized by a sharp pseudocapacitance peak lying at about −1.02 V, followed by two further peaks at about −1.10 V and −1.35 V. The first two peaks are ascribed to a cooperative reorientation of the lipid molecules, whereas the third one is due to their partial desorption [27]. Addition of the lipodepsipeptide depressed the peaks to a moderate extent and increased the capacitance along the flat region only at potentials negative of –0.70 V, where the SAM is known to be less stable. An EIS scan increased the effect of SP25A only slightly.

Here Figure 1

In all the above measurements, the SAM was formed before adding SP25A. In a few measurements, the SAM was also formed by immersing the mercury drop across the lipid film into an aqueous solution containing SP25A. In this case, the mercury drop dragged into the solution a lipid monolayer containing peptide molecules that may have previously interacted with the film in contact with the aqueous subphase; the effect of SP25A was found to be almost identical with that of the dashed curve in Fig. 1. The AC voltammograms at DOPC SAMs in aqueous solutions of 0.1 M KCl, pH 3 or 6.8, were even less influenced by the addition of SP25A. The EIS spectra recorded over the potential range of the flat capacitance region in Fig. 1 were only slightly affected by the addition of 0.2 μg/mL SP25A, with no relevant changes in the in-phase and quadrature components of the admittance. No differences were observed if the monovalent K^+ cation in the electrolyte was substituted by the divalent Ca^{+2} cation.

The effect of SP25A on the DOPS SAM in 0.1 M KCl was much stronger than that on the DOPC counterpart, at all the pH values investigated. Fig. 2 shows the AC voltammograms at a Hg-supported DOPS SAM in a buffer solution of 0.1 M KCl, pH 6.8, as obtained in the absence of SP25A (solid curve), immediately after the addition of 0.2 μg/mL SP25A (dashed curve) and after a complete EIS scan from –0.30 to –0.80 V (dash-dotted curve). The AC voltammogram recorded at a DOPS SAM in the absence of exogenous species (Fig. 2) differed from the counterpart measured at a DOPC SAM (Fig. 1) by the presence of a broader region of minimum capacitance, which extends up to –1.10 V and exhibits two pseudocapacitance peaks [25,31]. Since the potential region negative of the first pseudocapacitance peak, which lies at about –1.20 V, was not entirely reproducible, only the first peak is shown in Fig. 2. Addition of SP25A caused an immediate depression of the pseudocapacitance peak and an increase in the capacitance along the flat region at potentials negative of –0.7 V. A subsequent EIS scan suppressed the peak and increased the capacitance along the whole flat region.

Here Figure 2

The effect of SP25A on the AC voltammogram at a DOPS SAM increased slightly at pH 5.4, and to a greater extent at pH 3. At the latter pH value, the capacitance peak was completely suppressed upon the addition of SP25A (dashed curve at 75 Hz in Fig. 3). An EIS scan from –-0.30 to –0.80 V by 50 mV steps increased the capacitance *C* along the whole flat region (dash-dotted curve in Fig. 3). As distinct from the capacitance, the in-phase component of the admittance, *Y*', over the same potential range increased only slightly upon the addition of SP25A, at all the pH values investigated (data not shown). The AC voltammogram recorded after forming the DOPS SAM in a solution at pH 3 already containing 0.2 μg/mL SP25A showed no pseudocapacitance peak (gray curve in Fig. 3). Moreover, it practically coincided with the curve recorded in the absence of the lipodepsipeptide along the whole flat capacitance region. This strongly suggests that, when SP25A binds to a DOPS monolayer at its equilibrium spreading pressure on a water subphase, pH 3, it interacts mainly with the polar heads, without contacting the hydrocarbon tails. However, we cannot exclude the possibility that the short SP25A hydrocarbon chains may intercalate between the hydrocarbon tails of the lipid monolayer. Such an intercalation would not affect the capacitance along the flat region, since the polarizability of the SP25A hydrocarbon chains is comparable with that of the lipid hydrocarbon tails. Nonetheless, it would hinder the cooperative reorientation of the lipid molecules responsible for the pseudocapacitance peak, contributing to suppressing the latter. No differences were observed whenever the divalent cation Ca^{2+} was used instead of the monovalent K^+ one.

Here Figure 3

In this context, worth mentioning is the fact that a Hg-supported DOPS monolayer is positively charged at pH 3, neutral at pH 5.4 and negatively charged at higher pH values [32]. This behavior was explained by regarding the carboxyl and the amino groups of adjacent DOPS polar heads as being coplanar to the monolayer, and characterized by electrostatic dipole-dipole interactions. The phosphate group, whose pK_a is about 8, is buried inside the polar head region and almost completely protonated at pH 5.4, causing DOPS to be neutral and zwitterionic at this pH value. With a further decrease in the pH value, the carboxyl group, whose pK_a is around 3.3, undergoes a gradual protonation, inducing DOPS to become positively charged at low pH values. The electrostatic repulsion between the DOPS polar heads, which bear a positive charge at pH 3, and the positively charged SP25A octadepsipeptide moiety may oppose the penetration of the latter into a lipid monolayer suspended on an aqueous subphase and the resulting increase in monolayer capacitance. Only a negative electric potential, such as that applied to the Hg-supported lipid SAM, can move the octadepsipeptide moiety stably into the lipid monolayer.

The effect of SP25A at a Hg-supported DOPA SAM in an unbuffered solution of 0.1 M KCl, pH 5.4, was modest and comparable with that at a DOPC SAM. The two protonation constants of the DOPA phosphate group in biomimetic membranes have values close to 1×10^{-8} M^{-1} and 1×10^{-4} M^{-1} [33,34]. Hence, the phosphate group of DOPA is uncharged at pH 3 and monoanionic at pH 5.4. Repeated voltage scans over the range from –0.30 to –1.30 V yielded a stabilized AC voltammogramm with a flat capacitance region, followed by an abrupt capacitance rise at about –1.2 V terminating in a shoulder (Fig. 4). Addition of 0.2 μg/mL SP25A shifted the shoulder toward more negative potential values and increased the capacitance only at potentials negative of –0.90 V, leaving unaltered the largest part of the flat capacitance region. A subsequent EIS scan had no further effect.

Here Figure 4

The above findings raise the question on the factors responsible for the particular effectiveness of SP25A toward a DOPS SAM. The negative charge of a DOPS SAM at pH 6.8 might suggest an attractive electrostatic interaction with the positively charged octadepsipeptide moiety of SP25A. However, the observed effect is stronger at pH 3, a value at which the DOPS SAM is positively charged. Moreover, SP25A interaction with the negatively charged DOPA SAM is weak, just as that with the DOPC SAM. On this basis, the electrostatic interaction between SP25A and DOPS has to be ruled out as causative agent of the peptide penetration into the DOPS monolayer. At pH 5.4, the polar heads of both DOPS and DOPC are neutral and zwitterionic. The DOPC monolayer presents an arrangement of $(H_3C)_3N^+$-CH_2-CH_2-PO_3^- zwitterions that is coplanar to the monolayer, as a result of the electrostatic interactions between the trimethylammonium group and the phosphate group of adjacent polar heads. This results in the stabilization of the non-protonated form of the phosphate group [32]. On the other hand, the DOPS monolayer presents an arrangement of H_3N^+-CHR-CO_2^- zwitterions coplanar to the monolayer, with the protonated phosphate group buried inside the polar head region. In view of the above considerations, the experimental behavior observed strongly suggests that SP25A targets some structural features of the DOPS monolayer that are not present in the DOPC and DOPA monolayers.

In the absence of electroactive ions, the resistance of Hg-supported lipid SAMs along the flat capacitance region is slightly decreased by exogenous electroinactive species, even if they are able to induce defects and/or pores in the monolayer and to increase its capacitance to an appreciable extent. This is due to the lack of an ionic reservoir on the metal side of lipid SAMs, differently from tBLMs. The ability of an exogenous species to permeate a Hg-supported SAM

can be tested by exploiting the properties of inorganic ions that are electroreduced on mercury, with amalgam formation, over the potential range of stability of the lipid SAM [20,22,23]. In this case, the 'ionic reservoir' is provided by the mercury drop itself. For example, cadmium ion is electroreduced reversibly on bare mercury to Cd(Hg) amalgam, with a formal potential of –0.645 V in 0.1 M KCl [20,35], but its reduction is completely inhibited by a phospholipid SAM. In the presence of defects elicited by some exogenous species, the driving force of the electrode reaction moves Cd^{2+} ions along them across the SAM, generating a reduction current.

Fig. 5 shows the cyclic voltammograms (CVs) due to Cd^{2+} reduction and Cd(Hg) oxidation at a DOPS SAM in a solution of 0.1 M KCl, 4×10^{-5} M $CdSO_4$ and 0.2 μg/mL SP25A, at pH 6.8, 5.4 and 3. The height of the peaks decreased with a decrease in the pH value, and the negative peak at pH 3 evolved into a shoulder. The irreversibility of the electrode process, as measured by the separation between the positive and negative peaks, increased in passing from pH 6.8 to pH 5.4. While the ease of penetration of the SP25A molecules into the DOPS SAM increased with decreasing pH values, the permeability of this SAM to Cd^{2+} ions in the presence of SP25A decreased. This apparently anomalous behavior is explained by the charge on the DOPS polar heads being negative at pH 6.8 and positive at pH 3. Thus, it increased the cadmium ion concentration in the vicinity of the SAM with respect to its bulk value at the former pH, and decreased it at the latter. This behavior is not only due to a diffuse-layer effect. Rather, it is also and mainly due to the specific effect exerted by the charge of the DOPS polar heads, which can be regarded as a true specifically adsorbed charge, on the positively charged Cd^{2+} ions, as they start being deprived of their solvation sheath before entering into mercury. In fact, the rate constant of this electrode process is expected to decrease or increase depending on whether the charges of the DOPS polar heads and of cadmium ion have the same or opposite sign [36 and references therein].

Here Figure 5

3.2. DPTL/DOPS tBLM in a buffer solution, pH 6.8

The effect of SP25A on a Hg-supported DPTL/DOPC tBLM was reported in our previous paper [15]. The midpoint potential, $E_{1/2}$, between the positive and negative peaks in the CV at a DPTL/DOPC tBLM incorporating SP25A from aqueous 0.1 M KCl was found to shift toward less negative potentials with decreasing pH values. The magnitude of this shift was found to be practically identical with that observed at DPTL/DOPC and DPTL/DOPS tBLMs incorporating gramicidin [37], under otherwise identical conditions. Thus, with both ion channels, $E_{1/2}$ was found to be about equal to –0.65 V in a phosphate buffer at pH 6.8, –0.55 V in an unbuffered solution at pH 5.4, and –0.45 V in an unbuffered solution at pH 3. In view of the appreciable structural differences between the neutral dimeric gramicidin channel and the positively charged oligomeric SP25A channel, this common $E_{1/2}$ dependence upon pH value seems to depend more on the structural features of the phospholipid than on those of the ion channel, and a qualitative justification was provided. The cyclic voltammetry behavior of DPTL/DOPS tBLMs incorporating SP25A was in accord with this prediction. $E_{1/2}$ is the electric potential at which the ion flow into the hydrophilic spacer of the tBLM matches the corresponding outflow. Hence, it is equivalent to the zero transmembrane potential $\Delta\phi$ at a conventional symmetric BLM interposed between two identical solutions, where the flow of an ion in one direction matches that of the same ion in the opposite direction. Considering that the potential difference across the lipid

bilayer moiety of a Hg-supported DPTL/phospholipid (i.e., its transmembrane potential) is a fraction (about 0.72) of the potential difference across the whole mercury/solution interface [38], the product of 0.72 by the applied potential measured relative to $E_{1/2}$, $0.72(E–E_{1/2})$, can be directly compared with the transmembrane potential at a BLM. Hence, $0.72(E–E_{1/2})$ values more negative than those corresponding to the most negative transmembrane potential used in BLM measurements with SP25A [10,11,13], namely –200 mV, will be conventionally defined as non-physiological. While non-physiological negative $\Delta\phi$ values were required for incorporating SP25A into DPTL/DOPC tBLMs [15], physiological ones were sufficient for incorporating this peptide into DPTL/DOPS tBLMs at all the pH values we investigated.

The first EIS scan from –0.30 to –0.80 V, as reported at 10 Hz on a freshly prepared DPTL/DOPS tBLM incorporating SP25A from its 0.4 μg/mL solution in 0.1 M KCl, caused an appreciable increase in the capacitance (C) and the in-phase admittance (Y') over their background values, at potentials negative of about –0.60 ÷ –0.70 V, for all the pH values we investigated. The second EIS scan caused both C and Y' to increase over the whole potential range explored (data not shown). The impedance spectrum at a freshly prepared DPTL/DOPS tBLM in a buffer solution of 0.1 M KCl, pH 6.8, at –0.50 V is displayed in Fig. 6 on a ωZ' vs. –ωZ" plot (referred to as a modulus or M plot), both before and after the addition of 0.4 μg/mL SP25A. Lipodepsipeptide addition determined the appearance of a small semicircle partially fused with a roughly semicircular feature similar to that present before such an addition. It should be noted that a tBLM can be simulated by an equivalent circuit consisting of a series of '*RC* meshes', i.e., parallel combinations of a capacitance C and a resistance R. On a M plot, a single RC mesh yields a semicircle of diameter $1/C$ [24,39]. If some of the *RC* meshes simulating a tBLM have similar values of the time constant *RC*, the corresponding semicircles are partially overlapped in the M plot. The small semicircle elicited by the SP25A addition had a relatively high capacitance, 5 μF cm^{-2}, and a low resistance, 4 kΩ cm^2. It was quite similar to a small semicircle induced by the presence of the peptide melittin at a DPTL/lipid tBLM [17], and can likewise be ascribed to a monolayer of SP25A molecules intercalated with water molecules and adsorbed on top of the tBLM. After the first EIS scan over the whole range of physiological potentials, a subsequent impedance spectrum recorded at –0.5 V did not show this additional semicircle. At potentials negative of –0.50 V, no additional semicircle was observed at a freshly prepared tBLM even during the first recording of the impedance spectrum, denoting a stable penetration of the lipodepsipeptide molecules deeply into the lipid bilayer moiety of the tBLM, at these negative potentials.

Here Figure 6

This peculiar feature of the impedance spectrum was encountered neither with DPTL/DOPS tBLMs at pH 5.4 or 3, nor with DPTL/DOPC tBLMs at any of the three pH values we investigated. The impedance spectra of a DPTL/DOPS tBLM at pH 6.8, both in the absence and in the presence of 0.4 μg/mL SP25A, were analyzed over the potential range from –0.30 to –1.0 V, by fitting them with an equivalent circuit consisting of four *RC* meshes in series. The RC mesh of by far the lowest capacitance and resistance was common to all tBLMs and was ascribed to the aqueous solution adjacent to the tBLM; it will be ignored in what follows. Of the other three RC meshes, one had a capacitance of about 1 μF cm^{-2} and a resistance of a few MΩ cm^2 in the absence of SP25A; the peptide addition affected the capacitance only slightly and decreased the resistance by about three orders of magnitude at potentials negative of –0.50 V. This *RC* mesh was ascribed to the lipid bilayer moiety of the tBLM. The second *RC* mesh had a capacitance ranging from 3 to 5 μF cm^{-2} and a resistance of about 0.5 MΩ cm^2; SP25A addition

increased the capacitance by 2 or 3 times and left the resistance almost unaltered. This *RC* mesh was reasonably attributed to the dielectric layer in direct contact with the mercury surface. The potential dependence of the capacitance C and conductance $G = 1/R$ of the third RC mesh, as reported in Fig. 7, behaved differently from that at all other tBLMs examined. SP25A addition depressed both C and G at potentials positive of –0.60 V and increased them at more negative potential values. The relatively high capacitance and conductance of this *RC* mesh in the absence of the peptide are typical of the polar head region. Their apparently anomalous decrease at potentials positive of –0.60 V, upon addition of SP25A, is suggestive of a tight intercalation of the lipodepsipeptide molecules between the DOPS polar heads, whereas their subsequent increase at more negative potentials denotes a deeper penetration of the SP25A molecules into the lipid bilayer and a drop in polar head compactness.

Here Figure 7

Fig. 8 shows a series of charge transients recorded at a DPTL/DOPS tBLM in a buffer solution of 0.1 M KCl, pH 6.8, and 0.4 μg/mL SP25A by jumping from a fixed initial potential E_i = –0.30 V to progressively more negative final potentials E_f. These transients differ from those obtained at DPTL/DOPC tBLMs under otherwise identical conditions by two main features. Firstly, they constantly turn their concavity downwards, and hence do not show a two-stage flow of ionic charge, such as that in Fig. 5 of Ref. 15, where the two stages were separated by an inflection point. Secondly, extrapolation of the charge transient plateau at E_f = –0.80 V to t = 0 yields a charge density of about –50 μC cm^{-2}, which corresponds to a spacer saturation by the sole K^+ ions, whereas an analogous extrapolation of the two-stage charge transient at a DPTL/DOPC tBLM yielded a charge density of –60 μC cm^{-2} [15].

Before trying to explain these appreciable differences in behavior, it is convenient to summarize a number of results reported in previous works. At first, it must be mentioned that all peptides so far incorporated in our Hg-supported tBLMs (i.e. gramicidin [18], monazomicin [19], melittin [19], distinctin [20], trichogin GA IV [21], dermicidin [23], sarcolipin [40], phospholamban [41], syringomycin E [25]) yielded charge transients that attained a maximum charge density of –45 ± 5 μC cm^{-2}, with the only exception of SP25A in a DPTL/DOPC tBLM [15]. This maximum limiting charge density was explained by the limited spaciousness of the tetraethyleneoxy spacer moiety of the tBLM, which may accommodate a maximum amount of K^+ ions bearing a +45 ± 5 μC cm^{-2} charge density at the most negative E_f values. The equal and opposite charge density of –45 ± 5 μC cm^{-2} is due to the electrons accumulating on the mercury surface to ensure the electroneutrality of the whole electrified interface. Moreover, all peptides so far incorporated in our Hg-supported tBLMs exhibited a sigmoidal shape, with the only exception of gramicidin [18]. The sigmoidal shape was quantitatively explained by a mechanism of penetration of peptide monomers into the lipid bilayer, their nucleation, and growth of the resulting clusters, with channel formation [19]. The charge transients at a tBLM incorporating gramicidin also attained a maximum negative charge density of –45 ± 5 μC cm^{-2}, but did not exhibit a sigmoidal shape [18]. This simply depends on the nature of gramicidin channels, which consist of single N-terminus-to-N-terminus dimers and, hence, do not involve monomer clustering.

Here Figure 8

The fact that the maximum charge density attained by the two-stage transients of SP25A at a DPTL/DOPC tBLM significantly exceeded –45 ± 5 μC cm^{-2} was explained by assuming that,

differently from the other peptides so far examined by us, this lipodepsipeptide forms a channel that is open at the initial potential E_i = –0.30 V [15]. Since this applied potential corresponded to a positive transmembrane potential $\Delta\phi$, a certain amount of Cl^- ions was expected to be present in the hydrophilic spacer. The subsequent negative potential jump to E_f determined the outflow of Cl^- ions from the spacer, and the concomitant inflow of K^+ ions. Since the current due to the Cl^- outflow had the same negative sign as the current due to the K^+ inflow, at sufficiently negative final potentials both currents were expected to contribute to increasing the charge transient plateau beyond the $–45 \pm 5$ μC cm^{-2} value corresponding to spacer saturation by K^+ ions. The difference between the experimental value of –60 μC cm^{-2} and the above expected value yielded a charge density due to Cl^- outflow that amounted to about 15% of the overall K^+ inflow. Since the first stage of the charge transient for SP25A at the DPTL/DOPC tBLM was higher than the second one by more than 15%, we concluded that the first stage was necessarily determined by the concomitant Cl^- outflow and K^+ inflow, while the second stage was due to the sole K^+ ion inflow up to spacer saturation by this cation [15]. To justify the presence of two separate stages of the charge transient, we further postulated that the first stage was determined by Cl^- and K^+ flows along large SP25A ion channels, and the second stage by K^+ inflow along small SP25A ion channels.

The existence of both large and small SP25A ion channels was assumed on the basis of the detection of both large and small single-channel conductance fluctuations in SP25A single channel measurements at conventional BLMs [11,13,14]. Since the small fluctuations were found to be exactly one fourth of the large ones, Dalla Serra et al. [13] assumed that the large channels result from the tetrameric aggregation of the small channels, leading to their synchronous opening and closing, in analogy with the hexameric clusters proposed for syringomycin E [42]. In view of above results, we tentatively assumed that the first stage is mainly determined by ion flow along the large channels, which prevail over the small ones thanks to their higher level of conductance and much longer open state lifetime [15]. However, at more negative and non-physiological transmembrane potentials, the strong electric field may drag the positively charged cyclic moieties of the SP25A monomers composing the large channels deeper into the lipid bilayer. The resulting decrease in the dielectric constant of the immediate environment of the cationic octadepsipeptide moiety would then increase the mutual electrostatic repulsion among the small channels composing the tetrameric clusters, determining their abrupt disaggregation and causing the K^+ inflow to proceed exclusively along the small channels during the second charge-transient stage.

In the light of the above results on SP25A ion-channel activity, as reported by us [15] at a DPTL/DOPC tBLM and by others [11,13,14] at conventional BLMs, the following conclusions can be reasonably drawn about the charge transient behavior of this lipodepsipeptide at a DPTL/DOPS tBLM. The fact that the maximum limiting height of the charge transient plateau amounted to $–45 \pm 5$ μC cm^{-2} denotes that the SP25A ion channel is closed at the initial potential E_i = –0.30 V, and hence does not allow Cl^- inflow. In addition, the fact that the charge transients turned their concavity toward the time axis and did not show an inflection point, similarly to the gramicidin channel [18], indicates that these channels are not formed during the negative potential jump by a mechanism of nucleation and growth. Thus, they must be formed through a different rate-determining step during the potential jump or, more probably, they are already present at E_i, albeit in a closed state.

The CV in Fig. 9 at a DPTL/DOPS tBLM in an aqueous solution of 0.1 M KCl, pH 6.8, and 1 μg/mL SP25A was approximately centrosymmetric, with the inversion center located at the midpoint potential $E_{1/2}$ = –0.62 V between the positive and negative peaks. The trumpet-shaped enlargement of the CV at the most positive potentials is a specific feature that we observed only

in the CVs of SP25A at DPTL/DOPC tBLMs, at all the pH values we investigated [15]. It was explained on the basis of a modelistic calculation of CVs at a tBLM incorporating a non-selective ohmic channel, according to which the positive peak due to the anion inflow into the spacer and the negative peak due to its outflow fall at more positive potentials than the corresponding peaks for the in- and outflow of the monovalent cation (see Fig. 7 in Ref 15). This predicted behavior is due to the limited spaciousness of the spacer, which favors the accumulation of cations over anions at more negative potentials. A modest overlapping of anion and cation flow was only predicted at the junction between the negative peak due to anion outflow and the negative peak due to cation inflow, and between the reverse positive peak due to cation outflow and the positive peak due to anion inflow. Unfortunately, the positive potential range required to monitor the predicted massive anion in- and outflow is experimentally inaccessible on a Hg-supported tBLM, due to mercury surface oxidation. Nonetheless, the incipient small anion inflow (during the positive-going potential scan) and its subsequent outflow (during the negative-going scan) were revealed by the trumpet-shaped enlargement exhibited at the most positive potentials by the CV in Fig. 9. This conclusion seems to contradict the previous statement that the SP25A ion channel is closed at E_i. However, we must consider that cyclic voltammetry is a dynamic technique. Therefore, the rate of the voltage scan may prevent the channel from closing in the short time during which the applied potential E assumes values corresponding to positive transmembrane potentials. At the initial potential E_i of –0.30 V chosen for the chronocoulometric measurements in Fig. 8, the channel is closed because it is kept at this potential for a rest time long enough to permit its closure before each potential jump. Under all experimental conditions, the charge obtained by integrating the negative current peak in Fig. 9 turns out to be less negative than, or at most equal to, the opposite of the maximum cation charge that can be accommodated by the hydrophilic spacer (i.e., 45 ± 5 μC cm^{-2}) plus any anion charge moving away from the spacer, if the ion channel is open at the most positive potential covered by the voltage scan. *Mutatis mutandis*, analogous considerations apply to the corresponding positive peak.

Here Figure 9

The negative peak in Fig. 9 does not show a splitting such as that exhibited by the CV at a DPTL/DOPC tBLM (see Figs. 2 and 3 in Ref. 15). Such a splitting was ascribed to ion flow along the large channels at less negative potentials and along the small ones at more negative potentials [15]. The lack of splitting at a DPTL/DOPS tBML may be due either to the simultaneous presence of large and small channels or to the presence of the sole small channels, at all potentials. In the former case, the macroscopic current is clearly determined by the large channels, in view of their higher conductance and much longer lifetime. The latter case seems more probable at pH 6.8, where the DOPS polar heads are negatively charged, and may hinder the clustering of the small channels into the large ones. At pH 6.8, SP25A permeabilized the lipid bilayer to Tl^+ ions, yielding a CV of the Tl^+/Tl(Hg) couple almost identical with that obtained on bare mercury. This is shown in Fig. 10, which was recorded while maintaining the negative transmembrane potentials within the range of physiological values. This behavior differs from that at a DPTL/DOPC tBLM [15], which was totally impermeable to Tl^+ ions under the same conditions.

Here Figure 10

3.3. DPTL/DOPS tBLM in pH 3 and pH 5.4 unbuffered solutions

Fig. 11 shows the CVs at a DPTL/DOPS tBLM in aqueous solution of 0.1 M KCl and 0.4 μg/mL SP25A, at pH 5.4 and 3. The midpoint potential $E_{1/2}$ shifted gradually toward less negative potentials with decreasing pH, passing from –0.62 V at pH 6.8 to –0.56 V at pH 5.4 and to –0.42 V at pH 3. These midpoint potentials were in close agreement with those determined at the same pH values at DPTL/DOPS tBLMs incorporating gramicidin [37]. This confirms that the shift depends on the structural features of the lipid molecules interacting with those of a peptide at the mouth of ion channels, more than on the nature and charge of the particular peptide. Differently from pH 6.8, permeabilization of the DPTL/DOPS tBLM toward Tl^+ ions by SP25A was modest at pH 3 (dashed curve in Fig. 11). This is very likely due to the electrostatic interaction between Tl^+ ions and the DOPS distal monolayer. This interaction is repulsive at pH 3, where the lipid is positively charged, and attractive at pH 6.8, where it is negatively charged.

Here Figure 11

As distinct from the behavior of SP25A in a DPTL/DOPS tBLM at pH 6.8, chronocoulometric potential-step measurements carried out at pH 5.4 and 3, under otherwise identical conditions, yielded two-stage charge transients analogous to those occurring at DPTL/DOPC tBLMs at all the pH values we investigated [15]. The maximum charge density estimated by extrapolating the charge transient plateau at E_f = –0.90 V to t = 0 amounted to about –65 μC cm^{-2} at pH 5.4 (see Fig. 12) and to about –80 μC cm^{-2} at pH 3 (data not shown). This charge exceeded that, –45 ± 5 μC cm^{-2}, corresponding to spacer saturation by K^+ ions. Hence, an excess charge density of ~ –20 μC cm^{-2} at pH 5.4 and ~ –35 μC cm^{-2} at pH 3 must be ascribed to Cl^- outflow from the spacer during the potential jump. The lack of splitting in the negative peaks of the CVs in Fig. 11 seems to exclude the possibility for the first stage of the corresponding charge transients at pH 5.4 and 3 to be ascribed to ion flow along ion channels different from those active along the second stage, as hypothesized for the DPTL/DOPC tBLMs [15]. Hence, the amount of Cl^- ions contained in the hydrophilic spacer at the initial potential E_i = –0.30 V of the chronocoulometric potential jumps is responsible for practically the whole ion flow during the first stage of the charge transients. A positive potential jump from –0.80 to –0.30 V at a DPTL/DOPS tBLM in 0.1 M KCl and 0.4 μg/mL SP25A yielded a charge density practically equal in magnitude, but opposite in sign, to that obtained by stepping the potential from –0.30 to –0.80 V at all the pH values.

Here Figure 12

Summarizing the results reported in this note and in Ref. 15, the SP25A channel is open at positive transmembrane potentials in DPTL/DOPC tBLMs at all the pH values we investigated [15], and in DPTL/DOPS tBLMs at pH 5.4 and 3. Conversely, the SP25A channel is substantially closed at positive transmembrane potentials if it is incorporated in a DPTL/DOPS tBLM at pH 6.8. The latter peculiar behavior can be rationalized by assuming that the SP25A channel opens whenever the positive transmembrane potential succeeds in pushing the positively charged octadepsipeptide moiety slightly out of the membrane, as proposed by Dalla Serra et al. [13]. This occurs when the distal lipid monolayer is practically uncharged, namely with DPTL/DOPC tBLMs at all the pH values we investigated [15], with the DPTL/DOPS tBLM at pH 5.4, and, even more so, when the distal monolayer is positively charged, namely with the DPTL/DOPS tBLM at pH 3 [32]. On the other hand, when the distal monolayer is negatively charged, as in the case of a DPTL/DOPS tBLM at pH 6.8, the negative charge may prevent the octadepsipeptide moieties of the SP25A channel mouth from being pushed backwards by a positive

transmembrane potential, thus maintaining the channel closed state. The conformation assumed by the channel mouth under these conditions might possibly be related to the tight intercalation of the lipodepsipeptide molecules between the DOPS polar heads, as revealed by the impedance spectrum of Fig. 7, peculiar to the DOPS distal monolayer at pH 6.8.

The behavior of the distal monolayer of the DPTL/DOPS tBLM at pH 6.8 was shared by a conventional BLM formed from an equimolar mixture of DOPS and DOPE incorporating SP22A from a buffered solution of 0.1 M NaCl, pH 6 [11]. An opposite behavior was reported at a BLM consisting of a PC/PE/PS mixture in a 2:2:1 molar ratio at pH 6 [13], where the SP25A ion channel was open at positive transmembrane potentials. However, in this case the contribution to the overall lipid charge from PS was small, in view of its low mole fraction. It should be noted that the particular behavior of the SP25A channel at a DPTL/DOPS tBLM in a solution of 0.1 M KCl, pH 6.8, parallels that of the syringomycin E channel, which is closed at positive transmembrane potentials at a DOPS [43] and a DOPS/DOPE BLM in 0.1 M NaCl, pH 6 [44], while it is open at a DOPS/DOPE BLM in 0.1 M NaCl, pH 2, and at a diphytanoylPC BLM in 0.1 M NaCl, pH 6 [44].

To verify the effect of the absence of permeating anions in the solution bathing a DPTL/DOPS tBLM incorporating SP25A, a CV was recorded in a solution of 0.04 M Na_2H_2ATP, pH 3.3, and 0.4 μg/mL SP25A, using an external Ag/AgCl/(0.1M KCl) reference electrode. In fact, it is well known that ATP anions are too bulky to permeate lipid membranes along common ion channels and require the intervention of specific transporters [40]. After repeated voltage cycling, the stabilized CV showed an $E_{1/2}$ value of –0.48 V (dashed curve in Fig. 13). Addition of 0.2 M KCl to the bathing solution caused a gradual shift of the negative peak toward less negative potentials, while the positive peak remained unaltered. After stabilization, an almost centrosymmetric CV was obtained, with the inversion center located at the midpoint potential $E_{1/2}$ of –0.42 V (solid curve in Fig. 13). It is apparent that the trumpet-shaped enlargement occurred only upon Cl^- addition, proving beyond doubt that it was determined by an inflow and outflow of these anions at the less negative potentials.

Here Figure 13

Since $E_{1/2}$ is the potential at which ion inflow matches its outflow, it might be regarded as roughly equivalent to the reversal potential measured by the Goldman, Hodgkin and Katz (GHK) equation at BLMs and biomembranes. However, tBLMs are quite different from BLMs, since they are highly asymmetric and it is not possible to change the ionic composition in their hydrophilic spacer at will. Moreover, the electric potential range accessible to Hg-supported tBLMs is rather repulsive even toward anions easily translocated by the SP25A channel, such as Cl^- ion, making its permeability P_{Cl} quite low, other that at the less negative potentials. In practice, the hydrophilic spacer of a Hg-supported tBLM is almost exclusively occupied by monovalent cations. More precisely, each voltage cycle almost half-fills the spacer at the negative peak potential, and half-empties it at the positive peak potential (cf. Fig. 7 in Ref. 15). Hence, the $E_{1/2}$ value is largely determined by the monovalent cation. Nonetheless, the ATP anion, in spite of its extremely low permeability P_{ATP}, succeeded in shifting the $E_{1/2}$ value by about 40 mV toward more negative potentials with respect to corresponding value in 0.1 M KCl at pH 3, –0.44 V, i.e., in the direction predicted by the GHK equation. On the other hand, the subsequent addition of 0.2 M KCl shifted $E_{1/2}$ by about 20 mV toward more positive potentials with respect

to the $E_{1/2}$ value in 0.1 M KCl, possibly because of the higher cation concentration in the bathing solution.

3.4. DPTL/DOPA tBLM

The effect of SP25A at a DPTL/DOPA tBLM in an unbuffered solution of 0.1 M KCl, pH 5.4, was similar to that observed at a DPTL/DOPC tBLM. The CV obtained by scanning the potential between –0.20 and –0.90 V, thus maintaining the negative potentials within the limits of physiological transmembrane values, showed only a small current increase toward the more negative potentials, even after an EIS scan (dashed curve in Fig. 14). A slightly higher current increase was observed in a buffer solution, pH 6.8 (dotted curve in Fig. 14). Only upon extending the scanned potential range to the non-physiological value of –1.20 V, we obtained a well-formed CV. Its $E_{1/2}$ value of –0.57 V practically coincides with that obtained at DPTL/DOPC and DPTL/DOPS tBLMs incorporating gramicidin at the same pH value [37]. The particularly large trumpet-shaped enlargement denotes an appreciable Cl^- movement in and out of the spacer at potentials positive of –0.35 V. This was confirmed by the two-stage charge transients obtained by stepping the applied potential from –0.30 V to progressively more negative final values E_f (data not shown), which were similar to those in Fig. 12 for a DPTL/DOPS tBLM, at the same pH value. The height of the charge transient at E_f = –0.80 V amounted to ~ –80 μC cm^{-2}, indicating that, at the initial potential of –0.30 V, the Cl^- ions were present in the spacer in an amount bearing a charge of –30 μC cm^{-2}, before flowing out of the spacer during the first stage of the potential jump.

Here Figure 14

4. Conclusions

The particular ease with which SP25A targets and penetrates Hg-supported DOPS SAMs with respect to DOPC and DOPA SAMs not only at pH 6.8, where DOPS is negatively charged just as DOPA at pH 5.4, but also at pH 3, was confirmed by measurements at DPTL/phospholipid tBLMs. In the latter case, it was also possible to show that SP25A is incorporated at physiological transmembrane potentials in Hg-supported DPTL/DOPS tBLMs, whereas incorporation in DPTL/DOPC [15] and DPTL/DOPA tBLMs occurred only at non-physiological negative transmembrane potentials. Moreover, just as for DOPS SAMs, the attack of SP25A to DPTL/DOPS tBLMs took place irrespective of whether the DOPS molecules were negatively charged, neutral or positively charged. Interestingly, the effect of SP25A on the DOPS monolayer was stronger at pH 3 than at pH 6.8, in spite of the fact that the positively charged octadepsipeptide moieties of SP25A were expected to interact: *i*) attractively with the DOPS molecules at pH 6.8, where the latter species are negatively charged; *ii*) repulsively with the DOPS molecules at pH 3, where the latter species are positively charged. Taken together, the above findings lend support to the hypothesis that SP25A targets the structural feature that distinguishes DOPS monolayers from DOPC and DOPA monolayers at all pH values, namely the arrangement of the H_3N^+-CHR-CO_2^- zwitterions coplanar to the monolayer, due to electrostatic interactions between protonated amino groups and carboxylate groups of adjacent DOPS polar heads. We may tentatively explain this behavior by a competitive interaction of the latter groups with the protonated amino groups of Dab residues within SP25A. This interaction, mainly electrostatic, but possibly enhanced by some favorable conformation, might dismantle the typical

arrangement of the DOPS monolayer with amino•carboxylate pairs bridging contiguous DOPS polar heads.

The above results, albeit significant *per se*, might assume particular relevance in the light of the selective antimicrobial activity of SP25A, which targets G+ bacteria but not Gram-negative (G–) ones [5,6]. This molecular selectivity is consistent with the struggle for existence and self-defense undertaken by all living beings. In fact, it seems logical for the G– bacterium *Pseudomonas syringae* to produce peptides harmless for G– bacteria but potentially harmful to G+ ones. Since G– and G+ bacteria have similar DOPS amounts in their biomembranes [45], other molecular features distinguishing the above-mentioned bacterial groups have to be considered to rationalize SP25A selectivity. In this respect, the main peculiar feature of G+ bacteria is represented by their outer envelope, which consists of a 20 ÷ 80 nm thick layer of peptidoglycan (PG). This layer is composed of long strands of alternating residues of *N*-acetylglucosamine (GluNAc) and *N*-acetylmuramic acids (MurNAc) (called glycan strands), with one (L-Ala^1 – D-Glu^2 – m-Dap^3 –D-Ala^4 – D-Ala^5) pentapeptide chain linked to each MurNAc residue; m-Dap stands for meso-diaminopimelic acid and the superscript denotes the amino acid position, as counted from the MurNAc residue. Previous studies on PG biosynthesis demonstrated that the corresponding precursor (lipid II) is assembled within the cytoplasm of G+ bacteria [46,47], and consists of a phosphorylated undecaprenyl-GluNAc-MurNAc molecule also bearing the pentapeptide moiety (see Fig. 15). After biosynthesis, lipid II is flipped across the cytoplasmic membrane, still maintaining its undecaprenyl chain firmly inserted into the membrane and the remaining part exposed to the periplasmic space [47]. Biosynthesis of the PG layer finally occurs via binding of contiguous MurNAc-GluNAc chains through transglycosylation (TG), with glycan strand formation, in parallel with cross-linking of the pentapeptides bound to adjacent glycan stands via transpeptidation (TP).

Here Figure 15

The whole biosynthetic process is highly dynamic and is compatible with the large PG envelope changes occurring during bacterial duplication and division phases. The final PG biosynthetic steps are carried out by monofunctional transglycosylases (containing a TG domain), monofunctional transpeptidases (containing a TP domain), and bifunctional transglycosylases / transpeptidases, which harbor both a TG and a TP domain and are referred to as class A penicillin-binding proteins (PBPs) [47]. Both TG and TP domains are located in the periplasm. Cross-linking of the peptides occurs between the D-Ala^4 residue of the donor peptide bound to one strand and the m-Dap^3 residue of the acceptor peptide bound to an adjacent strand. The energy for this reaction is gained from the cleavage of the D-Ala^4 – D-Ala^5 bond of the donor peptide [48].

In this context, we may tentatively hypothesize that a significant amount of R-CO_2^-•$^+NH_3$-R' pairs may exist in the outer envelope of G+ bacteria before the TP reaction. These pairs might form as a result of the electrostatic interaction between the protonated amino group of the m-Dap residue from one pentapeptide and the carboxylate group of the D-Glu^2 or C-terminal D-Ala^5 group from the pentapeptide of an adjacent PG strand. This situation resembles that described above for DOPS monolayers, where $^+NH_3$-CHR-CO_2^-•$^+NH_3$-CHR-CO_2^- pairs, resulting from the electrostatic interaction between the protonated amino and carboxylate groups of adjacent phospholipid polar heads, were shown to be the preferential molecular target of the cationic SP25A, highly modulating the lipodepsipeptide affinity toward DOPS monolayers. Thus, the postulated existence of R-CO_2^-•$^+NH_3$-R' peptidoglycan pairs reported above should promote the attractive interaction of SP25A toward the outer envelope of G+ bacteria. SP25A binding to non-

mature PG might possibly be reinforced by the dual electrostatic interaction of its contiguous protonated Dab residues toward the carboxylate groups of two of the three D-Ala^5, m-Dap^3 and D-Glu^2 residues pertaining to the same pentapeptide moiety in a PG strand, as schematically depicted in Fig. 15. This interaction, followed by peptide insertion and pore formation into the corresponding membrane according to the mechanism reported before [11-14], might possibly justify the reported antimicrobial selectivity of this lipodepsipeptide.

Differently from G+ bacteria, the outer envelope of G– bacteria consists of a lipid bilayer containing integral proteins and lipopolysaccharides, whose inner core is negatively charged as a result of the presence of several phosphate groups. Although the shell of these bacteria also includes a thin layer of PG, this is not exposed to the extracellular fluid, from which it is separated by the outer membrane and a first periplasmic space.

The outer envelope of G+ bacteria is also negatively charged as a result of the presence of teichoic acids, which are polysaccharides having some of their negative phosphate groups covalently linked to the terminal D-Ala residues of the peptidoglycan network. In this context, Bensaci and Takemoto [6] demonstrated that SP25A is more effective in inhibiting the growth of G+ *Bacillus subtilis* mutant strains deleted in the genes encoding the enzymes that facilitate the transport of activated D-Ala to the lipoteichoic acid, than the wild-type strain. No such an effect was observed for SP22A. The lack of D-alanylation of the wall-linked teichoic acid during the growth of the mutant strains increases the number of negative phosphate groups of teichoic acid. Thus, it was suggested that the inhibitory effect of SP25A is promoted by the interaction between the positive charge of its Dab residues and the negative phosphate groups of bacterial teichoic acids. However, the cationic properties of SP25A do not seem sufficient *per se* to selectively inhibit the growth of G+ bacteria, as also admitted by Bensaci and Takemoto [6]. In fact, among other things, similar attractive electrostatic interactions would also be operative toward G– bacteria, whose outer covering presents a significant negative net charge due to lipopolysaccharides, as mentioned above.

By demonstrating the greatest preference of SP25A for interacting with DOPS monolayers than with DOPC or DOPA ones, our electrochemical measurements at Hg-supported lipid mono- and bilayers may provide a novel clue toward understanding the antimicrobial activity of this lipodepsipeptide against G+ bacteria. From a more general point of view, the above results demonstrate the potential of Hg-supported DPTL/phospholipid tBLMs in monitoring the ion flow along ion channels incorporated in the lipid bilayer moiety by exploiting the well-defined spaciousness of the hydrophilic spacer, through the use of potential-step chronocoulometry and cyclic voltammetry.

Acknowledgments

This study was partially supported by grants from the Italian Ministry of Economy and Finance for the project "Innovazione e Sviluppo del Mezzogiorno - Conoscenze Integrate per Sostenibilità ed Innovazione del *Made in Italy* Agroalimentare - Legge n. 191/2009" and from Regione Campania for the project "Nuovi Processi e Prodotti per la Nutraceutica, la Cosmeceutica e la Nutrizione umana" (BenTeN) - P.O.R. Campania Region (Italy) 2007/2013, objectives 2.1". Thanks are due to Prof. Adrian Schwan (University of Guelph, Guelph, Ontario, Canada) for providing us with the DPTL thiolipid.

References

1 - A. Ballio, D. Barra, F. Bossa, A. Collina, I. Grgurina, G. Marino, G. Moneti, M. Paci, P. Pucci, A. Segre, M. Simmaco, Syringopeptins, new phytotoxic lipodepsipeptides of *Pseudomonas syringae* pv. *syringae*, FEBS Lett. 291 (1991) 109-112.

2 - A. Isogai, H. Iguchi, J. Nakayama, A. Kusai, J.Y. Takemoto, A. Suzuki, Structural analysis of new syringopeptins by tandem mass spectroscopy, Biosci. Biotechnol. Biochem. 59 (1995) 1374-1376.

3 - A. Ballio, F. Bossa, D. Di Giorgio, A. Di Nola, C. Manetti, M. Paci, A. Scaloni, A.L. Segre, Solution conformation of the *Pseudomonas syringae* pv. *syringae* phytotoxic lipodepsipeptide syringopeptin 25-A. Two-dimensional NMR, distance geometry and molecular dynamics, Eur. J. Biochem. 234 (1995) 747-758.

4 - E. Mátyus, K. Blaskó, J. Fidy, D.P. Tieleman, Structure and dynamics of the antifungal molecules syringotoxin-B and syringopeptin-25A from molecular dynamics simulation, Eur. Biophys. J. 37 (2008) 495-502.

5 - I. Grgurina, M. Bensaci, G. Pocsfalvi, L. Mannina, O. Cruciani, A. Fiore, V. Fogliano, K. N. Sorensen, J. Y. Takemoto, Novel cyclic lipodepsipeptide from *Pseudomonas syringae* pv. lachrymans strain 508 and syringopeptin antimicrobial activities, Antimicrob. Agents Chemother. 49 (2005) 5037-5045.

6 -M. F. Bensaci, J. Y. Takemoto, Syringopeptin SP25A-mediated killing of gram-positive bacteria and the role of the teichoic acid D-alanylation, FEMS Microbiol. Lett. 268 (2007) 106-111.

7 - D. Di Giorgio, L. Camoni, A. Ballio, Toxins of *Pseudomonas syringae* pv. *syringae* affect H^+-transport across the plasma membrane of maize, Physiol. Plant. 91 (1994) 741-746.

8 - N.S. Iacobellis, P. Lavermicocca, I.Grgurina, M. Simmaco, A. Ballio, Phytotoxic properties of *Pseudomonas syringae* pv. *syringae* toxins, Physiol. Mol. Plant Pathol. 40 (1992) 107-116.

9 - M.L. Hutchison, D.C. Gross, Lipopeptide phytotoxins produced by *Pseudomonas syringae* pv. *syringae:* Comparison of the biosurfactant and ion channel-forming activities of syringopeptin and syringomycin, Mol. Plant-Microbe Inter., 10 (1997) 347-354.

10 - A. Carpaneto, M. Dalla Serra, G. Menestrina, V. Fogliano, F. Gambale, The phytotoxin lipodepsipeptide syringopeptin 25A from *Pseudomonas syringae* pv. *syringae* forms ion channels in sugar beet vacuoles, J. Membrane Biol. 188 (2002) 237-248.

11 - M.F. Bensaci, P.H. Gurnev, S.M. Bezrukov, J.Y. Takemoto, Fungal activities and mechanisms of action of *Pseudomonas syringae* pv. *syringae* lipodepsipeptide syringopeptins 22A and 25A, Front. Microbiol. 2 (2011) Article 216, 1-6.

12 - M. Dalla Serra, G. Fagiuoli, P. Nordera, I. Bernhart, C. Della Volpe, D. Di Giorgio, A. Ballio, G. Menestrina, The interaction of lipodepsipeptide toxins from *Pseudomonas syringae* pv. *syringae* with biological and model membranes: A comparison of syringotoxins, syringomycin and two syringopeptins, Mol. Plant-Microbe Inter., 12 (1999) 391-400.

13 - M. Dalla Serra, I. Bernhart, P. Nordera, D. Di Giorgio, A. Ballio, G. Menestrina, Conductive properties and gating channels formed by syringopeptin 25A, a bioactive lipodepsipeptide from *Pseudomonas syringae* pv. *syringae*, in planar lipid membranes, Mol. Plant-Microbe Inter., 12 (1999) 401-409.

14 - G. Agner, Y.A. Kaulin, P.A. Gurnev, Z. Szabo, L.V. Schagina, J.Y. Takemoto, K. Blasko, Membrane-permeabilizing activities of cyclic lipodepsipeptides, syringopeptin 22A and syringomycin E from *Pseudomonas syringae* pv. *syringae* in human red blood cells and in bilayer lipid membranes, Bioelectrochemistry, 52 (2000) 161-167.

15 - L. Becucci, M. Rossi, A. Fiore, A. Scaloni, R. Guidelli, Channel-forming activity of syringopeptin 25A in mercury-supported lipid bilayers with a phosphatidylcholine distal leaflet, Bioelectrochemistry 108 (2016) 28-35.
16 - S.M. Schiller, R. Naumann, K. Lovejoy, H. Kunz, W. Knoll, Archaea analogue thiolipids for tethered bilayer lipid membranes on ultrasmooth gold surfaces, Angew. Chem. Int. Ed. Engl. 42 (2003) 208-211.
17 - L. Becucci, R. Romero Léon, M.R. Moncelli, P. Rovero, R. Guidelli, Electrochemical investigation of melittin reconstituted into a mercury-supported lipid bilayer, Langmuir 22 (2006) 6644-6650.
18 - L. Becucci, A. Santucci, R. Guidelli, Gramicidin conducting dimers in lipid bilayers are stabilized by single-file ionic flux along them, J. Phys. Chem. B 111 (2007) 9814-9820.
19 - L. Becucci, R. Guidelli, Kinetics of channel formation in bilayer lipid membranes (BLMs) and tethered BLMs: monazomycin and melittin, Langmuir 23 (2007) 5601-5608.
20 - L. Becucci, M. Papini, D. Muller, A. Scaloni, G. Veglia, R. Guidelli, Probing membrane permeabilization by the antimicrobial peptide distinctin in mercury-supported biomimetic membranes, Biochim. Biophys. Acta 1808 (2011) 2745-2752.
21 - L. Becucci, F. Maran, R. Guidelli, Probing membrane permeabilization by the antibiotic lipopeptaibol trichogin GA IV in a tethered bilayer lipid membrane, Biochim. Biophys. Acta 1818 (2012) 1656-1662.
22 - L. Becucci, M. Innocenti, S. Bellandi, R. Guidelli, Permeabilization of mercury-supported biomimetic membranes by amphotericin B and the role of calcium ions, Electrochim. Acta 112 (2013) 719-726.
23 - L. Becucci, D. Valensin, M. Innocenti, R. Guidelli, Dermcidin, an anionic antibiotic peptide: influence of lipid charge, pH and Zn^{2+} on its interaction with a biomimetic membrane, Soft Matter 10 (2014) 616-626.
24 - L. Becucci, R. Guidelli, Mercury-supported biomimetic membranes for the investigation of antimicrobial peptides, Pharmaceuticals 7 (2014) 136-168.
25 - L. Becucci, V. Tramonti, A. Fiore, V. Fogliano, A. Scaloni, R. Guidelli, Channel-forming activity of syringomycin E in two mercury-supported biomimetic membranes, Biochim. Biophys. Acta 1848 (2015) 932-941.
26 - M.R. Moncelli, L. Becucci, A novel model of the hanging mercury drop electrode, J. Electroanal. Chem. 433 (1997) 91-96.
27 - D. Bizzotto, A. Nelson, Continuing electrochemical studies of phospholipid monolayers of dioleoyl phosphatidylcholine at the mercury-electrolyte interface, Langmuir 14 (1998) 6269-6273.
28 - A. Nelson, N. Auffret, J. Borlakoglu, Interaction of hydrophobic organic compounds with mercury adsorbed dioleoylphosphatidylcholine monolayers, Biochim. Biophys. Acta 1021 (1990) 205-216.
29 - M.-F. Lecompte, A.-C. Bras, N. Dousset, I. Portas, R. Salvayre, M. Ayrault-Jarrier, Binding steps of apolipoprotein A-I with phospholipid monolayers: Adsorption and penetration, Biochemistry 37 (1998) 16165-16171.
30 - R. Stoodley, J. Shepherd, K. M. Wasan, D. Bizzotto, Amphotericin B interactions with a DOPC monolayer. Electrochemical investigations, Biochim. Biophys. Acta 1564 (2002) 289-297.
31 - A. Nelson, F.A. M. Leermakers, Substrate-induced structural changes in electrode-adsorbed lipid layers. Experimental evidence for the behaviour of phospholipid layers on the mercury-water interface, J. Electroanal. Chem. 278 (1990) 73-83.

32 - M.R. Moncelli, L. Becucci, R. Guidelli, The intrinsic pK_a values for phosphatidylcholine, phosphatidylethanolamine, and phosphatidylserine in monolayers deposited on mercury electrodes, Biophys. J. 66 (1994) 1969-1980.
33 - P. W. M. Van Dijck, B. De Kruijff, A. J. Verkleij, L. L. M. Van Deenen, J. De Gier, Comparative study on the effects of pH and Ca^{2+} on bilayers of various negatively charged phospholipids and their mixtures with phosphatidylcholine, Biochim. Biophys Acta 512 (1978) 84-96.
34 - M. R. Moncelli, L. Becucci, The intrinsic pK_a values for phosphatidic acid in monolayers deposited on mercury electrodes, J. Electroanal. Chem. 385 (1995) 183-189.
35 - W. Furness, Changes in potential of the dropping mercury electrode during drop formation and measurement of potential in polarographic analysis, Analyst 77 (1952) 345–355.
36 – R. Guidelli, A comparison between some recent theories on the effect of ionic specific adsorption upon electrode kinetics, J. Electoanal. Chem. 53 (1974) 205-218.
37 - L. Becucci, R. Guidelli, Can gramicidin ion channel affect the dipole potential of neighboring phospholipid headgroups?, Bioelectrochemistry, 106 (2015) 343-352.
38 - R. Guidelli and L. Becucci, Estimate of the potential difference across metal/water interfaces and across the lipid bilayer moiety of biomimetic membranes: an approach, Soft Matter, 7 (2011) 2195-2201.
39 - R. Guidelli, L. Becucci, Electrochemistry of biomimetic membranes, in: N. Eliaz, (Ed.), Applications of Electrochemistry and Nanotechnology in Biology and Medicine, Vol 53 of the Series: Modern Aspects of Electrochemistry, Springer, New York, 2011, pp.147-265.
40 - L. Becucci, R. Guidelli, C.B. Karim, D.D. Thomas, G. Veglia: An electrochemical investigation of sarcolipin reconstituted into a mercury-supported lipid bilayer. Biophys. J. 93 (2007) 2678-2687.
41 - L. Becucci, M. Papini, R. Verardi, G. Veglia, R. Guidelli, Phospholamban and its phosphorylated form require non-physiological transmembrane potentials to translocate ions Soft Matter 8 (2012) 3881-3888.
42- A.M. Feigin, J.Y. Takemoto, R. Wangspa, J.H. Teeter, J.G. Brand, Properties of voltage-gated ion channels formed by syringomycin E in planar lipid bilayers, J. Membr. Biol. 149 (1996) 41- 47.
43 – Y. A. Kaulin, L. Schagina, S. M. Bezrukov, V. V. Malev, A. M. Feigin, J. Y. Takemoto, J. H. Teeter, J. G. Brand, Cluster organization of ion channels formed by the antibiotic syringomycin E in bilayer lipid membranes, Biophys. J. 74 (1998) 2918-2925.
44 - V.V. Malev, L.V. Schagina, P.A. Gurnev, J.Y. Takemoto, E.M. Nestorovich, S.M. Bezrukov, Syringomycin E channel: A lipidic pore stabilized by lipopetide?, Biophys. J. 82 (2002) 1985-1994.
45 - R. M. Epand, R. F. Epand, Functional consequences of the lateral organization of biological membranes, in: P. L. Yeagle (Ed.), The Structure of Biological Membranes, 3rd Edition, CRC Press, Boca Raton, pp. 133-152.
46 - W. A. van der Donk, Lighting up the nascent cell wall, ACS Chem. Biol. 1 (2006) 425-428.
47 – W. Vollmer, U. Bertsche, Biochim. Biophys. Acta, Murein (peptidoglycan) structure, architecture and biosynthesis in *Escherichia coli*, 1778 (2008) 1714-1734.
48 – M. Terrak, T. K. Ghosh, J. van Heijenoort, J. Van Beeumen, M. Lampilas, J. Aszodi, J. A. Ayala, J. M. Ghuysen, M. Nguyen-Disteche, The catalytic, glycosyl transferase and acyl transferase modules of the cell wall peptidoglycan-polymerizing penicillin-binding protein 1b of *Escherichia coli*, Mol. Microbiol. 34 (1999) 350-364.

Legends for figures

Fig. 1 - AC voltammograms at a DOPC SAM in an unbuffered solution of 0.1 M KCl, pH 5.4, in the absence of SP25A (solid curve), immediately after the addition of 0.2 μg/mL SP25A (dashed curve) and after a complete EIS scan from –0.30 to –0.80 V (dash-dotted curve). Frequency = 75 Hz.

Fig. 2 - AC voltammograms at a DOPS SAM in a buffer solution of 0.1 M KCl, pH 6.8, in the absence of SP25A (solid curve), immediately after the addition of 0.2 μg/mL SP25A (dashed curve) and after a complete EIS scan from –0.30 to –0.80 V (dash-dotted curve). Frequency = 75 Hz.

Fig. 3 - AC voltammograms at a DOPS SAM in a solution of 0.1 M KCl, pH 3, in the absence of SP25A (solid curve), immediately after the addition of 0.2 μg/mL SP25A (dashed curve) and after a complete EIS scan from –0.30 V to –0.80 V (dash-dotted curve). The grey curve corresponds to an AC voltammogram recorded after forming a DOPS SAM in a solution of 0.1 M KCl, pH 3, containing 0.2 μg/mL SP25A. Frequency = 75 Hz.

Fig. 4 - Stabilized AC voltammograms at a DOPA SAM in an unbuffered solution of 0.1 M KCl, pH 5.4, in the absence (solid curve) and in the presence of 0.2 μg/mL SP25A (dashed curve). Frequency = 75 Hz.

Fig. 5 - CVs due to Cd^{2+} reduction and Cd(Hg) oxidation at a DOPS SAM in an aqueous solution of 0.1 M KCl, 4×10^{-5} M $CdSO_4$ and 0.2 μg/mL SP25A, at pH 6.8 (dash-dotted curve), 5.4 (dashed curve) and 3 (solid curve). Scan rate = 50 mV/s. The gray curve represents the CV of an aqueous solution of 0.1 M KCl and 4×10^{-5} M $CdSO_4$ on bare mercury.

Fig. 6 - Plot of $\omega Z'$ against $-\omega Z''$ at –0.50 V at a freshly prepared DPTL/DOPS tBLM in a buffer solution of 0.1 M KCl, pH 6.8, in the absence of SP25A (solid circles) and in the presence of 0.4 μg/mL SP25A during the first frequency scan (solid triangles) and during the second and subsequent ones (open squares). The impedance spectrum at –0.5 V was obtained starting from a bias potential of –0.30 V and shifting it gradually by –50 mV increments up to the attainment of –0.50 V.

Fig. 7 - Plots of capacitance C (circles) and conductance G (squares) against the applied potential for the RC mesh ascribed to the polar head region, at a DPTL/DOPS tBLM in a buffer solution of 0.1 M KCl, pH 6.8, in the absence (solid symbols) and in the presence of 0.4 μg/mL SP25A (open symbols). The impedance spectra were recorded proceeding toward progressively more negative bias potentials, starting from a value of –0.30 V.

Fig. 8 - Charge transients at a DPTL/DOPS tBLM in a buffer solution of 0.1 M KCl, pH 6.8, and 0.4 μg/mL SP25A, obtained by jumping from E_i = –0.30 V to final potential values varying from –0.50 to –0.80 V by –50 mV increments.

Fig. 9 - CV at a DPTL/DOPS tBLM in a buffer solution of 0.1 M KCl, pH 6.8, and 1 μg/mL SP25A, recorded between –0.20 and –0.90 V (solid curve), and between –0.20 and –1.20 V (dashed curve). The gray curve corresponds to the CV in the absence of SP25A. Scan rate = 50 mV/s.

Fig. 10 - CV at a DPTL/DOPS tBLM in a buffer solution of 0.1 M KCl, pH 6.8, and 1 μg/mL SP25A, before (dash-dotted curve) and after addition of 1×10^{-4} M $TlNO_3$ (dashed curve). The gray curve corresponds to the CV at bare mercury in 0.1 M KCl and 1×10^{-4} M $TlNO_3$. Scan rate = 50 mV/s.

Fig. 11 - CVs at a DPTL/DOPS tBLM in unbuffered solutions of 0.1 M KCl and 0.4 μg/mL SP25A at pH pH 5.4 (solid curve) and pH 3 (grey curve). The dashed curve corresponds to the CV at pH 3 after addition of 1×10^{-4} M $TlNO_3$. Scan rate = 50 mV/s.

Fig. 12 - Charge transients at a DPTL/DOPS tBLM in an unbuffered solution of 0.1 M KCl and 0.4 μg/mL SP25A, pH 5.4, obtained by jumping from E_i = –0.30 V to final potentials varying from –0.55 to –0.80 V by –50 mV increments.

Fig. 13 - CV at a DPTL/DOPS tBLM in a solution of 0.04 M Na_2H_2ATP and 0.4 μg/mL SP25A, pH 3.3, before (dashed curve) and after the addition of 0.2 M KCl (solid curve). The grey curve corresponds to the CV in the absence of SP25A.

Fig. 14 - CVs at a DPTL/DOPA tBLM in 0.1 M KCl and 0.4 μg/mL SP25A, recorded between –0.20 and –0.90 V at pH 5.4 (dashed curve) and pH 6.8 (dotted curve), and recorded between –0.20 and –1.20 V at pH 5.4 (solid curve).

Fig. 15 - Peptidoglycan synthesis catalyzed by a Class A PBP and tentative intervention of SP25A octadepsipeptide before the start of this synthesis. The functional groups of some residues, which are possibly relevant to such an intervention, have been evidenced. The glycan strand is elongated by transglycosylation (TG) with lipid II and forms cross-links by transpeptidation (TP), via release of D-Ala^5. Gray bars, MurNAc linked to pentapeptides represented either in detail or as arrows, for simplicity; white bars, GlcNAc; zigzag line, undecaprenyl residue; black circles, phosphate groups; gray octahedron, SP25A octadepsipeptide.

Figure 1

Click here to download high resolution image

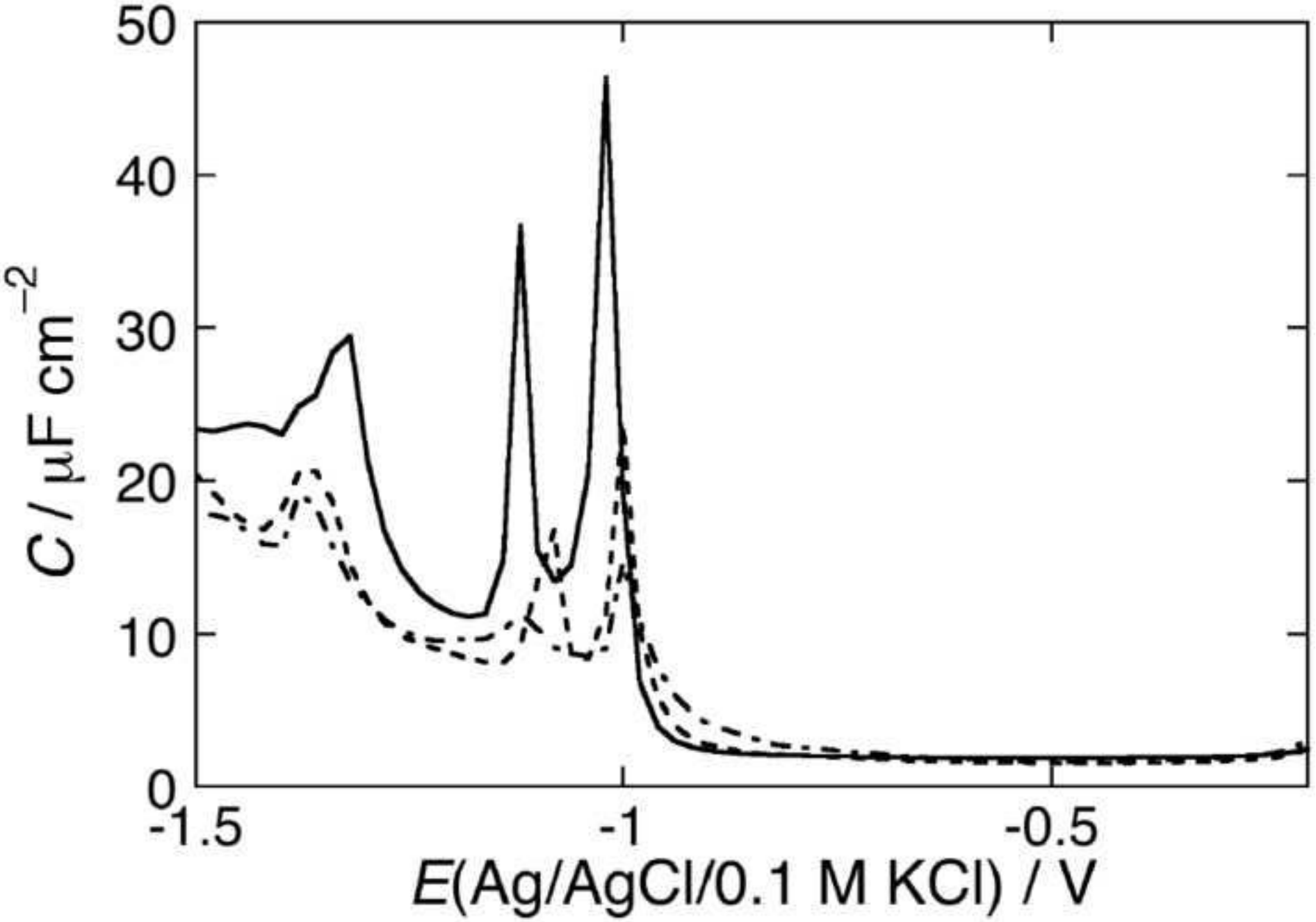

Figure 2

Click here to download high resolution image

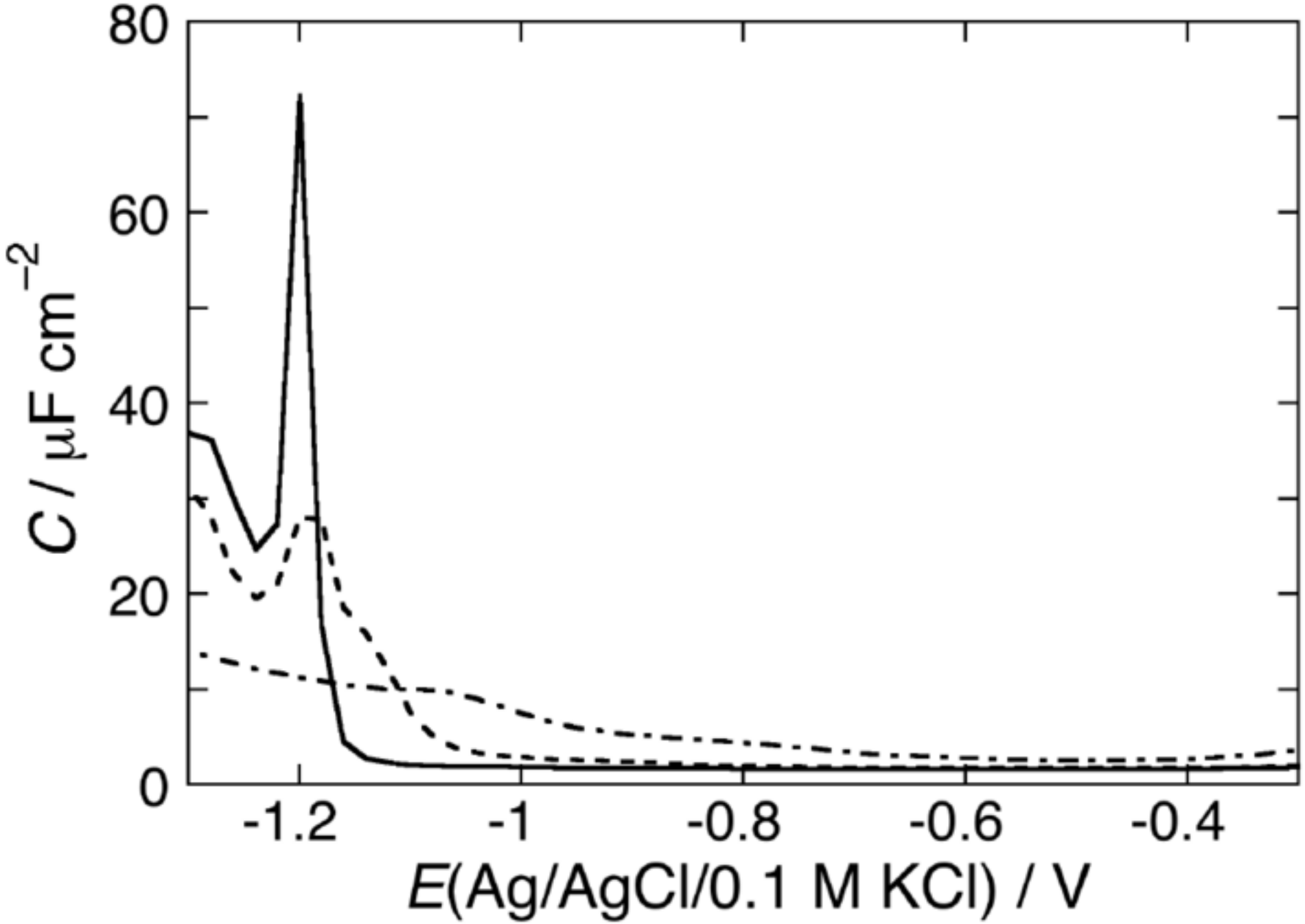

Figure 3

Click here to download high resolution image

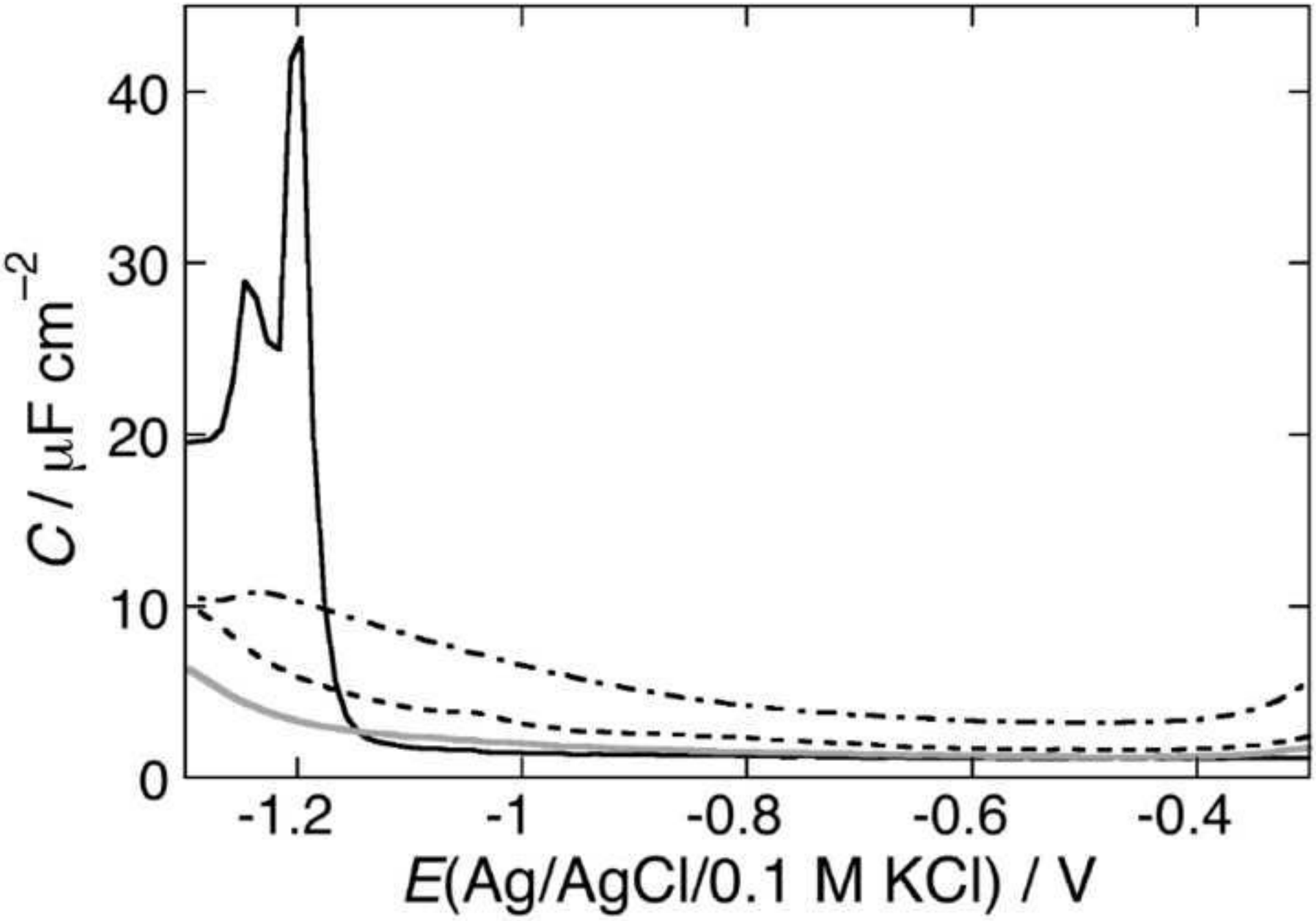

Figure 4
Click here to download high resolution image

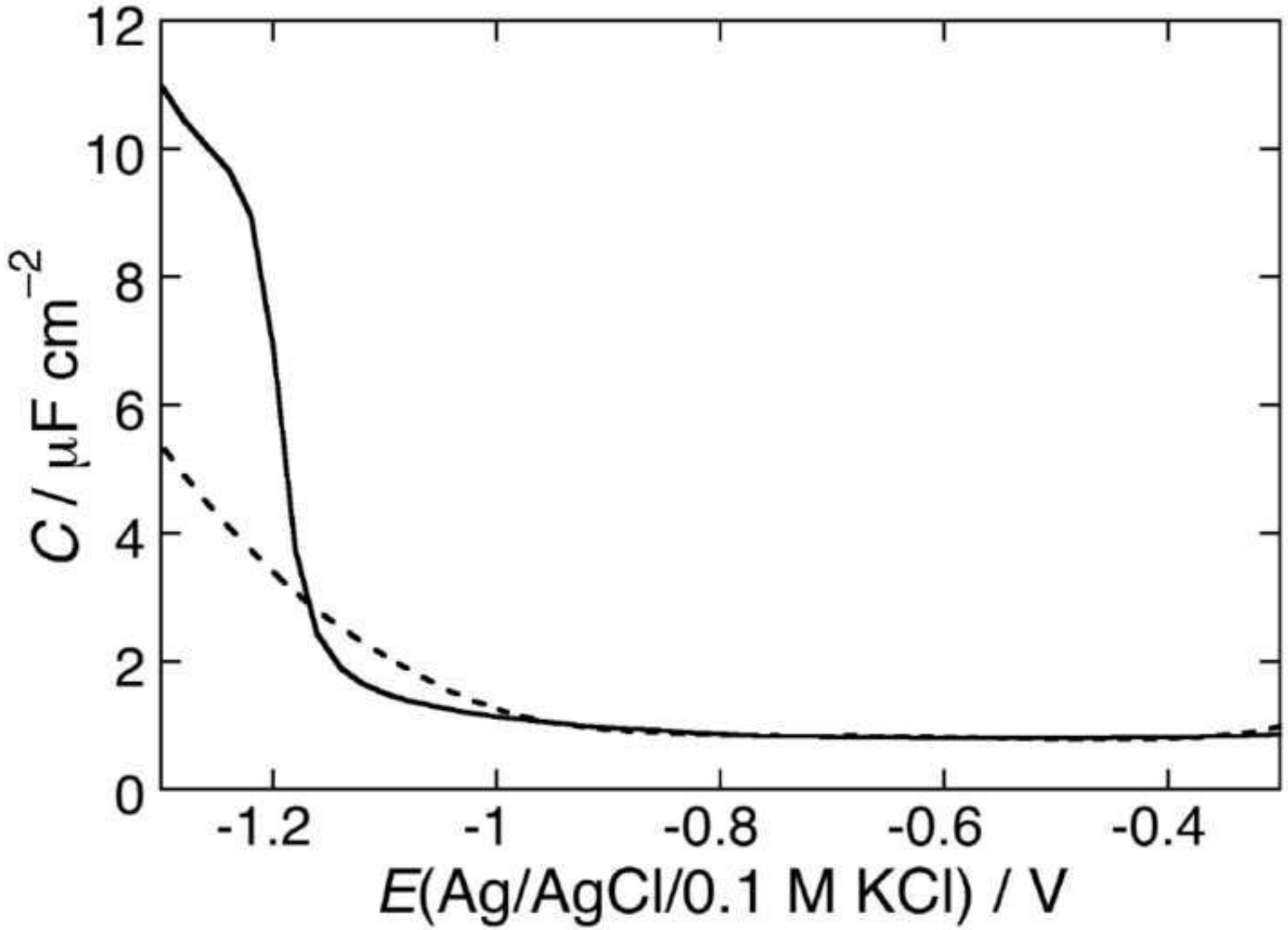

Figure 5
Click here to download high resolution image

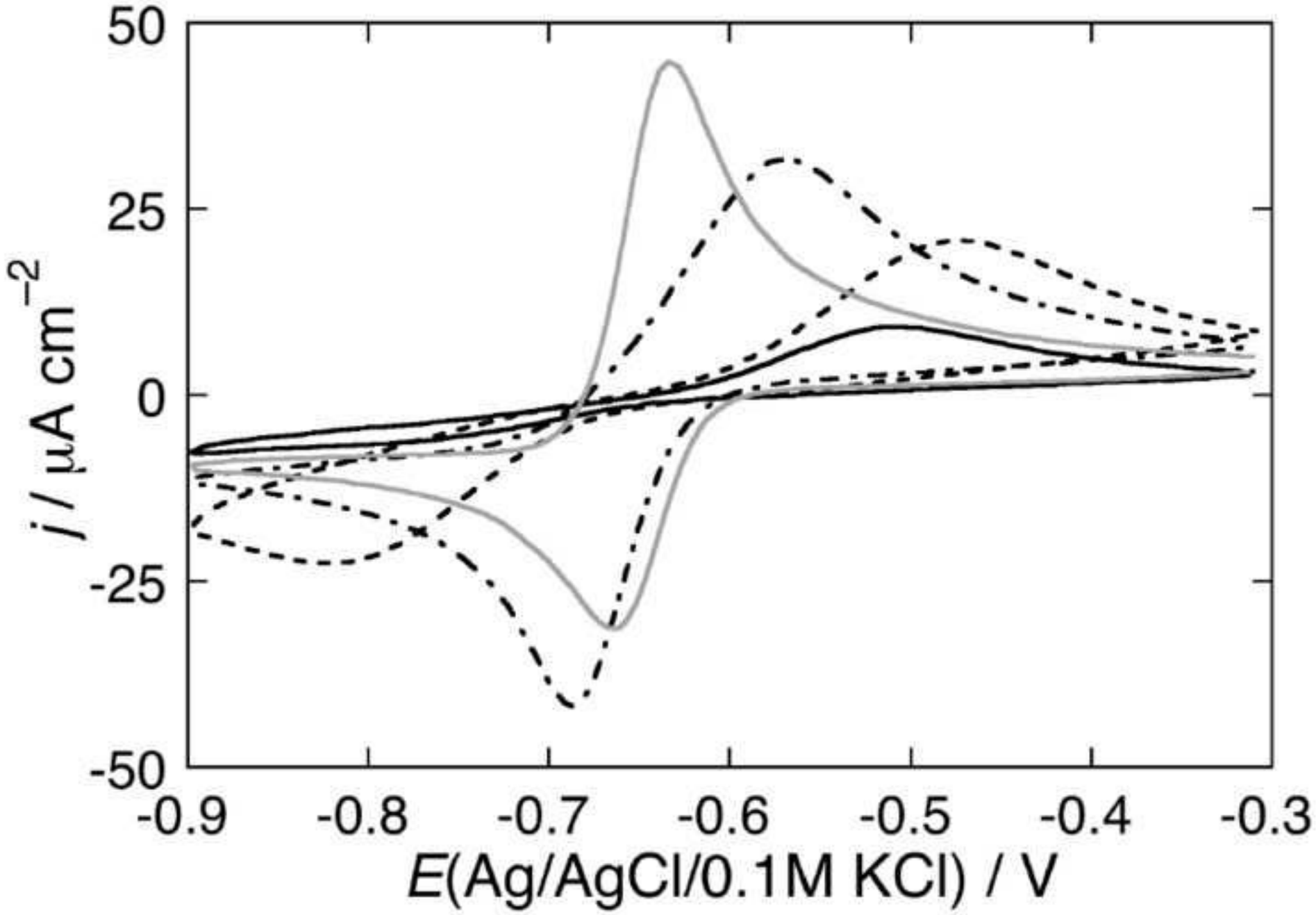

Figure 6
Click here to download high resolution image

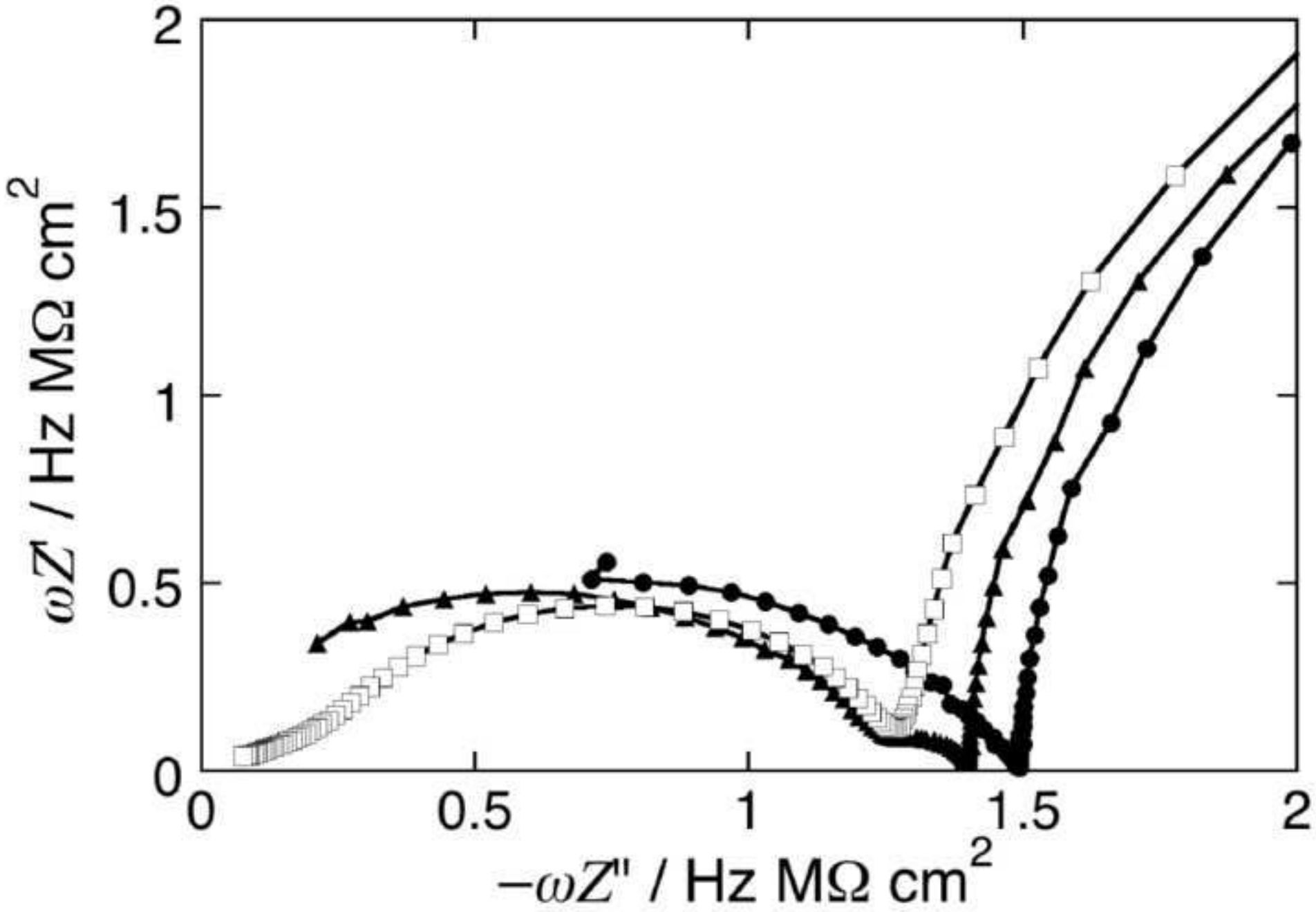

Figure 7

Click here to download high resolution image

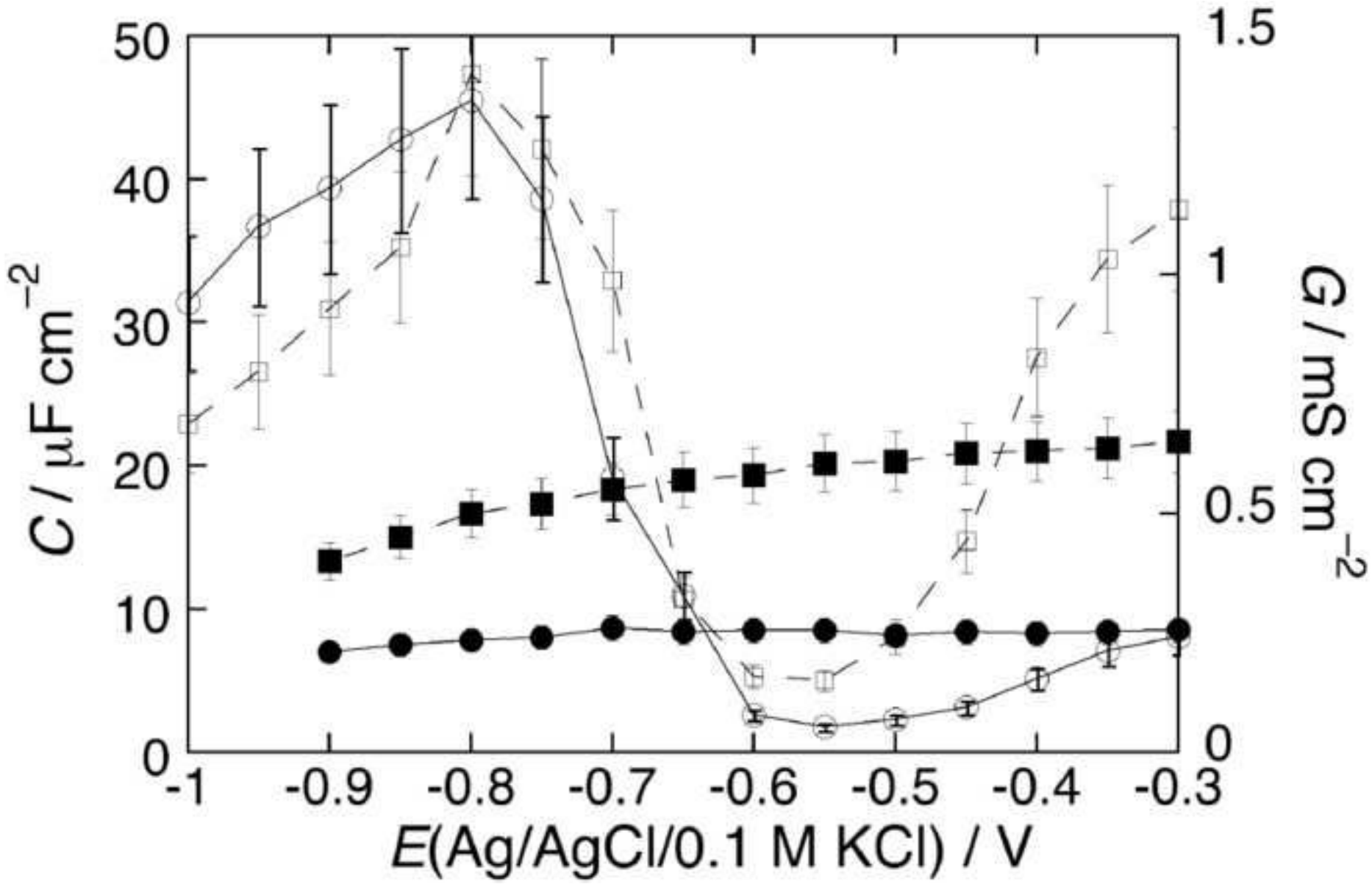

Figure 8
Click here to download high resolution image

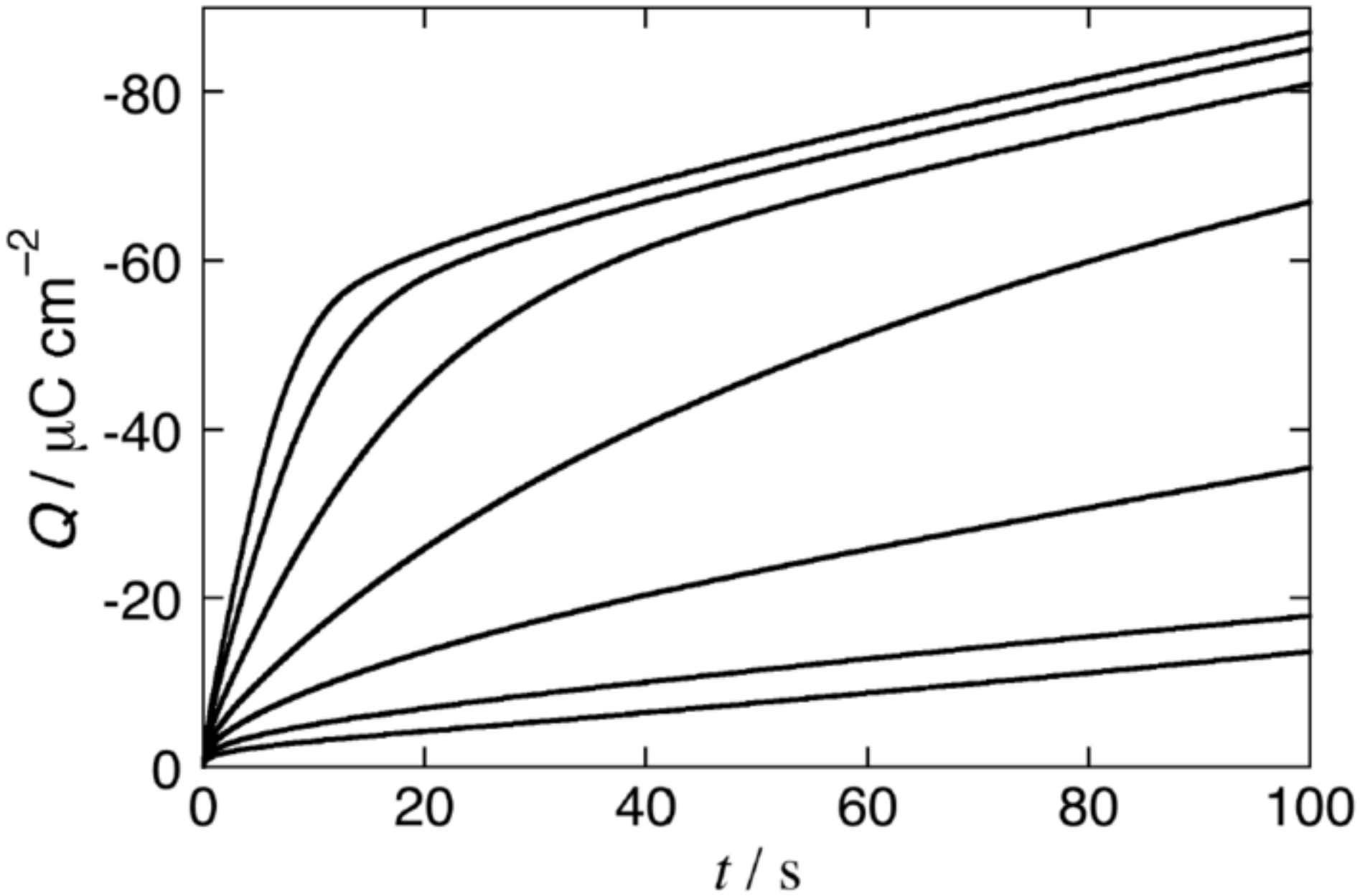

Figure 9
Click here to download high resolution image

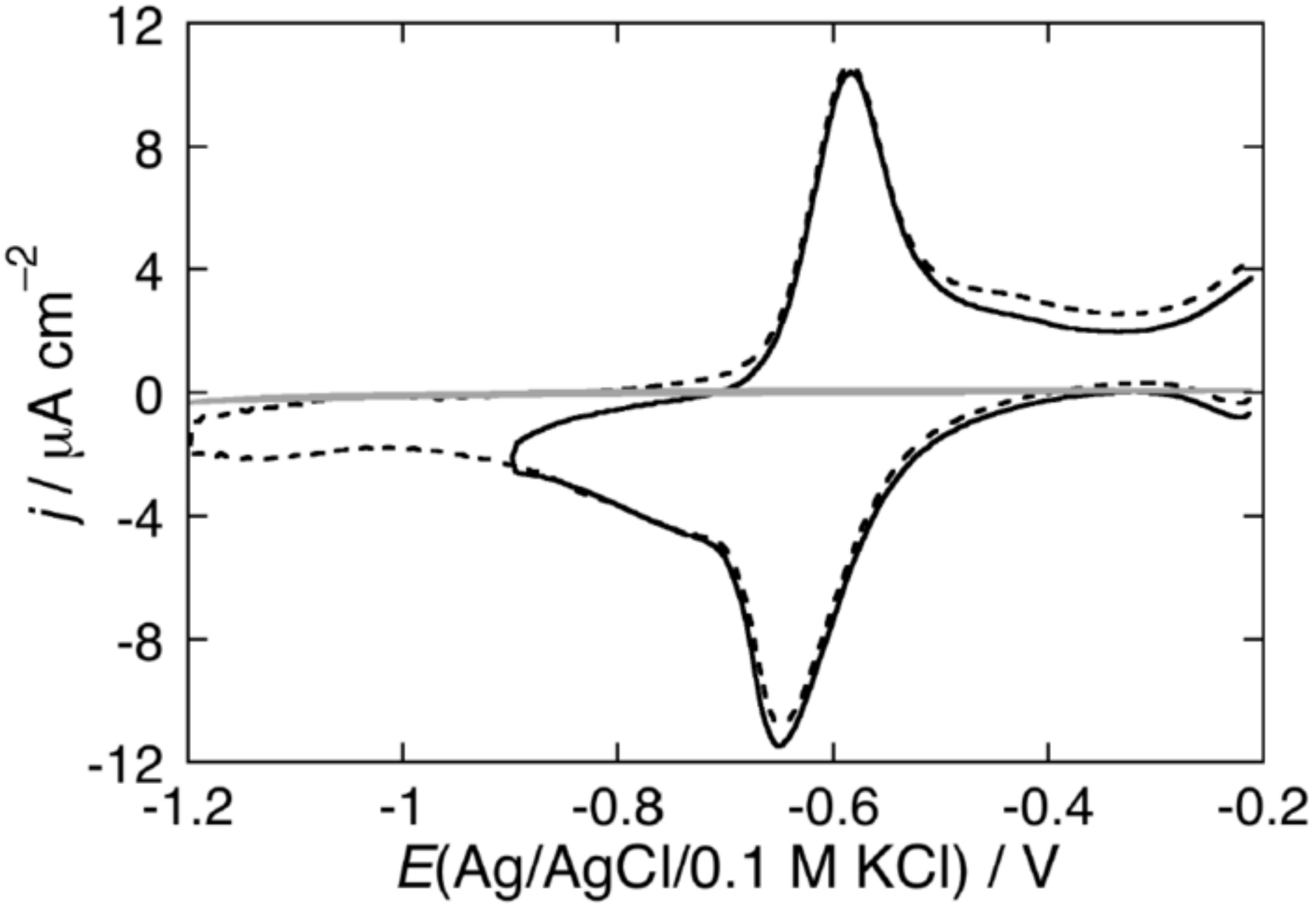

Figure 10
Click here to download high resolution image

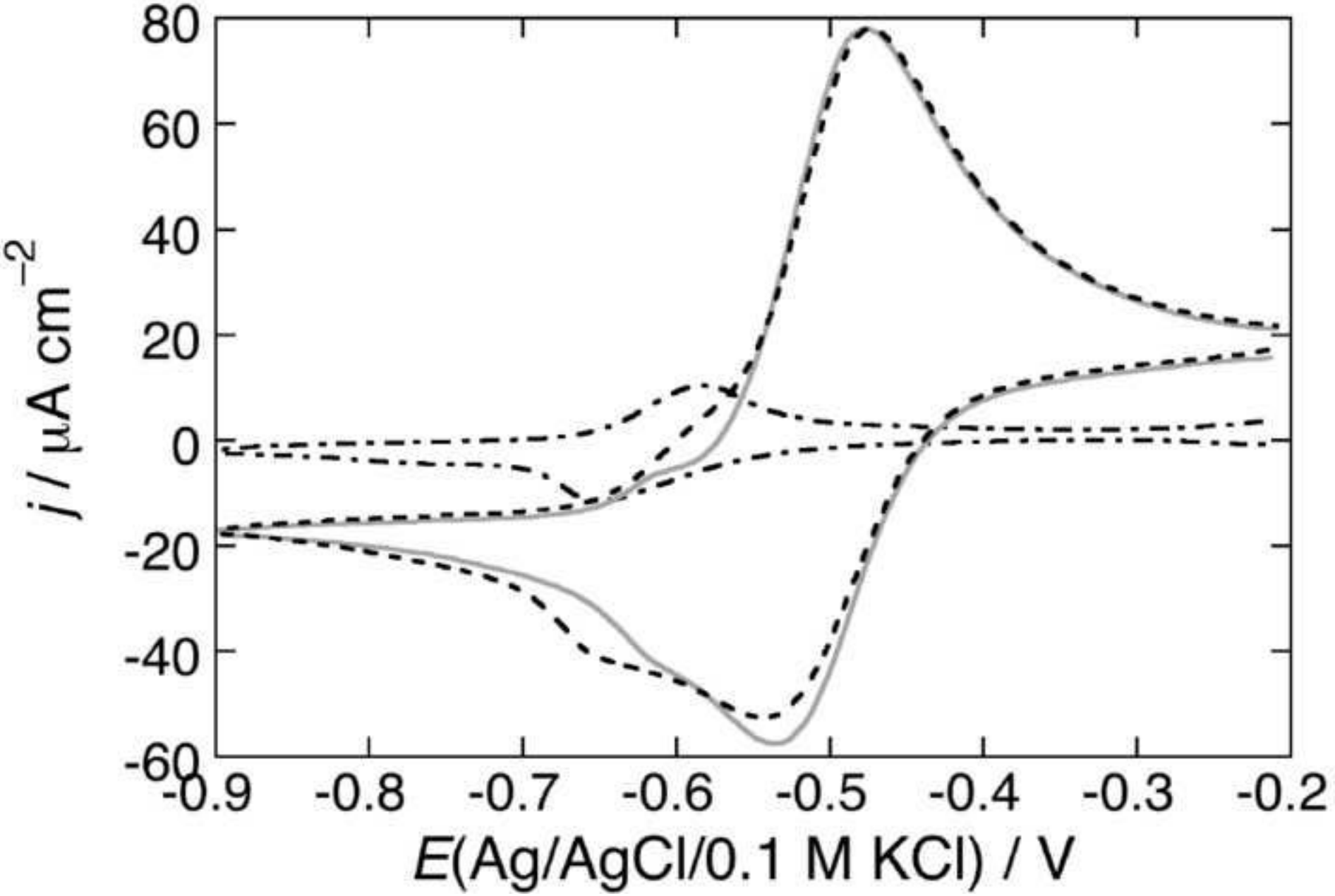

Figure 11
Click here to download high resolution image

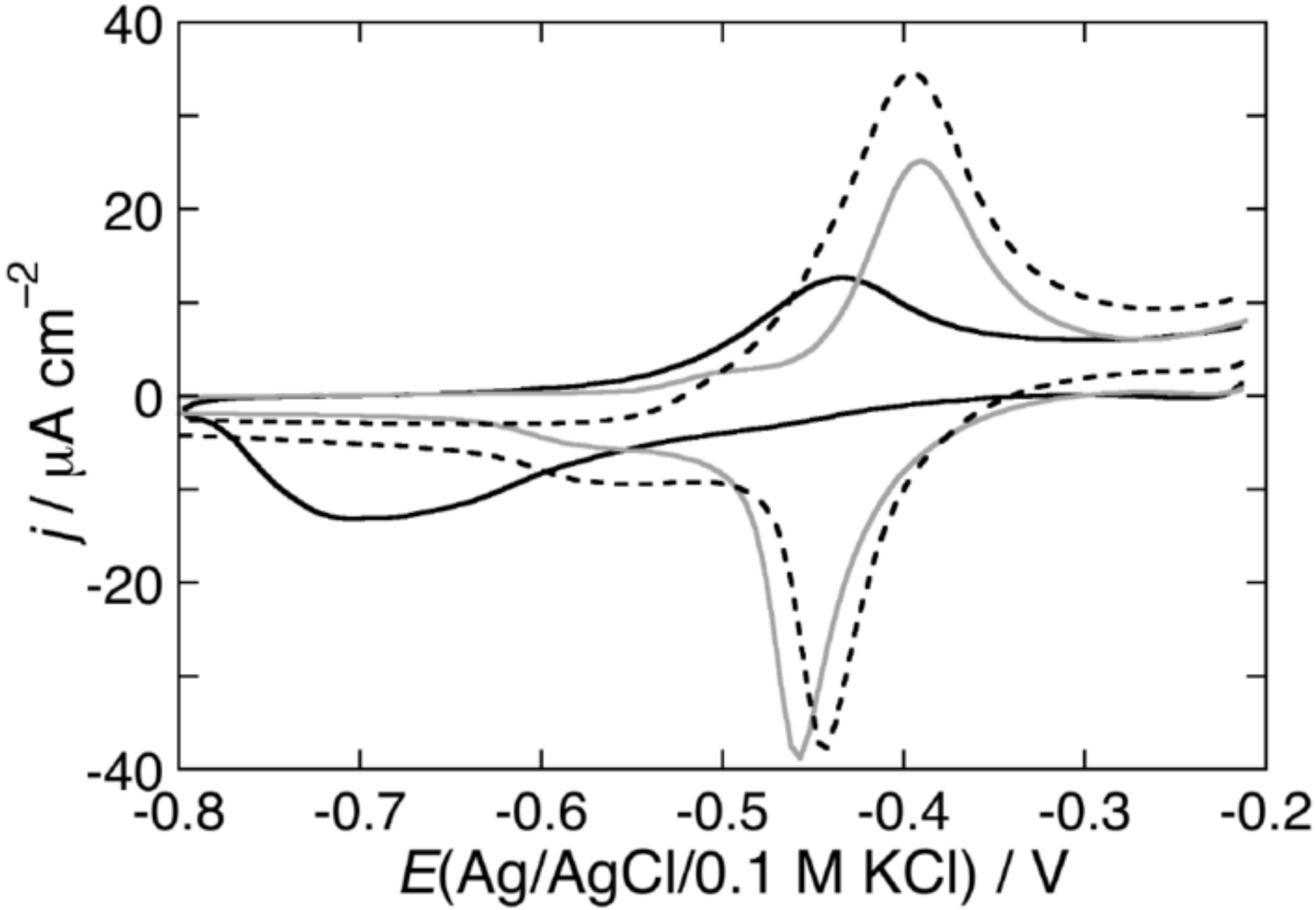

Figure 12
Click here to download high resolution image

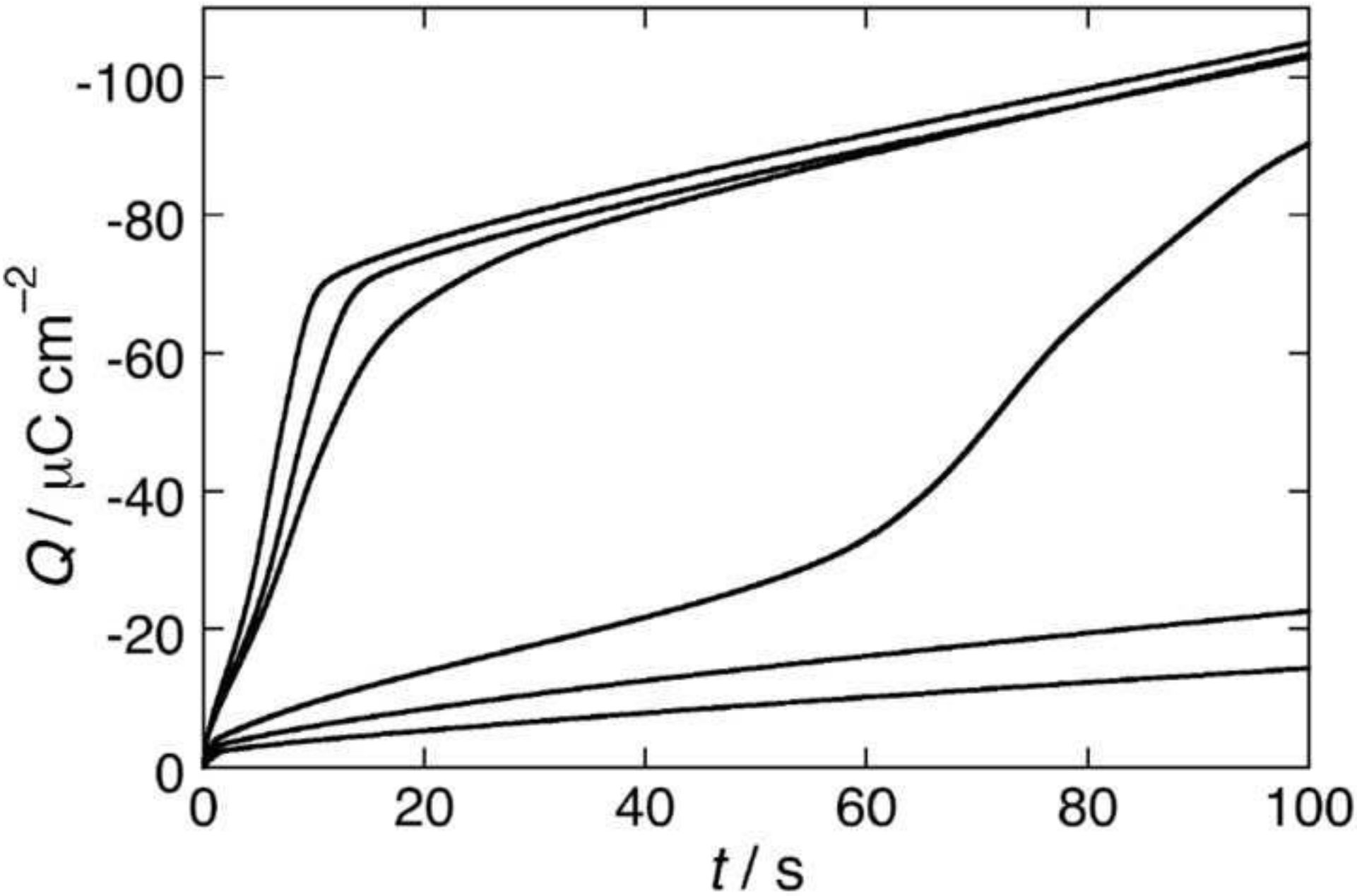

Figure 13

Click here to download high resolution image

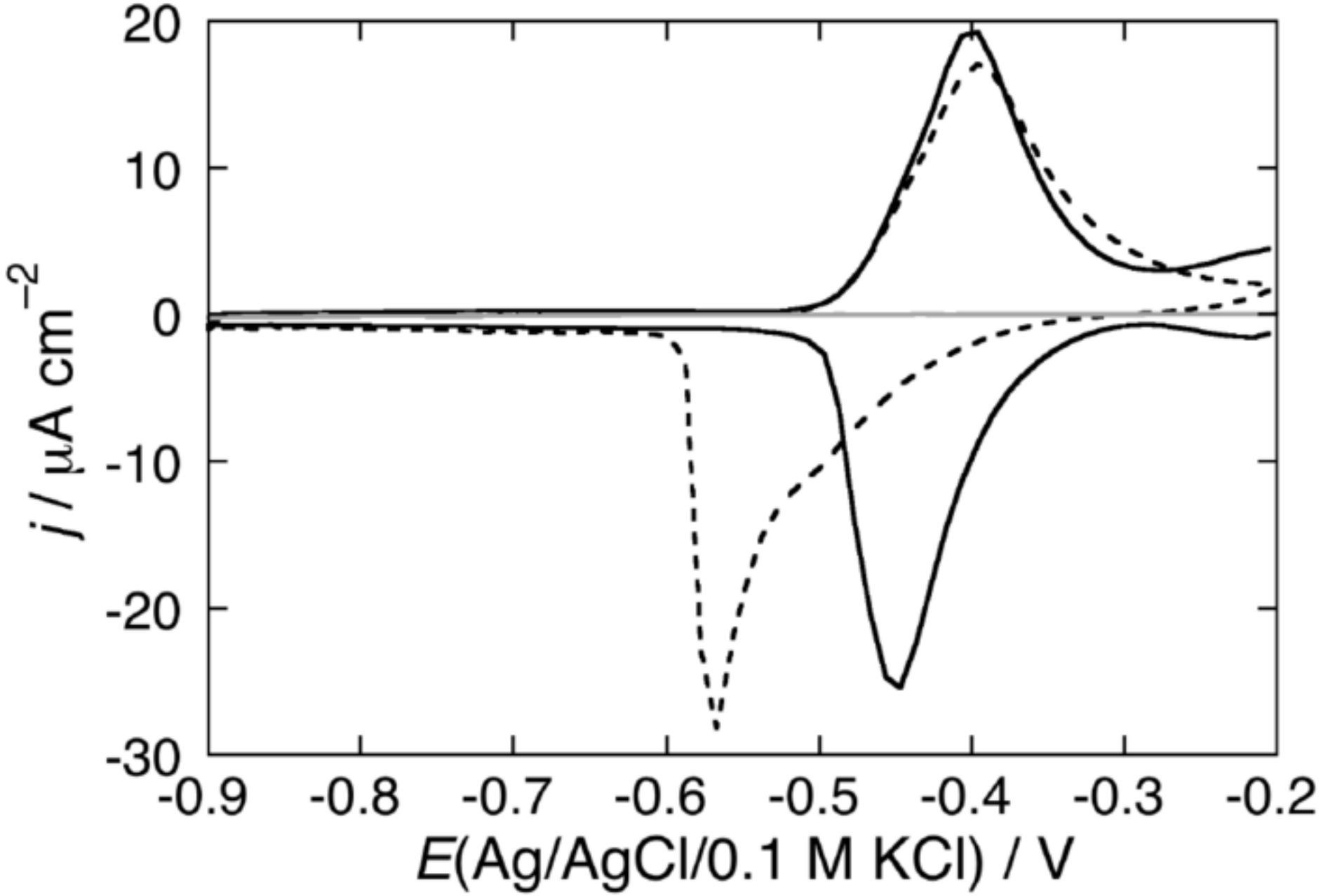

Figure 14
Click here to download high resolution image

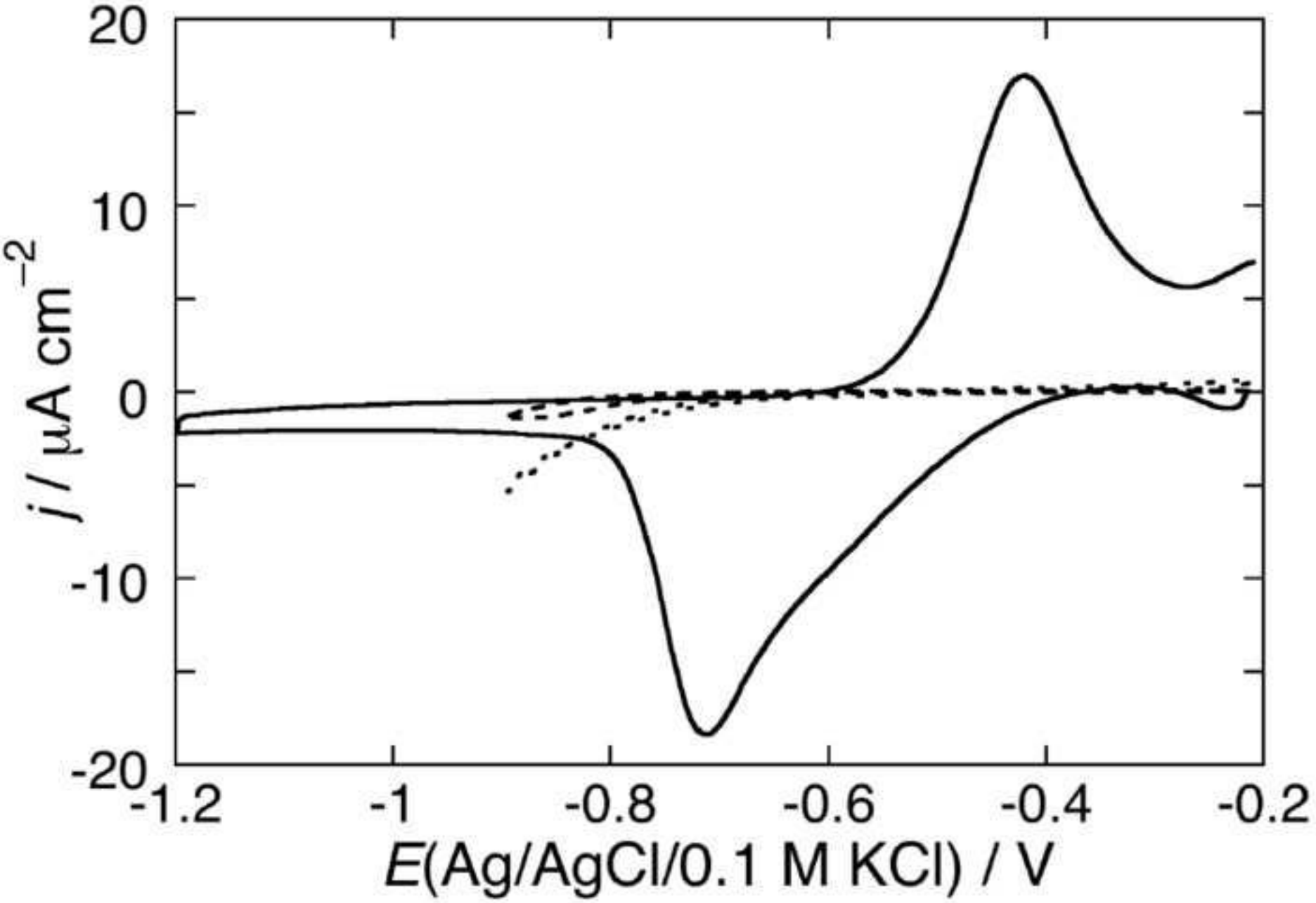

Figure 15

Click here to download high resolution image

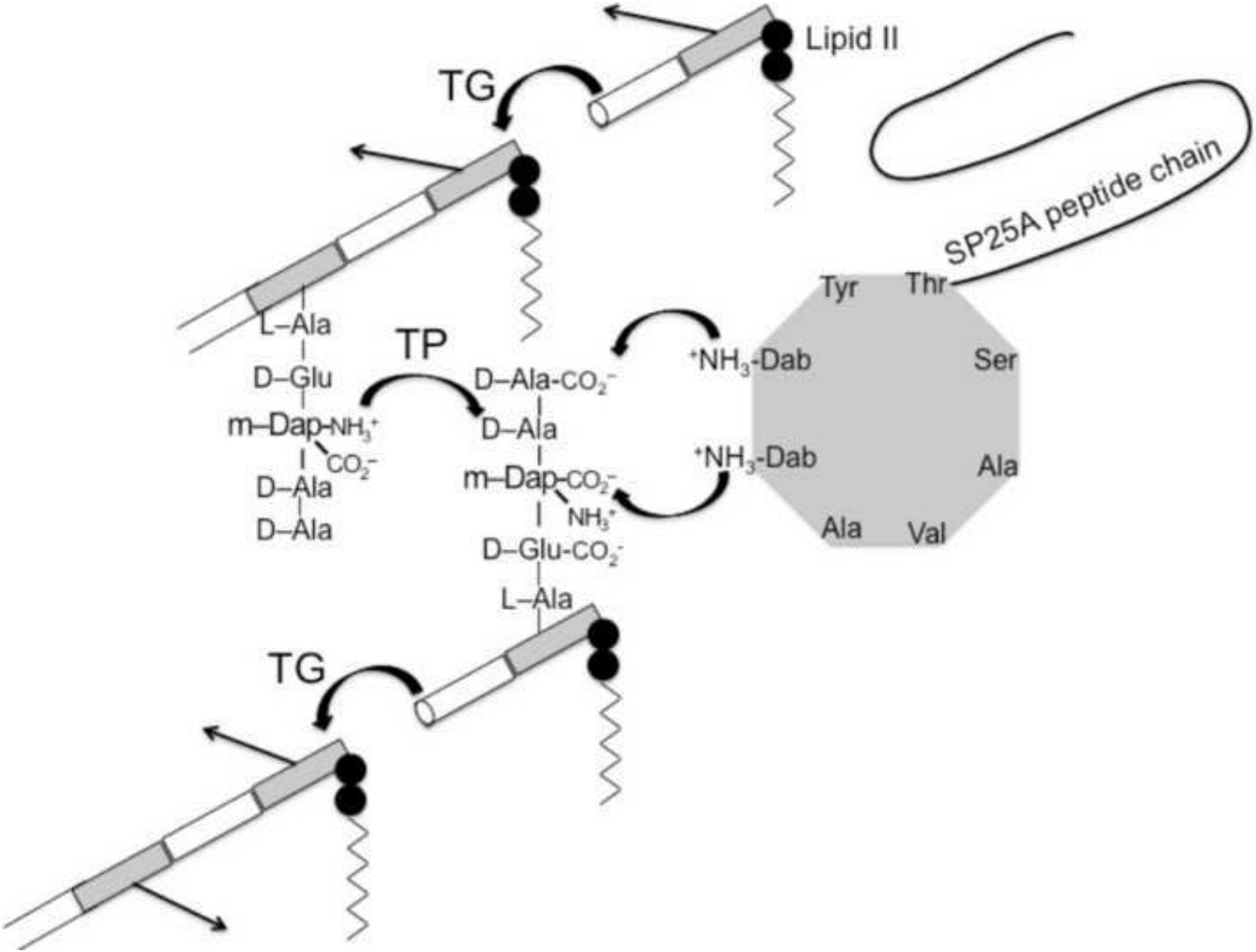

***Highlights**

- ✓ syringopeptin 25A (SP25A) targets a dioleoylphosphatidylserine (DOPS) SAM
- ✓ SP25A forms ion channels in tethered BLMs with a DOPS distal monolayer
- ✓ The target is NH_3-CHR-CO_2^-•$^+NH_3$-CHR-CO_2^-pair between adjacent DOPS polar heads
- ✓ Similar pairs may exist in premature peptidoglycan of Gram-positive bacteria
- ✓ This might explain SP25A antimicrobial activity against Gram-positive bacteria

Channel-forming activity of syringopeptin 25A in mercury-supported phospholipid monolayers and negatively charged bilayers

Lucia Becucci[#†,&], Arianna Toppi[†], Alberto Fiore [‡≠], Andrea Scaloni [¥], and Rolando Guidelli[1]

[†] *Department of Chemistry, Florence University, via della Lastruccia 3, 50019 Sesto Fiorentino (Firenze), Italy*

[&] *Department of Chemistry, University of Padova, Via Marzolo 1, 35131 Padova, Italy*

[‡] *Department of Agricultural and Food Science, University of Naples "Federico II", 80055 Portici, Italy*

[¥] *Proteomics & Mass Spectrometry Laboratory, ISPAAM-National Research Council, 80147 Naples, Italy*

[≠] *School of Science, Engineering & Technology, Division of Food & Life Sciences, Abertay University, Kydd Building, Dundee, DD1 1HG, UK*

Abstract

Interactions of the cationic lipodepsipeptide syringopeptin 25A (SP25A) with mercury-supported dioleoylphosphatidylcholine (DOPC), dioleoylphosphatidylserine (DOPS) and dioeleoylphosphatidic acid (DOPA) self-assembled monolayers (SAMs) were investigated by AC voltammetry in 0.1 M KCl at pH 3, 5.4 and 6.8. SP25A targets and penetrates the DOPS SAM much more effectively than the other SAMs not only at pH 6.8, where the DOPS SAM is negatively charged, but also at pH 3, where it is positively charged just as SP25A. Similar investigations at tethered bilayer lipid membranes (tBLMs) consisting of a thiolipid called DPTL anchored to mercury, with a DOPS, DOPA or DOPC distal monolayer on top of it, showed that, at physiological transmembrane potentials, SP25A forms ion channels spanning the tBLM only if DOPS is the distal monolayer. The distinguishing chemical feature of the DOPS SAM is the ionic interaction between the protonated amino group of a DOPS molecule and the carboxylate group of an adjacent phospholipid molecule. Under the reasonable assumption that SP25A preferentially interacts with this ion pair, the selective lipodepsipeptide antimicrobial activity against Gram-positive bacteria may be tentatively explained by its affinity for similar protonated amino-carboxylate pairs, which are expected to be present in the peptide moieties of peptidoglycan strands.

Keywords: Antimicrobial peptides; lipodepsipeptides; ion channels; lipid monolayers self-assembled on mercury; tethered bilayer lipid membranes; cyclic voltammetry

---

[#] Corresponding author. Telephone: (+39) 055-457-3095. Fax: (+39) 055-457-3385

E-mail: luci_be@tiscali.it; lucia.becucci@unifi.it

[1] Former Professor at Florence University

1. Introduction

In addition to the lipodepsinonapeptides syringomycin (SR) and syringotoxin, the plant pathogenic bacterium *Pseudomonas syringae* pv. *syringae* produces syringopeptins SP22 and SP25, which contain 22 and 25 amino acids, respectively. Combined biochemical approaches demonstrated that the latter lipodepsipeptides have common structural characteristics, e.g. a similar peptide chain preferentially made of hydrophobic D-amino acids, a similar C-terminal octadepsipeptide ring containing 2,4-diaminobutanoic acid, and N-terminal 3-hydroxy-decanoic or 3-hydroxy-dodecanoic acid moieties generating A or B molecular isoforms, respectively [1,2]. NMR investigations in aqueous solution showed that SP25A assumes a conformation having distinct structural portions, e.g. a loop region (amino acids 2-6), a left-handed helical region (amino acids 8-15), and an octadepsipeptide moiety (amino acids 18-25) that resembles the seam of a tennis ball [3,4]. Syringopeptins have phytotoxic, antifungal and antibacterial properties. The latter action seems mainly directed against Gram-positive (G+) organisms, seemingly toward their teichoic acid-containing peptidoglycan layer [5,6]. It was demonstrated that syringopeptins have a stronger phytotoxic activity than SR [7,8], and disrupt erythrocytes and tobacco protoplasts below their critical micellar concentration [9]. Even though the main plant target is the cellular plasma membrane, these lipodepsipeptides may also lyse intracellular membranes [10].

When assayed for the induction of macroscopic conductance on neutral dioleoylphosphatidylcholine (DOPC) bilayers, syringopeptins were found to be more effective than SR [10]. This property was associated with their long hydrophobic peptide chain, which may strongly interact with lipids. Differently from SR, which presents an increased activity on phospholipid vesicles in the presence of sterols, syringopeptins do not require the latter molecules to elicit their potential. Measurements of single- and multi-channel currents induced by syringopeptins at conventional bilayer lipid membranes (BLMs) have been performed by different groups [11-14]. Both small and large single-channel conductance fluctuations were observed, which present a 4-6 fold difference in their level of conductance and in the corresponding open state lifetime [11,13,14]. The latter parameter ranges from several sec (for the higher conductance levels) to a few tens of msec (for the lower ones). When SP25A was added to the *cis* side of a BLM consisting of 2:2:1 phosphatidylcholine (PC), phosphatidylethanolamine (PE) and phosphatidylserine (PS) mixture, bathed by an electrolyte solution, lipodepsipeptide incorporation induced a multichannel current upon applying a positive transmembrane potential ($\Delta\phi$) at the *trans* side [13], which tended exponentially to a constant limiting value. A symmetrically opposite behavior was observed when a negative potential of the same magnitude was quickly applied. On this basis, the SP25A channel seems to open at positive $\Delta\phi$ values, whereas a step-like voltage sign reversal induces its closure in about 10 sec. Single channel currents obtained from voltage sign reversal measurements at the same BLM, once reported against $\Delta\phi$, yielded a plot exhibiting a higher slope at positive $\Delta\phi$ values than at negative ones [13]. Therefore, the corresponding estimated single channel conductance was higher at positive $\Delta\phi$ values. This behavior was associated with the positive charge of the cyclic moieties present at the mouth of the lipodepsipeptide channel. This positive charge attracts anions, increasing their local concentration at this site, while decreasing that of cations. Thus, anions are moved by a positive $\Delta\phi$ value along the SP25A channel more favorably than cations by the negative $\Delta\phi$ counterpart. A similar phenomenon was observed with a DOPC-containing BLM incorporating SP25A, when the peptide was dissolved in an electrolyte solution, pH 6 [11]. Measurements performed with reversed $\Delta\phi$ values pointed to a modest anion selectivity [13].

We have recently evaluated some aspects of the SP25A ion-channel activity at a biomimetic membrane in relation to transmembrane potential and pH values [15]. To this purpose, use was made of a Hg-supported biomimetic membrane consisting of a monolayer of a thiolipid, called DPTL, with a DOPC monolayer on top of it. DPTL is made of a tetraethyleneoxy hydrophilic chain, called spacer, ending at one side with a lipoic acid residue (for anchoring to the mercury surface). At the other side, it is covalently linked to two phytanyl chains that mimic the hydrocarbon tails of a lipid [16]. The hydrophobic interactions between the phytanyl chains and the overlying phospholipid monolayer give rise to a lipid bilayer interposed between the tetraethyleneoxy chain and the bulk aqueous solution. The spacer may accommodate a number of water molecules and ions, thus acting as an ionic reservoir. The incorporation of SP25A in the DPTL/DOPC tBLM required the application of non-physiological $\Delta\phi$ values. Nonetheless, once incorporated, SP25A formed stable ion channels over the narrower range of physiological $\Delta\phi$ values. Ion flow into and out of the spacer through the lipid bilayer moiety of the tBLM was monitored by potential step chronocoulometry and cyclic voltammetry, at different pH values. Potassium ion flow into the hydrophilic spacer along the SP25A channels during the negative potential scan was found to proceed in two stages.

The present work aims at investigating the behavior of SP25A in Hg-supported lipid mono- and bi-layers composed of DOPC, dioleoylphosphatidylserine (DOPS) or dioleoylphosphatidic acid (DOPA). The variation of the lipid composition intends to simulate the different lipid films that SP25A may encounter *in vivo*, in order to verify the possible effect of their nature on its activity. The effect of a change of pH in aqueous 0.1 M KCl was also evaluated. In addition to Hg-supported DPTL/DOPS and DPTL/DOPA tBLMs, self-assembled monolayers (SAMs) of DOPC, DOPS and DOPA were used. Mercury provides a defect free, fluid and readily renewable surface to both SAMs and tBLMs. Moreover, it imparts to the lipid molecules of the whole film a lateral mobility comparable with that of biomembranes. Hg-supported tBLMs have been extensively used in our laboratory for the investigation of ion channels [17-25]. Thanks to its partially hydrophobic nature, mercury is also an excellent substrate for phospholipid monolayers. Phospholipid molecules self-assemble onto the mercury surface with the hydrocarbon tails directed toward the metal and the polar heads facing the bathing solution. Lacking a hydrophilic spacer and one of the two lipid leaflets, Hg-supported lipid SAMs represent a poorer biomimetic membrane with respect to tBLMs. Nonetheless, their dielectric properties are extremely sensitive to the presence of exogenous molecules. This has stimulated the use of SAMs to investigate the effect of the interaction of peptides and small proteins with the outer leaflet of biological membranes [20,22-25]. Combining the features of this interaction with those of SP25A penetration into tBLMs may reveal novel insights into the mechanism of action of this lipodepsipeptide on biomembranes.

2. Material and methods

Water was obtained by an inverted osmosis unit; it was then distilled once and redistilled from alkaline permanganate. Suprapur® KCl (Merck, Darmstadt, Germany) was baked at 500 °C before use to remove any organic impurities. Adenosine-5'-triphosphate disodium salt (Na_2H_2ATP) from Fluka (Milwaukee, WI, USA), dimethylsulfoxide (DMSO), HCl and $TlNO_3$ from Sigma-Aldrich (St. Louis, MO, USA) and KH_2PO_4 and K_2HPO_4 from Merck were used without further purification. DOPC, DOPS and DOPA were purchased in chloroform solution from Avanti Polar Lipids (Birmingham, AL, USA). 2,3,di-O-phytanyl-*sn*-glycerol-1-tetraethylene-glycol-D,L-α lipoic acid ester thiolipid (DPTL) was provided by Prof. Adrian Schwan (Department of Chemistry, University of Guelph, Canada). Solutions of 0.2 mg/mL

DPTL in ethanol were prepared from a 2 mg/mL solution of DPTL in ethanol. Stock solutions of this thiolipid were stored at –18 °C. SP25A was obtained from *P. syringae* pv. *syringae* culture broths and purified as already reported [1]. SP25A stock solutions (1 mg/mL) in DMSO were stored at 4 °C.

All measurements were carried out with a homemade hanging mercury drop electrode (HMDE) described elsewhere [26]. A homemade glass capillary with a finely tapered tip (about 1 mm in outer diameter) was employed. Capillary and mercury reservoir were thermostated at 25 ± 0.1 °C in a water-jacketed box to avoid any changes in drop area due to temperature changes. The HMDE acted as the working electrode in a three-electrode system, with an Ag/AgCl (0.1 M KCl) reference electrode and a platinum coil counter electrode.

Phospholipid monolayers were obtained by first spreading a DOPC, DOPS or DOPA solution in pentane on the surface of a buffered or unbuffered 0.1 M KCl aqueous solution, in an amount corresponding to about five phospholipid monolayers, and allowing the solvent to evaporate. The lipid film so formed was a monolayer at its equilibrium spreading pressure (about 45 mN m^{-1}), in equilibrium with the bulk phase of the surfactant, which consisted of floating 'icebergs' [27]. A HMDE was then immersed into the solution across the formed lipid film, at a controlled rate. Preparation of these lipid SAMs did not require any electrochemical stabilization. Hg-supported tBLMs were obtained by tethering a DPTL monolayer to a HMDE upon keeping the mercury drop immersed in a 0.2 mg/mL DPTL solution in ethanol, for about 20 min [18]. The mercury drop was then extracted from the solution, and ethanol was allowed to evaporate under N_2 atmosphere. A lipid monolayer was subsequently self-assembled on top of the DPTL monolayer by the same procedure adopted to form it on a bare mercury drop. The tBLM was subjected to repeated potential scans over a potential range from –0.20 to –1.20 V, while continuously monitoring the curve of the quadrature component of the current at 75 Hz against the applied potential (E) using AC voltammetry, until a stable curve was attained.

Electrochemical impedance spectroscopy (EIS), potential-step chronocoulometry, phase-sensitive AC voltammetry and cyclic voltammetry measurements were carried out with an Autolab instrument PGSTAT12 (Echo Chemie, Utrecht, The Netherlands) supplied with FRA2 module for impedance measurements, SCAN-GEN scan generator and GPES 4.9007 software. All AC voltammetry and EIS measurements were carried out by superimposing an AC voltage of 10 mV peak-to-peak amplitude to the bias potential E. In EIS measurements the frequency was varied between 10^{-1} and 10^5 Hz. Potentials were measured *vs*. a Ag/AgCl electrode immersed in the 0.1 M KCl working solution, and are referred to this reference electrode.

3. Results and discussion

3.1. Lipid SAMs

A self-assembled lipid monolayer can be regarded as the first barrier that a peptide encounters in its attempt to penetrate a membrane. Nonetheless, the interactions of the peptide with the hydrocarbon tail region of a SAM are generally different from those occurring with a lipid bilayer, especially if its length is appreciably greater than the SAM thickness, as is often the case. In fact, the peptide can only intercalate partially between the hydrocarbon tails, without being capable of assuming the conformation otherwise present in a biomembrane. Conversely, its interactions with the polar heads of a SAM may realistically reproduce those with the outer leaflet of a biomembrane. AC voltammograms are plots of the quadrature component of the current against the applied potential (E) at constant frequency (f); the current is converted into a capacitance (C) by calibrating the instrument with a high precision capacitor in place of the electrochemical cell. All lipid SAMs are characterized by a potential region of low and almost

constant capacitance, followed by two or more pseudo-capacitance peaks at more negative potentials. The less negative peak is ascribed to a cooperative reorientation of the lipid molecules, whereas the most negative one is due to their partial desorption [27]. As a rule, molecules capable of penetrating the hydrocarbon tail region of the phospholipid monolayer increase its capacitance over the potential range of the flat capacitance minimum, with respect to its value in the absence of foreign species, provided that their polarizability is appreciably higher than that of the lipid molecules. Conversely, they affect the monolayer capacitance only slightly if they have a low polarizability [28]. In both cases, whenever their concentration in the lipid monolayer is sufficiently high, their intercalation with the lipid molecules prevents the latter molecules from undergoing a sufficiently sharp cooperative reorientation, thus broadening and depressing the pseudo-capacitance peaks. Molecules adsorbed on top of the lipid monolayer, but unable to penetrate it, alter and depress the pseudo-capacitance peaks by interacting with the polar heads [29,30]; they may also decrease the capacitance over the potential range of the flat capacitance minimum, whenever they form a sufficiently compact layer, thus increasing the thickness of the whole adsorbed material [28].

Scanning the potential from –0.20 V to potentials negative with respect to one or two peaks may allow the penetration of exogenous molecules present in the solution into the SAM or, at least, into its polar head region, provided they have some affinity for it. Another procedure adopted to favor the possible penetration of an exogenous molecule consists in carrying out a series of electrochemical impedance spectra, at regular intervals of the bias potential, over the potential range of stability of the SAM; this procedure will be briefly referred to as an 'EIS scan'. In this case, incorporation may be favored by the relatively long time during which the SAM is maintained at each of the stepwise varied potentials over its stability range, and/or by some effect of the small AC signals covering the frequency range from 10^{-1} to 10^{5} Hz. The AC voltammetry profile of a lipid SAM is its outright fingerprint, just as its alteration upon addition of an exogenous species is a measure of the nature and extent of its interaction with the SAM. In the absence of interacting species, Hg-supported lipid SAMs constitute an impenetrable barrier to inorganic ions. If a peptide alters the compact and well-organized structure of the SAM, it may induce defects and/or pores (not ion channels) allowing the penetration of ions. These structural changes affect both the capacitance and, to a lesser extent, the resistance, in a frequency dependent manner. Thus, the effect of SP25A was investigated at DOPC and DOPS SAMs in unbuffered solutions, pH 3 and 5.4, and in a phosphate buffer solution, pH 6.8, as well as at a DOPA SAM in an unbuffered solution, pH 5.4.

Fig. 1 shows the AC voltammograms at a Hg-supported DOPC SAM in an unbuffered solution of 0.1 M KCl, pH 5.4, as obtained in the absence of SP25A (solid curve), immediately after the addition of 0.2 μg/mL SP25A (dashed curve) and after a complete EIS scan from –0.30 to –0.80 V (dash-dotted curve). In the absence of SP25A, the DOPC SAM was characterized by a sharp pseudocapacitance peak lying at about −1.02 V, followed by two further peaks at about −1.10 V and −1.35 V. The first two peaks are ascribed to a cooperative reorientation of the lipid molecules, whereas the third one is due to their partial desorption [27]. Addition of the lipodepsipeptide depressed the peaks to a moderate extent and increased the capacitance along the flat region only at potentials negative of –0.70 V, where the SAM is known to be less stable. An EIS scan increased the effect of SP25A only slightly.

Here Figure 1

In all the above measurements, the SAM was formed before adding SP25A. In a few measurements, the SAM was also formed by immersing the mercury drop across the lipid film into an aqueous solution containing SP25A. In this case, the mercury drop dragged into the solution a lipid monolayer containing peptide molecules that may have previously interacted with the film in contact with the aqueous subphase; the effect of SP25A was found to be almost identical with that of the dashed curve in Fig. 1. The AC voltammograms at DOPC SAMs in aqueous solutions of 0.1 M KCl, pH 3 or 6.8, were even less influenced by the addition of SP25A. The EIS spectra recorded over the potential range of the flat capacitance region in Fig. 1 were only slightly affected by the addition of 0.2 μg/mL SP25A, with no relevant changes in the in-phase and quadrature components of the admittance. No differences were observed if the monovalent K^+ cation in the electrolyte was substituted by the divalent Ca^{+2} cation.

The effect of SP25A on the DOPS SAM in 0.1 M KCl was much stronger than that on the DOPC counterpart, at all the pH values investigated. Fig. 2 shows the AC voltammograms at a Hg-supported DOPS SAM in a buffer solution of 0.1 M KCl, pH 6.8, as obtained in the absence of SP25A (solid curve), immediately after the addition of 0.2 μg/mL SP25A (dashed curve) and after a complete EIS scan from –0.30 to –0.80 V (dash-dotted curve). The AC voltammogram recorded at a DOPS SAM in the absence of exogenous species (Fig. 2) differed from the counterpart measured at a DOPC SAM (Fig. 1) by the presence of a broader region of minimum capacitance, which extends up to –1.10 V and exhibits two pseudocapacitance peaks [25,31]. Since the potential region negative of the first pseudocapacitance peak, which lies at about –1.20 V, was not entirely reproducible, only the first peak is shown in Fig. 2. Addition of SP25A caused an immediate depression of the pseudocapacitance peak and an increase in the capacitance along the flat region at potentials negative of –0.7 V. A subsequent EIS scan suppressed the peak and increased the capacitance along the whole flat region.

Here Figure 2

The effect of SP25A on the AC voltammogram at a DOPS SAM increased slightly at pH 5.4, and to a greater extent at pH 3. At the latter pH value, the capacitance peak was completely suppressed upon the addition of SP25A (dashed curve at 75 Hz in Fig. 3). An EIS scan from –-0.30 to –0.80 V by 50 mV steps increased the capacitance *C* along the whole flat region (dash-dotted curve in Fig. 3). As distinct from the capacitance, the in-phase component of the admittance, *Y*', over the same potential range increased only slightly upon the addition of SP25A, at all the pH values investigated (data not shown). The AC voltammogram recorded after forming the DOPS SAM in a solution at pH 3 already containing 0.2 μg/mL SP25A showed no pseudocapacitance peak (gray curve in Fig. 3). Moreover, it practically coincided with the curve recorded in the absence of the lipodepsipeptide along the whole flat capacitance region. This strongly suggests that, when SP25A binds to a DOPS monolayer at its equilibrium spreading pressure on a water subphase, pH 3, it interacts mainly with the polar heads, without contacting the hydrocarbon tails. However, we cannot exclude the possibility that the short SP25A hydrocarbon chains may intercalate between the hydrocarbon tails of the lipid monolayer. Such an intercalation would not affect the capacitance along the flat region, since the polarizability of the SP25A hydrocarbon chains is comparable with that of the lipid hydrocarbon tails. Nonetheless, it would hinder the cooperative reorientation of the lipid molecules responsible for the pseudocapacitance peak, contributing to suppressing the latter. No differences were observed whenever the divalent cation Ca^{2+} was used instead of the monovalent K^+ one.

Here Figure 3

In this context, worth mentioning is the fact that a Hg-supported DOPS monolayer is positively charged at pH 3, neutral at pH 5.4 and negatively charged at higher pH values [32]. This behavior was explained by regarding the carboxyl and the amino groups of adjacent DOPS polar heads as being coplanar to the monolayer, and characterized by electrostatic dipole-dipole interactions. The phosphate group, whose pK_a is about 8, is buried inside the polar head region and almost completely protonated at pH 5.4, causing DOPS to be neutral and zwitterionic at this pH value. With a further decrease in the pH value, the carboxyl group, whose pK_a is around 3.3, undergoes a gradual protonation, inducing DOPS to become positively charged at low pH values. The electrostatic repulsion between the DOPS polar heads, which bear a positive charge at pH 3, and the positively charged SP25A octadepsipeptide moiety may oppose the penetration of the latter into a lipid monolayer suspended on an aqueous subphase and the resulting increase in monolayer capacitance. Only a negative electric potential, such as that applied to the Hg-supported lipid SAM, can move the octadepsipeptide moiety stably into the lipid monolayer.

The effect of SP25A at a Hg-supported DOPA SAM in an unbuffered solution of 0.1 M KCl, pH 5.4, was modest and comparable with that at a DOPC SAM. The two protonation constants of the DOPA phosphate group in biomimetic membranes have values close to 1×10^{-8} M^{-1} and 1×10^{-4} M^{-1} [33,34]. Hence, the phosphate group of DOPA is uncharged at pH 3 and monoanionic at pH 5.4. Repeated voltage scans over the range from –0.30 to –1.30 V yielded a stabilized AC voltammogramm with a flat capacitance region, followed by an abrupt capacitance rise at about –1.2 V terminating in a shoulder (Fig. 4). Addition of 0.2 μg/mL SP25A shifted the shoulder toward more negative potential values and increased the capacitance only at potentials negative of –0.90 V, leaving unaltered the largest part of the flat capacitance region. A subsequent EIS scan had no further effect.

Here Figure 4

The above findings raise the question on the factors responsible for the particular effectiveness of SP25A toward a DOPS SAM. The negative charge of a DOPS SAM at pH 6.8 might suggest an attractive electrostatic interaction with the positively charged octadepsipeptide moiety of SP25A. However, the observed effect is stronger at pH 3, a value at which the DOPS SAM is positively charged. Moreover, SP25A interaction with the negatively charged DOPA SAM is weak, just as that with the DOPC SAM. On this basis, the electrostatic interaction between SP25A and DOPS has to be ruled out as causative agent of the peptide penetration into the DOPS monolayer. At pH 5.4, the polar heads of both DOPS and DOPC are neutral and zwitterionic. The DOPC monolayer presents an arrangement of $(H_3C)_3N^+$-CH_2-CH_2-PO_3^- zwitterions that is coplanar to the monolayer, as a result of the electrostatic interactions between the trimethylammonium group and the phosphate group of adjacent polar heads. This results in the stabilization of the non-protonated form of the phosphate group [32]. On the other hand, the DOPS monolayer presents an arrangement of H_3N^+-CHR-CO_2^- zwitterions coplanar to the monolayer, with the protonated phosphate group buried inside the polar head region. In view of the above considerations, the experimental behavior observed strongly suggests that SP25A targets some structural features of the DOPS monolayer that are not present in the DOPC and DOPA monolayers.

In the absence of electroactive ions, the resistance of Hg-supported lipid SAMs along the flat capacitance region is slightly decreased by exogenous electroinactive species, even if they are able to induce defects and/or pores in the monolayer and to increase its capacitance to an appreciable extent. This is due to the lack of an ionic reservoir on the metal side of lipid SAMs, differently from tBLMs. The ability of an exogenous species to permeate a Hg-supported SAM

can be tested by exploiting the properties of inorganic ions that are electroreduced on mercury, with amalgam formation, over the potential range of stability of the lipid SAM [20,22,23]. In this case, the 'ionic reservoir' is provided by the mercury drop itself. For example, cadmium ion is electroreduced reversibly on bare mercury to Cd(Hg) amalgam, with a formal potential of –0.645 V in 0.1 M KCl [20,35], but its reduction is completely inhibited by a phospholipid SAM. In the presence of defects elicited by some exogenous species, the driving force of the electrode reaction moves Cd^{2+} ions along them across the SAM, generating a reduction current.

Fig. 5 shows the cyclic voltammograms (CVs) due to Cd^{2+} reduction and Cd(Hg) oxidation at a DOPS SAM in a solution of 0.1 M KCl, 4×10^{-5} M $CdSO_4$ and 0.2 μg/mL SP25A, at pH 6.8, 5.4 and 3. The height of the peaks decreased with a decrease in the pH value, and the negative peak at pH 3 evolved into a shoulder. The irreversibility of the electrode process, as measured by the separation between the positive and negative peaks, increased in passing from pH 6.8 to pH 5.4. While the ease of penetration of the SP25A molecules into the DOPS SAM increased with decreasing pH values, the permeability of this SAM to Cd^{2+} ions in the presence of SP25A decreased. This apparently anomalous behavior is explained by the charge on the DOPS polar heads being negative at pH 6.8 and positive at pH 3. Thus, it increased the cadmium ion concentration in the vicinity of the SAM with respect to its bulk value at the former pH, and decreased it at the latter. This behavior is not only due to a diffuse-layer effect. Rather, it is also and mainly due to the specific effect exerted by the charge of the DOPS polar heads, which can be regarded as a true specifically adsorbed charge, on the positively charged Cd^{2+} ions, as they start being deprived of their solvation sheath before entering into mercury. In fact, the rate constant of this electrode process is expected to decrease or increase depending on whether the charges of the DOPS polar heads and of cadmium ion have the same or opposite sign [36 and references therein].

Here Figure 5

3.2. DPTL/DOPS tBLM in a buffer solution, pH 6.8

The effect of SP25A on a Hg-supported DPTL/DOPC tBLM was reported in our previous paper [15]. The midpoint potential, $E_{1/2}$, between the positive and negative peaks in the CV at a DPTL/DOPC tBLM incorporating SP25A from aqueous 0.1 M KCl was found to shift toward less negative potentials with decreasing pH values. The magnitude of this shift was found to be practically identical with that observed at DPTL/DOPC and DPTL/DOPS tBLMs incorporating gramicidin [37], under otherwise identical conditions. Thus, with both ion channels, $E_{1/2}$ was found to be about equal to –0.65 V in a phosphate buffer at pH 6.8, –0.55 V in an unbuffered solution at pH 5.4, and –0.45 V in an unbuffered solution at pH 3. In view of the appreciable structural differences between the neutral dimeric gramicidin channel and the positively charged oligomeric SP25A channel, this common $E_{1/2}$ dependence upon pH value seems to depend more on the structural features of the phospholipid than on those of the ion channel, and a qualitative justification was provided. The cyclic voltammetry behavior of DPTL/DOPS tBLMs incorporating SP25A was in accord with this prediction. $E_{1/2}$ is the electric potential at which the ion flow into the hydrophilic spacer of the tBLM matches the corresponding outflow. Hence, it is equivalent to the zero transmembrane potential $\Delta\phi$ at a conventional symmetric BLM interposed between two identical solutions, where the flow of an ion in one direction matches that of the same ion in the opposite direction. Considering that the potential difference across the lipid

bilayer moiety of a Hg-supported DPTL/phospholipid (i.e., its transmembrane potential) is a fraction (about 0.72) of the potential difference across the whole mercury/solution interface [38], the product of 0.72 by the applied potential measured relative to $E_{1/2}$, $0.72(E–E_{1/2})$, can be directly compared with the transmembrane potential at a BLM. Hence, $0.72(E–E_{1/2})$ values more negative than those corresponding to the most negative transmembrane potential used in BLM measurements with SP25A [10,11,13], namely –200 mV, will be conventionally defined as non-physiological. While non-physiological negative $\Delta\phi$ values were required for incorporating SP25A into DPTL/DOPC tBLMs [15], physiological ones were sufficient for incorporating this peptide into DPTL/DOPS tBLMs at all the pH values we investigated.

The first EIS scan from –0.30 to –0.80 V, as reported at 10 Hz on a freshly prepared DPTL/DOPS tBLM incorporating SP25A from its 0.4 μg/mL solution in 0.1 M KCl, caused an appreciable increase in the capacitance (C) and the in-phase admittance (Y') over their background values, at potentials negative of about –0.60 ÷ –0.70 V, for all the pH values we investigated. The second EIS scan caused both C and Y' to increase over the whole potential range explored (data not shown). The impedance spectrum at a freshly prepared DPTL/DOPS tBLM in a buffer solution of 0.1 M KCl, pH 6.8, at –0.50 V is displayed in Fig. 6 on a ωZ' vs. –ωZ" plot (referred to as a modulus or M plot), both before and after the addition of 0.4 μg/mL SP25A. Lipodepsipeptide addition determined the appearance of a small semicircle partially fused with a roughly semicircular feature similar to that present before such an addition. It should be noted that a tBLM can be simulated by an equivalent circuit consisting of a series of '*RC* meshes', i.e., parallel combinations of a capacitance C and a resistance R. On a M plot, a single RC mesh yields a semicircle of diameter $1/C$ [24,39]. If some of the *RC* meshes simulating a tBLM have similar values of the time constant RC, the corresponding semicircles are partially overlapped in the M plot. The small semicircle elicited by the SP25A addition had a relatively high capacitance, 5 μF cm^{-2}, and a low resistance, 4 $k\Omega cm^2$. It was quite similar to a small semicircle induced by the presence of the peptide melittin at a DPTL/lipid tBLM [17], and can likewise be ascribed to a monolayer of SP25A molecules intercalated with water molecules and adsorbed on top of the tBLM. After the first EIS scan over the whole range of physiological potentials, a subsequent impedance spectrum recorded at –0.5 V did not show this additional semicircle. At potentials negative of –0.50 V, no additional semicircle was observed at a freshly prepared tBLM even during the first recording of the impedance spectrum, denoting a stable penetration of the lipodepsipeptide molecules deeply into the lipid bilayer moiety of the tBLM, at these negative potentials.

Here Figure 6

This peculiar feature of the impedance spectrum was encountered neither with DPTL/DOPS tBLMs at pH 5.4 or 3, nor with DPTL/DOPC tBLMs at any of the three pH values we investigated. The impedance spectra of a DPTL/DOPS tBLM at pH 6.8, both in the absence and in the presence of 0.4 μg/mL SP25A, were analyzed over the potential range from –0.30 to –1.0 V, by fitting them with an equivalent circuit consisting of four *RC* meshes in series. The RC mesh of by far the lowest capacitance and resistance was common to all tBLMs and was ascribed to the aqueous solution adjacent to the tBLM; it will be ignored in what follows. Of the other three RC meshes, one had a capacitance of about 1 μF cm^{-2} and a resistance of a few $M\Omega\ cm^2$ in the absence of SP25A; the peptide addition affected the capacitance only slightly and decreased the resistance by about three orders of magnitude at potentials negative of –0.50 V. This *RC* mesh was ascribed to the lipid bilayer moiety of the tBLM. The second *RC* mesh had a capacitance ranging from 3 to 5 μF cm^{-2} and a resistance of about 0.5 $M\Omega\ cm^2$; SP25A addition

increased the capacitance by 2 or 3 times and left the resistance almost unaltered. This *RC* mesh was reasonably attributed to the dielectric layer in direct contact with the mercury surface. The potential dependence of the capacitance C and conductance $G = 1/R$ of the third RC mesh, as reported in Fig. 7, behaved differently from that at all other tBLMs examined. SP25A addition depressed both C and G at potentials positive of –0.60 V and increased them at more negative potential values. The relatively high capacitance and conductance of this *RC* mesh in the absence of the peptide are typical of the polar head region. Their apparently anomalous decrease at potentials positive of –0.60 V, upon addition of SP25A, is suggestive of a tight intercalation of the lipodepsipeptide molecules between the DOPS polar heads, whereas their subsequent increase at more negative potentials denotes a deeper penetration of the SP25A molecules into the lipid bilayer and a drop in polar head compactness.

Here Figure 7

Fig. 8 shows a series of charge transients recorded at a DPTL/DOPS tBLM in a buffer solution of 0.1 M KCl, pH 6.8, and 0.4 μg/mL SP25A by jumping from a fixed initial potential $E_i = –0.30$ V to progressively more negative final potentials E_f. These transients differ from those obtained at DPTL/DOPC tBLMs under otherwise identical conditions by two main features. Firstly, they constantly turn their concavity downwards, and hence do not show a two-stage flow of ionic charge, such as that in Fig. 5 of Ref. 15, where the two stages were separated by an inflection point. Secondly, extrapolation of the charge transient plateau at $E_f = –0.80$ V to $t = 0$ yields a charge density of about –50 μC cm^{-2}, which corresponds to a spacer saturation by the sole K^+ ions, whereas an analogous extrapolation of the two-stage charge transient at a DPTL/DOPC tBLM yielded a charge density of –60 μC cm^{-2} [15].

Before trying to explain these appreciable differences in behavior, it is convenient to summarize a number of results reported in previous works. At first, it must be mentioned that all peptides so far incorporated in our Hg-supported tBLMs (i.e. gramicidin [18], monazomicin [19], melittin [19], distinctin [20], trichogin GA IV [21], dermicidin [23], sarcolipin [40], phospholamban [41], syringomycin E [25]) yielded charge transients that attained a maximum charge density of –45 ± 5 μC cm^{-2}, with the only exception of SP25A in a DPTL/DOPC tBLM [15]. This maximum limiting charge density was explained by the limited spaciousness of the tetraethyleneoxy spacer moiety of the tBLM, which may accommodate a maximum amount of K^+ ions bearing a +45 ± 5 μC cm^{-2} charge density at the most negative E_f values. The equal and opposite charge density of –45 ± 5 μC cm^{-2} is due to the electrons accumulating on the mercury surface to ensure the electroneutrality of the whole electrified interface. Moreover, all peptides so far incorporated in our Hg-supported tBLMs exhibited a sigmoidal shape, with the only exception of gramicidin [18]. The sigmoidal shape was quantitatively explained by a mechanism of penetration of peptide monomers into the lipid bilayer, their nucleation, and growth of the resulting clusters, with channel formation [19]. The charge transients at a tBLM incorporating gramicidin also attained a maximum negative charge density of –45 ± 5 μC cm^{-2}, but did not exhibit a sigmoidal shape [18]. This simply depends on the nature of gramicidin channels, which consist of single N-terminus-to-N-terminus dimers and, hence, do not involve monomer clustering.

Here Figure 8

The fact that the maximum charge density attained by the two-stage transients of SP25A at a DPTL/DOPC tBLM significantly exceeded –45 ± 5 μC cm^{-2} was explained by assuming that,

differently from the other peptides so far examined by us, this lipodepsipeptide forms a channel that is open at the initial potential E_i = –0.30 V [15]. Since this applied potential corresponded to a positive transmembrane potential $\Delta\phi$, a certain amount of Cl^- ions was expected to be present in the hydrophilic spacer. The subsequent negative potential jump to E_f determined the outflow of Cl^- ions from the spacer, and the concomitant inflow of K^+ ions. Since the current due to the Cl^- outflow had the same negative sign as the current due to the K^+ inflow, at sufficiently negative final potentials both currents were expected to contribute to increasing the charge transient plateau beyond the –45 ± 5 μC cm^{-2} value corresponding to spacer saturation by K^+ ions. The difference between the experimental value of –60 μC cm^{-2} and the above expected value yielded a charge density due to Cl^- outflow that amounted to about 15% of the overall K^+ inflow. Since the first stage of the charge transient for SP25A at the DPTL/DOPC tBLM was higher than the second one by more than 15%, we concluded that the first stage was necessarily determined by the concomitant Cl^- outflow and K^+ inflow, while the second stage was due to the sole K^+ ion inflow up to spacer saturation by this cation [15]. To justify the presence of two separate stages of the charge transient, we further postulated that the first stage was determined by Cl^- and K^+ flows along large SP25A ion channels, and the second stage by K^+ inflow along small SP25A ion channels.

The existence of both large and small SP25A ion channels was assumed on the basis of the detection of both large and small single-channel conductance fluctuations in SP25A single channel measurements at conventional BLMs [11,13,14]. Since the small fluctuations were found to be exactly one fourth of the large ones, Dalla Serra et al. [13] assumed that the large channels result from the tetrameric aggregation of the small channels, leading to their synchronous opening and closing, in analogy with the hexameric clusters proposed for syringomycin E [42]. In view of above results, we tentatively assumed that the first stage is mainly determined by ion flow along the large channels, which prevail over the small ones thanks to their higher level of conductance and much longer open state lifetime [15]. However, at more negative and non-physiological transmembrane potentials, the strong electric field may drag the positively charged cyclic moieties of the SP25A monomers composing the large channels deeper into the lipid bilayer. The resulting decrease in the dielectric constant of the immediate environment of the cationic octadepsipeptide moiety would then increase the mutual electrostatic repulsion among the small channels composing the tetrameric clusters, determining their abrupt disaggregation and causing the K^+ inflow to proceed exclusively along the small channels during the second charge-transient stage.

In the light of the above results on SP25A ion-channel activity, as reported by us [15] at a DPTL/DOPC tBLM and by others [11,13,14] at conventional BLMs, the following conclusions can be reasonably drawn about the charge transient behavior of this lipodepsipeptide at a DPTL/DOPS tBLM. The fact that the maximum limiting height of the charge transient plateau amounted to –45 ± 5 μC cm^{-2} denotes that the SP25A ion channel is closed at the initial potential E_i = –0.30 V, and hence does not allow Cl^- inflow. In addition, the fact that the charge transients turned their concavity toward the time axis and did not show an inflection point, similarly to the gramicidin channel [18], indicates that these channels are not formed during the negative potential jump by a mechanism of nucleation and growth. Thus, they must be formed through a different rate-determining step during the potential jump or, more probably, they are already present at E_i, albeit in a closed state.

The CV in Fig. 9 at a DPTL/DOPS tBLM in an aqueous solution of 0.1 M KCl, pH 6.8, and 1 μg/mL SP25A was approximately centrosymmetric, with the inversion center located at the midpoint potential $E_{1/2}$ = –0.62 V between the positive and negative peaks. The trumpet-shaped enlargement of the CV at the most positive potentials is a specific feature that we observed only

in the CVs of SP25A at DPTL/DOPC tBLMs, at all the pH values we investigated [15]. It was explained on the basis of a modelistic calculation of CVs at a tBLM incorporating a non-selective ohmic channel, according to which the positive peak due to the anion inflow into the spacer and the negative peak due to its outflow fall at more positive potentials than the corresponding peaks for the in- and outflow of the monovalent cation (see Fig. 7 in Ref 15). This predicted behavior is due to the limited spaciousness of the spacer, which favors the accumulation of cations over anions at more negative potentials. A modest overlapping of anion and cation flow was only predicted at the junction between the negative peak due to anion outflow and the negative peak due to cation inflow, and between the reverse positive peak due to cation outflow and the positive peak due to anion inflow. Unfortunately, the positive potential range required to monitor the predicted massive anion in- and outflow is experimentally inaccessible on a Hg-supported tBLM, due to mercury surface oxidation. Nonetheless, the incipient small anion inflow (during the positive-going potential scan) and its subsequent outflow (during the negative-going scan) were revealed by the trumpet-shaped enlargement exhibited at the most positive potentials by the CV in Fig. 9. This conclusion seems to contradict the previous statement that the SP25A ion channel is closed at E_i. However, we must consider that cyclic voltammetry is a dynamic technique. Therefore, the rate of the voltage scan may prevent the channel from closing in the short time during which the applied potential E assumes values corresponding to positive transmembrane potentials. At the initial potential E_i of –0.30 V chosen for the chronocoulometric measurements in Fig. 8, the channel is closed because it is kept at this potential for a rest time long enough to permit its closure before each potential jump. Under all experimental conditions, the charge obtained by integrating the negative current peak in Fig. 9 turns out to be less negative than, or at most equal to, the opposite of the maximum cation charge that can be accommodated by the hydrophilic spacer (i.e., 45 ± 5 μC cm^{-2}) plus any anion charge moving away from the spacer, if the ion channel is open at the most positive potential covered by the voltage scan. *Mutatis mutandis*, analogous considerations apply to the corresponding positive peak.

Here Figure 9

The negative peak in Fig. 9 does not show a splitting such as that exhibited by the CV at a DPTL/DOPC tBLM (see Figs. 2 and 3 in Ref. 15). Such a splitting was ascribed to ion flow along the large channels at less negative potentials and along the small ones at more negative potentials [15]. The lack of splitting at a DPTL/DOPS tBML may be due either to the simultaneous presence of large and small channels or to the presence of the sole small channels, at all potentials. In the former case, the macroscopic current is clearly determined by the large channels, in view of their higher conductance and much longer lifetime. The latter case seems more probable at pH 6.8, where the DOPS polar heads are negatively charged, and may hinder the clustering of the small channels into the large ones. At pH 6.8, SP25A permeabilized the lipid bilayer to Tl^+ ions, yielding a CV of the Tl^+/Tl(Hg) couple almost identical with that obtained on bare mercury. This is shown in Fig. 10, which was recorded while maintaining the negative transmembrane potentials within the range of physiological values. This behavior differs from that at a DPTL/DOPC tBLM [15], which was totally impermeable to Tl^+ ions under the same conditions.

Here Figure 10

3.3. DPTL/DOPS tBLM in pH 3 and pH 5.4 unbuffered solutions

Fig. 11 shows the CVs at a DPTL/DOPS tBLM in aqueous solution of 0.1 M KCl and 0.4 μg/mL SP25A, at pH 5.4 and 3. The midpoint potential $E_{1/2}$ shifted gradually toward less negative potentials with decreasing pH, passing from –0.62 V at pH 6.8 to –0.56 V at pH 5.4 and to –0.42 V at pH 3. These midpoint potentials were in close agreement with those determined at the same pH values at DPTL/DOPS tBLMs incorporating gramicidin [37]. This confirms that the shift depends on the structural features of the lipid molecules interacting with those of a peptide at the mouth of ion channels, more than on the nature and charge of the particular peptide. Differently from pH 6.8, permeabilization of the DPTL/DOPS tBLM toward Tl^+ ions by SP25A was modest at pH 3 (dashed curve in Fig. 11). This is very likely due to the electrostatic interaction between Tl^+ ions and the DOPS distal monolayer. This interaction is repulsive at pH 3, where the lipid is positively charged, and attractive at pH 6.8, where it is negatively charged.

Here Figure 11

As distinct from the behavior of SP25A in a DPTL/DOPS tBLM at pH 6.8, chronocoulometric potential-step measurements carried out at pH 5.4 and 3, under otherwise identical conditions, yielded two-stage charge transients analogous to those occurring at DPTL/DOPC tBLMs at all the pH values we investigated [15]. The maximum charge density estimated by extrapolating the charge transient plateau at E_f = –0.90 V to t = 0 amounted to about –65 μC cm^{-2} at pH 5.4 (see Fig. 12) and to about –80 μC cm^{-2} at pH 3 (data not shown). This charge exceeded that, –45 ± 5 μC cm^{-2}, corresponding to spacer saturation by K^+ ions. Hence, an excess charge density of ~ –20 μC cm^{-2} at pH 5.4 and ~ –35 μC cm^{-2} at pH 3 must be ascribed to Cl^- outflow from the spacer during the potential jump. The lack of splitting in the negative peaks of the CVs in Fig. 11 seems to exclude the possibility for the first stage of the corresponding charge transients at pH 5.4 and 3 to be ascribed to ion flow along ion channels different from those active along the second stage, as hypothesized for the DPTL/DOPC tBLMs [15]. Hence, the amount of Cl^- ions contained in the hydrophilic spacer at the initial potential E_i = –0.30 V of the chronocoulometric potential jumps is responsible for practically the whole ion flow during the first stage of the charge transients. A positive potential jump from –0.80 to –0.30 V at a DPTL/DOPS tBLM in 0.1 M KCl and 0.4 μg/mL SP25A yielded a charge density practically equal in magnitude, but opposite in sign, to that obtained by stepping the potential from –0.30 to –0.80 V at all the pH values.

Here Figure 12

Summarizing the results reported in this note and in Ref. 15, the SP25A channel is open at positive transmembrane potentials in DPTL/DOPC tBLMs at all the pH values we investigated [15], and in DPTL/DOPS tBLMs at pH 5.4 and 3. Conversely, the SP25A channel is substantially closed at positive transmembrane potentials if it is incorporated in a DPTL/DOPS tBLM at pH 6.8. The latter peculiar behavior can be rationalized by assuming that the SP25A channel opens whenever the positive transmembrane potential succeeds in pushing the positively charged octadepsipeptide moiety slightly out of the membrane, as proposed by Dalla Serra et al. [13]. This occurs when the distal lipid monolayer is practically uncharged, namely with DPTL/DOPC tBLMs at all the pH values we investigated [15], with the DPTL/DOPS tBLM at pH 5.4, and, even more so, when the distal monolayer is positively charged, namely with the DPTL/DOPS tBLM at pH 3 [32]. On the other hand, when the distal monolayer is negatively charged, as in the case of a DPTL/DOPS tBLM at pH 6.8, the negative charge may prevent the octadepsipeptide moieties of the SP25A channel mouth from being pushed backwards by a positive

transmembrane potential, thus maintaining the channel closed state. The conformation assumed by the channel mouth under these conditions might possibly be related to the tight intercalation of the lipodepsipeptide molecules between the DOPS polar heads, as revealed by the impedance spectrum of Fig. 7, peculiar to the DOPS distal monolayer at pH 6.8.

The behavior of the distal monolayer of the DPTL/DOPS tBLM at pH 6.8 was shared by a conventional BLM formed from an equimolar mixture of DOPS and DOPE incorporating SP22A from a buffered solution of 0.1 M NaCl, pH 6 [11]. An opposite behavior was reported at a BLM consisting of a PC/PE/PS mixture in a 2:2:1 molar ratio at pH 6 [13], where the SP25A ion channel was open at positive transmembrane potentials. However, in this case the contribution to the overall lipid charge from PS was small, in view of its low mole fraction. It should be noted that the particular behavior of the SP25A channel at a DPTL/DOPS tBLM in a solution of 0.1 M KCl, pH 6.8, parallels that of the syringomycin E channel, which is closed at positive transmembrane potentials at a DOPS [43] and a DOPS/DOPE BLM in 0.1 M NaCl, pH 6 [44], while it is open at a DOPS/DOPE BLM in 0.1 M NaCl, pH 2, and at a diphytanoylPC BLM in 0.1 M NaCl, pH 6 [44].

To verify the effect of the absence of permeating anions in the solution bathing a DPTL/DOPS tBLM incorporating SP25A, a CV was recorded in a solution of 0.04 M Na_2H_2ATP, pH 3.3, and 0.4 μg/mL SP25A, using an external Ag/AgCl/(0.1M KCl) reference electrode. In fact, it is well known that ATP anions are too bulky to permeate lipid membranes along common ion channels and require the intervention of specific transporters [40]. After repeated voltage cycling, the stabilized CV showed an $E_{1/2}$ value of –0.48 V (dashed curve in Fig. 13). Addition of 0.2 M KCl to the bathing solution caused a gradual shift of the negative peak toward less negative potentials, while the positive peak remained unaltered. After stabilization, an almost centrosymmetric CV was obtained, with the inversion center located at the midpoint potential $E_{1/2}$ of –0.42 V (solid curve in Fig. 13). It is apparent that the trumpet-shaped enlargement occurred only upon Cl^- addition, proving beyond doubt that it was determined by an inflow and outflow of these anions at the less negative potentials.

Here Figure 13

Since $E_{1/2}$ is the potential at which ion inflow matches its outflow, it might be regarded as roughly equivalent to the reversal potential measured by the Goldman, Hodgkin and Katz (GHK) equation at BLMs and biomembranes. However, tBLMs are quite different from BLMs, since they are highly asymmetric and it is not possible to change the ionic composition in their hydrophilic spacer at will. Moreover, the electric potential range accessible to Hg-supported tBLMs is rather repulsive even toward anions easily translocated by the SP25A channel, such as Cl^- ion, making its permeability P_{Cl} quite low, other that at the less negative potentials. In practice, the hydrophilic spacer of a Hg-supported tBLM is almost exclusively occupied by monovalent cations. More precisely, each voltage cycle almost half-fills the spacer at the negative peak potential, and half-empties it at the positive peak potential (cf. Fig. 7 in Ref. 15). Hence, the $E_{1/2}$ value is largely determined by the monovalent cation. Nonetheless, the ATP anion, in spite of its extremely low permeability P_{ATP}, succeeded in shifting the $E_{1/2}$ value by about 40 mV toward more negative potentials with respect to corresponding value in 0.1 M KCl at pH 3, –0.44 V, i.e., in the direction predicted by the GHK equation. On the other hand, the subsequent addition of 0.2 M KCl shifted $E_{1/2}$ by about 20 mV toward more positive potentials with respect

to the $E_{1/2}$ value in 0.1 M KCl, possibly because of the higher cation concentration in the bathing solution.

3.4. DPTL/DOPA tBLM

The effect of SP25A at a DPTL/DOPA tBLM in an unbuffered solution of 0.1 M KCl, pH 5.4, was similar to that observed at a DPTL/DOPC tBLM. The CV obtained by scanning the potential between –0.20 and –0.90 V, thus maintaining the negative potentials within the limits of physiological transmembrane values, showed only a small current increase toward the more negative potentials, even after an EIS scan (dashed curve in Fig. 14). A slightly higher current increase was observed in a buffer solution, pH 6.8 (dotted curve in Fig. 14). Only upon extending the scanned potential range to the non-physiological value of –1.20 V, we obtained a well-formed CV. Its $E_{1/2}$ value of –0.57 V practically coincides with that obtained at DPTL/DOPC and DPTL/DOPS tBLMs incorporating gramicidin at the same pH value [37]. The particularly large trumpet-shaped enlargement denotes an appreciable Cl^- movement in and out of the spacer at potentials positive of –0.35 V. This was confirmed by the two-stage charge transients obtained by stepping the applied potential from –0.30 V to progressively more negative final values E_f (data not shown), which were similar to those in Fig. 12 for a DPTL/DOPS tBLM, at the same pH value. The height of the charge transient at E_f = –0.80 V amounted to ~ –80 μC cm^{-2}, indicating that, at the initial potential of –0.30 V, the Cl^- ions were present in the spacer in an amount bearing a charge of –30 μC cm^{-2}, before flowing out of the spacer during the first stage of the potential jump.

Here Figure 14

4. Conclusions

The particular ease with which SP25A targets and penetrates Hg-supported DOPS SAMs with respect to DOPC and DOPA SAMs not only at pH 6.8, where DOPS is negatively charged just as DOPA at pH 5.4, but also at pH 3, was confirmed by measurements at DPTL/phospholipid tBLMs. In the latter case, it was also possible to show that SP25A is incorporated at physiological transmembrane potentials in Hg-supported DPTL/DOPS tBLMs, whereas incorporation in DPTL/DOPC [15] and DPTL/DOPA tBLMs occurred only at non-physiological negative transmembrane potentials. Moreover, just as for DOPS SAMs, the attack of SP25A to DPTL/DOPS tBLMs took place irrespective of whether the DOPS molecules were negatively charged, neutral or positively charged. Interestingly, the effect of SP25A on the DOPS monolayer was stronger at pH 3 than at pH 6.8, in spite of the fact that the positively charged octadepsipeptide moieties of SP25A were expected to interact: *i*) attractively with the DOPS molecules at pH 6.8, where the latter species are negatively charged; *ii*) repulsively with the DOPS molecules at pH 3, where the latter species are positively charged. Taken together, the above findings lend support to the hypothesis that SP25A targets the structural feature that distinguishes DOPS monolayers from DOPC and DOPA monolayers at all pH values, namely the arrangement of the H_3N^+-CHR-CO_2^- zwitterions coplanar to the monolayer, due to electrostatic interactions between protonated amino groups and carboxylate groups of adjacent DOPS polar heads. We may tentatively explain this behavior by a competitive interaction of the latter groups with the protonated amino groups of Dab residues within SP25A. This interaction, mainly electrostatic, but possibly enhanced by some favorable conformation, might dismantle the typical

arrangement of the DOPS monolayer with amino•carboxylate pairs bridging contiguous DOPS polar heads.

The above results, albeit significant *per se*, might assume particular relevance in the light of the selective antimicrobial activity of SP25A, which targets G+ bacteria but not Gram-negative (G–) ones [5,6]. This molecular selectivity is consistent with the struggle for existence and self-defense undertaken by all living beings. In fact, it seems logical for the G– bacterium *Pseudomonas syringae* to produce peptides harmless for G– bacteria but potentially harmful to G+ ones. Since G– and G+ bacteria have similar DOPS amounts in their biomembranes [45], other molecular features distinguishing the above-mentioned bacterial groups have to be considered to rationalize SP25A selectivity. In this respect, the main peculiar feature of G+ bacteria is represented by their outer envelope, which consists of a 20 ÷ 80 nm thick layer of peptidoglycan (PG). This layer is composed of long strands of alternating residues of *N*-acetylglucosamine (GluNAc) and *N*-acetylmuramic acids (MurNAc) (called glycan strands), with one (L-Ala^1 – D-Glu^2 – m-Dap^3 –D-Ala^4 – D-Ala^5) pentapeptide chain linked to each MurNAc residue; m-Dap stands for meso-diaminopimelic acid and the superscript denotes the amino acid position, as counted from the MurNAc residue. Previous studies on PG biosynthesis demonstrated that the corresponding precursor (lipid II) is assembled within the cytoplasm of G+ bacteria [46,47], and consists of a phosphorylated undecaprenyl-GluNAc-MurNAc molecule also bearing the pentapeptide moiety (see Fig. 15). After biosynthesis, lipid II is flipped across the cytoplasmic membrane, still maintaining its undecaprenyl chain firmly inserted into the membrane and the remaining part exposed to the periplasmic space [47]. Biosynthesis of the PG layer finally occurs via binding of contiguous MurNAc-GluNAc chains through transglycosylation (TG), with glycan strand formation, in parallel with cross-linking of the pentapeptides bound to adjacent glycan stands via transpeptidation (TP).

Here Figure 15

The whole biosynthetic process is highly dynamic and is compatible with the large PG envelope changes occurring during bacterial duplication and division phases. The final PG biosynthetic steps are carried out by monofunctional transglycosylases (containing a TG domain), monofunctional transpeptidases (containing a TP domain), and bifunctional transglycosylases / transpeptidases, which harbor both a TG and a TP domain and are referred to as class A penicillin-binding proteins (PBPs) [47]. Both TG and TP domains are located in the periplasm. Cross-linking of the peptides occurs between the D-Ala^4 residue of the donor peptide bound to one strand and the m-Dap^3 residue of the acceptor peptide bound to an adjacent strand. The energy for this reaction is gained from the cleavage of the D-Ala^4 – D-Ala^5 bond of the donor peptide [48].

In this context, we may tentatively hypothesize that a significant amount of R-CO_2^-•$^+NH_3$-R' pairs may exist in the outer envelope of G+ bacteria before the TP reaction. These pairs might form as a result of the electrostatic interaction between the protonated amino group of the m-Dap residue from one pentapeptide and the carboxylate group of the D-Glu^2 or C-terminal D-Ala^5 group from the pentapeptide of an adjacent PG strand. This situation resembles that described above for DOPS monolayers, where $^+NH_3$-CHR-CO_2^-•$^+NH_3$-CHR-CO_2^- pairs, resulting from the electrostatic interaction between the protonated amino and carboxylate groups of adjacent phospholipid polar heads, were shown to be the preferential molecular target of the cationic SP25A, highly modulating the lipodepsipeptide affinity toward DOPS monolayers. Thus, the postulated existence of R-CO_2^-•$^+NH_3$-R' peptidoglycan pairs reported above should promote the attractive interaction of SP25A toward the outer envelope of G+ bacteria. SP25A binding to non-

mature PG might possibly be reinforced by the dual electrostatic interaction of its contiguous protonated Dab residues toward the carboxylate groups of two of the three D-Ala^5, m-Dap^3 and D-Glu^2 residues pertaining to the same pentapeptide moiety in a PG strand, as schematically depicted in Fig. 15. This interaction, followed by peptide insertion and pore formation into the corresponding membrane according to the mechanism reported before [11-14], might possibly justify the reported antimicrobial selectivity of this lipodepsipeptide.

Differently from G+ bacteria, the outer envelope of G– bacteria consists of a lipid bilayer containing integral proteins and lipopolysaccharides, whose inner core is negatively charged as a result of the presence of several phosphate groups. Although the shell of these bacteria also includes a thin layer of PG, this is not exposed to the extracellular fluid, from which it is separated by the outer membrane and a first periplasmic space.

The outer envelope of G+ bacteria is also negatively charged as a result of the presence of teichoic acids, which are polysaccharides having some of their negative phosphate groups covalently linked to the terminal D-Ala residues of the peptidoglycan network. In this context, Bensaci and Takemoto [6] demonstrated that SP25A is more effective in inhibiting the growth of G+ *Bacillus subtilis* mutant strains deleted in the genes encoding the enzymes that facilitate the transport of activated D-Ala to the lipoteichoic acid, than the wild-type strain. No such an effect was observed for SP22A. The lack of D-alanylation of the wall-linked teichoic acid during the growth of the mutant strains increases the number of negative phosphate groups of teichoic acid. Thus, it was suggested that the inhibitory effect of SP25A is promoted by the interaction between the positive charge of its Dab residues and the negative phosphate groups of bacterial teichoic acids. However, the cationic properties of SP25A do not seem sufficient *per se* to selectively inhibit the growth of G+ bacteria, as also admitted by Bensaci and Takemoto [6]. In fact, among other things, similar attractive electrostatic interactions would also be operative toward G– bacteria, whose outer covering presents a significant negative net charge due to lipopolysaccharides, as mentioned above.

By demonstrating the greatest preference of SP25A for interacting with DOPS monolayers than with DOPC or DOPA ones, our electrochemical measurements at Hg-supported lipid mono- and bilayers may provide a novel clue toward understanding the antimicrobial activity of this lipodepsipeptide against G+ bacteria. From a more general point of view, the above results demonstrate the potential of Hg-supported DPTL/phospholipid tBLMs in monitoring the ion flow along ion channels incorporated in the lipid bilayer moiety by exploiting the well-defined spaciousness of the hydrophilic spacer, through the use of potential-step chronocoulometry and cyclic voltammetry.

Acknowledgments

This study was partially supported by grants from the Italian Ministry of Economy and Finance for the project "Innovazione e Sviluppo del Mezzogiorno - Conoscenze Integrate per Sostenibilità ed Innovazione del *Made in Italy* Agroalimentare - Legge n. 191/2009" and from Regione Campania for the project "Nuovi Processi e Prodotti per la Nutraceutica, la Cosmeceutica e la Nutrizione umana" (BenTeN) - P.O.R. Campania Region (Italy) 2007/2013, objectives 2.1". Thanks are due to Prof. Adrian Schwan (University of Guelph, Guelph, Ontario, Canada) for providing us with the DPTL thiolipid.

References

1 - A. Ballio, D. Barra, F. Bossa, A. Collina, I. Grgurina, G. Marino, G. Moneti, M. Paci, P. Pucci, A. Segre, M. Simmaco, Syringopeptins, new phytotoxic lipodepsipeptides of *Pseudomonas syringae* pv. *syringae*, FEBS Lett. 291 (1991) 109-112.

2 - A. Isogai, H. Iguchi, J. Nakayama, A. Kusai, J.Y. Takemoto, A. Suzuki, Structural analysis of new syringopeptins by tandem mass spectroscopy, Biosci. Biotechnol. Biochem. 59 (1995) 1374-1376.

3 - A. Ballio, F. Bossa, D. Di Giorgio, A. Di Nola, C. Manetti, M. Paci, A. Scaloni, A.L. Segre, Solution conformation of the *Pseudomonas syringae* pv. *syringae* phytotoxic lipodepsipeptide syringopeptin 25-A. Two-dimensional NMR, distance geometry and molecular dynamics, Eur. J. Biochem. 234 (1995) 747-758.

4 - E. Mátyus, K. Blaskó, J. Fidy, D.P. Tieleman, Structure and dynamics of the antifungal molecules syringotoxin-B and syringopeptin-25A from molecular dynamics simulation, Eur. Biophys. J. 37 (2008) 495-502.

5 - I. Grgurina, M. Bensaci, G. Pocsfalvi, L. Mannina, O. Cruciani, A. Fiore, V. Fogliano, K. N. Sorensen, J. Y. Takemoto, Novel cyclic lipodepsipeptide from *Pseudomonas syringae* pv. lachrymans strain 508 and syringopeptin antimicrobial activities, Antimicrob. Agents Chemother. 49 (2005) 5037-5045.

6 -M. F. Bensaci, J. Y. Takemoto, Syringopeptin SP25A-mediated killing of gram-positive bacteria and the role of the teichoic acid D-alanylation, FEMS Microbiol. Lett. 268 (2007) 106-111.

7 - D. Di Giorgio, L. Camoni, A. Ballio, Toxins of *Pseudomonas syringae* pv. *syringae* affect H^+-transport across the plasma membrane of maize, Physiol. Plant. 91 (1994) 741-746.

8 - N.S. Iacobellis, P. Lavermicocca, I.Grgurina, M. Simmaco, A. Ballio, Phytotoxic properties of *Pseudomonas syringae* pv. *syringae* toxins, Physiol. Mol. Plant Pathol. 40 (1992) 107-116.

9 - M.L. Hutchison, D.C. Gross, Lipopeptide phytotoxins produced by *Pseudomonas syringae* pv. *syringae:* Comparison of the biosurfactant and ion channel-forming activities of syringopeptin and syringomycin, Mol. Plant-Microbe Inter., 10 (1997) 347-354.

10 - A. Carpaneto, M. Dalla Serra, G. Menestrina, V. Fogliano, F. Gambale, The phytotoxin lipodepsipeptide syringopeptin 25A from *Pseudomonas syringae* pv. *syringae* forms ion channels in sugar beet vacuoles, J. Membrane Biol. 188 (2002) 237-248.

11 - M.F. Bensaci, P.H. Gurnev, S.M. Bezrukov, J.Y. Takemoto, Fungal activities and mechanisms of action of *Pseudomonas syringae* pv. *syringae* lipodepsipeptide syringopeptins 22A and 25A, Front. Microbiol. 2 (2011) Article 216, 1-6.

12 - M. Dalla Serra, G. Fagiuoli, P. Nordera, I. Bernhart, C. Della Volpe, D. Di Giorgio, A. Ballio, G. Menestrina, The interaction of lipodepsipeptide toxins from *Pseudomonas syringae* pv. *syringae* with biological and model membranes: A comparison of syringotoxins, syringomycin and two syringopeptins, Mol. Plant-Microbe Inter., 12 (1999) 391-400.

13 - M. Dalla Serra, I. Bernhart, P. Nordera, D. Di Giorgio, A. Ballio, G. Menestrina, Conductive properties and gating channels formed by syringopeptin 25A, a bioactive lipodepsipeptide from *Pseudomonas syringae* pv. *syringae*, in planar lipid membranes, Mol. Plant-Microbe Inter., 12 (1999) 401-409.

14 - G. Agner, Y.A. Kaulin, P.A. Gurnev, Z. Szabo, L.V. Schagina, J.Y. Takemoto, K. Blasko, Membrane-permeabilizing activities of cyclic lipodepsipeptides, syringopeptin 22A and syringomycin E from *Pseudomonas syringae* pv. *syringae* in human red blood cells and in bilayer lipid membranes, Bioelectrochemistry, 52 (2000) 161-167.

15 - L. Becucci, M. Rossi, A. Fiore, A. Scaloni, R. Guidelli, Channel-forming activity of syringopeptin 25A in mercury-supported lipid bilayers with a phosphatidylcholine distal leaflet, Bioelectrochemistry 108 (2016) 28-35.
16 - S.M. Schiller, R. Naumann, K. Lovejoy, H. Kunz, W. Knoll, Archaea analogue thiolipids for tethered bilayer lipid membranes on ultrasmooth gold surfaces, Angew. Chem. Int. Ed. Engl. 42 (2003) 208-211.
17 - L. Becucci, R. Romero Léon, M.R. Moncelli, P. Rovero, R. Guidelli, Electrochemical investigation of melittin reconstituted into a mercury-supported lipid bilayer, Langmuir 22 (2006) 6644-6650.
18 - L. Becucci, A. Santucci, R. Guidelli, Gramicidin conducting dimers in lipid bilayers are stabilized by single-file ionic flux along them, J. Phys. Chem. B 111 (2007) 9814-9820.
19 - L. Becucci, R. Guidelli, Kinetics of channel formation in bilayer lipid membranes (BLMs) and tethered BLMs: monazomycin and melittin, Langmuir 23 (2007) 5601-5608.
20 - L. Becucci, M. Papini, D. Muller, A. Scaloni, G. Veglia, R. Guidelli, Probing membrane permeabilization by the antimicrobial peptide distinctin in mercury-supported biomimetic membranes, Biochim. Biophys. Acta 1808 (2011) 2745-2752.
21 - L. Becucci, F. Maran, R. Guidelli, Probing membrane permeabilization by the antibiotic lipopeptaibol trichogin GA IV in a tethered bilayer lipid membrane, Biochim. Biophys. Acta 1818 (2012) 1656-1662.
22 - L. Becucci, M. Innocenti, S. Bellandi, R. Guidelli, Permeabilization of mercury-supported biomimetic membranes by amphotericin B and the role of calcium ions, Electrochim. Acta 112 (2013) 719-726.
23 - L. Becucci, D. Valensin, M. Innocenti, R. Guidelli, Dermcidin, an anionic antibiotic peptide: influence of lipid charge, pH and Zn^{2+} on its interaction with a biomimetic membrane, Soft Matter 10 (2014) 616-626.
24 - L. Becucci, R. Guidelli, Mercury-supported biomimetic membranes for the investigation of antimicrobial peptides, Pharmaceuticals 7 (2014) 136-168.
25 - L. Becucci, V. Tramonti, A. Fiore, V. Fogliano, A. Scaloni, R. Guidelli, Channel-forming activity of syringomycin E in two mercury-supported biomimetic membranes, Biochim. Biophys. Acta 1848 (2015) 932-941.
26 - M.R. Moncelli, L. Becucci, A novel model of the hanging mercury drop electrode, J. Electroanal. Chem. 433 (1997) 91-96.
27 - D. Bizzotto, A. Nelson, Continuing electrochemical studies of phospholipid monolayers of dioleoyl phosphatidylcholine at the mercury-electrolyte interface, Langmuir 14 (1998) 6269-6273.
28 - A. Nelson, N. Auffret, J. Borlakoglu, Interaction of hydrophobic organic compounds with mercury adsorbed dioleoylphosphatidylcholine monolayers, Biochim. Biophys. Acta 1021 (1990) 205-216.
29 - M.-F. Lecompte, A.-C. Bras, N. Dousset, I. Portas, R. Salvayre, M. Ayrault-Jarrier, Binding steps of apolipoprotein A-I with phospholipid monolayers: Adsorption and penetration, Biochemistry 37 (1998) 16165-16171.
30 - R. Stoodley, J. Shepherd, K. M. Wasan, D. Bizzotto, Amphotericin B interactions with a DOPC monolayer. Electrochemical investigations, Biochim. Biophys. Acta 1564 (2002) 289-297.
31 - A. Nelson, F.A. M. Leermakers, Substrate-induced structural changes in electrode-adsorbed lipid layers. Experimental evidence for the behaviour of phospholipid layers on the mercury-water interface, J. Electroanal. Chem. 278 (1990) 73-83.

32 - M.R. Moncelli, L. Becucci, R. Guidelli, The intrinsic pK_a values for phosphatidylcholine, phosphatidylethanolamine, and phosphatidylserine in monolayers deposited on mercury electrodes, Biophys. J. 66 (1994) 1969-1980.
33 - P. W. M. Van Dijck, B. De Kruijff, A. J. Verkleij, L. L. M. Van Deenen, J. De Gier, Comparative study on the effects of pH and Ca^{2+} on bilayers of various negatively charged phospholipids and their mixtures with phosphatidylcholine, Biochim. Biophys Acta 512 (1978) 84-96.
34 - M. R. Moncelli, L. Becucci, The intrinsic pK_a values for phosphatidic acid in monolayers deposited on mercury electrodes, J. Electroanal. Chem. 385 (1995) 183-189.
35 - W. Furness, Changes in potential of the dropping mercury electrode during drop formation and measurement of potential in polarographic analysis, Analyst 77 (1952) 345–355.
36 – R. Guidelli, A comparison between some recent theories on the effect of ionic specific adsorption upon electrode kinetics, J. Electoanal. Chem. 53 (1974) 205-218.
37 - L. Becucci, R. Guidelli, Can gramicidin ion channel affect the dipole potential of neighboring phospholipid headgroups?, Bioelectrochemistry, 106 (2015) 343-352.
38 - R. Guidelli and L. Becucci, Estimate of the potential difference across metal/water interfaces and across the lipid bilayer moiety of biomimetic membranes: an approach, Soft Matter, 7 (2011) 2195-2201.
39 - R. Guidelli, L. Becucci, Electrochemistry of biomimetic membranes, in: N. Eliaz, (Ed.), Applications of Electrochemistry and Nanotechnology in Biology and Medicine, Vol 53 of the Series: Modern Aspects of Electrochemistry, Springer, New York, 2011, pp.147-265.
40 - L. Becucci, R. Guidelli, C.B. Karim, D.D. Thomas, G. Veglia: An electrochemical investigation of sarcolipin reconstituted into a mercury-supported lipid bilayer. Biophys. J. 93 (2007) 2678-2687.
41 - L. Becucci, M. Papini, R. Verardi, G. Veglia, R. Guidelli, Phospholamban and its phosphorylated form require non-physiological transmembrane potentials to translocate ions Soft Matter 8 (2012) 3881-3888.
42- A.M. Feigin, J.Y. Takemoto, R. Wangspa, J.H. Teeter, J.G. Brand, Properties of voltage-gated ion channels formed by syringomycin E in planar lipid bilayers, J. Membr. Biol. 149 (1996) 41- 47.
43 – Y. A. Kaulin, L. Schagina, S. M. Bezrukov, V. V. Malev, A. M. Feigin, J. Y. Takemoto, J. H. Teeter, J. G. Brand, Cluster organization of ion channels formed by the antibiotic syringomycin E in bilayer lipid membranes, Biophys. J. 74 (1998) 2918-2925.
44 - V.V. Malev, L.V. Schagina, P.A. Gurnev, J.Y. Takemoto, E.M. Nestorovich, S.M. Bezrukov, Syringomycin E channel: A lipidic pore stabilized by lipopetide?, Biophys. J. 82 (2002) 1985-1994.
45 - R. M. Epand, R. F. Epand, Functional consequences of the lateral organization of biological membranes, in: P. L. Yeagle (Ed.), The Structure of Biological Membranes, 3rd Edition, CRC Press, Boca Raton, pp. 133-152.
46 - W. A. van der Donk, Lighting up the nascent cell wall, ACS Chem. Biol. 1 (2006) 425-428.
47 – W. Vollmer, U. Bertsche, Biochim. Biophys. Acta, Murein (peptidoglycan) structure, architecture and biosynthesis in *Escherichia coli*, 1778 (2008) 1714-1734.
48 – M. Terrak, T. K. Ghosh, J. van Heijenoort, J. Van Beeumen, M. Lampilas, J. Aszodi, J. A. Ayala, J. M. Ghuysen, M. Nguyen-Disteche, The catalytic, glycosyl transferase and acyl transferase modules of the cell wall peptidoglycan-polymerizing penicillin-binding protein 1b of *Escherichia coli*, Mol. Microbiol. 34 (1999) 350-364.

Legends for figures

Fig. 1 - AC voltammograms at a DOPC SAM in an unbuffered solution of 0.1 M KCl, pH 5.4, in the absence of SP25A (solid curve), immediately after the addition of 0.2 μg/mL SP25A (dashed curve) and after a complete EIS scan from –0.30 to –0.80 V (dash-dotted curve). Frequency = 75 Hz.

Fig. 2 - AC voltammograms at a DOPS SAM in a buffer solution of 0.1 M KCl, pH 6.8, in the absence of SP25A (solid curve), immediately after the addition of 0.2 μg/mL SP25A (dashed curve) and after a complete EIS scan from –0.30 to –0.80 V (dash-dotted curve). Frequency = 75 Hz.

Fig. 3 - AC voltammograms at a DOPS SAM in a solution of 0.1 M KCl, pH 3, in the absence of SP25A (solid curve), immediately after the addition of 0.2 μg/mL SP25A (dashed curve) and after a complete EIS scan from –0.30 V to –0.80 V (dash-dotted curve). The grey curve corresponds to an AC voltammogram recorded after forming a DOPS SAM in a solution of 0.1 M KCl, pH 3, containing 0.2 μg/mL SP25A. Frequency = 75 Hz.

Fig. 4 - Stabilized AC voltammograms at a DOPA SAM in an unbuffered solution of 0.1 M KCl, pH 5.4, in the absence (solid curve) and in the presence of 0.2 μg/mL SP25A (dashed curve). Frequency = 75 Hz.

Fig. 5 - CVs due to Cd^{2+} reduction and Cd(Hg) oxidation at a DOPS SAM in an aqueous solution of 0.1 M KCl, 4×10^{-5} M $CdSO_4$ and 0.2 μg/mL SP25A, at pH 6.8 (dash-dotted curve), 5.4 (dashed curve) and 3 (solid curve). Scan rate = 50 mV/s. The gray curve represents the CV of an aqueous solution of 0.1 M KCl and 4×10^{-5} M $CdSO_4$ on bare mercury.

Fig. 6 - Plot of $\omega Z'$ against $-\omega Z''$ at –0.50 V at a freshly prepared DPTL/DOPS tBLM in a buffer solution of 0.1 M KCl, pH 6.8, in the absence of SP25A (solid circles) and in the presence of 0.4 μg/mL SP25A during the first frequency scan (solid triangles) and during the second and subsequent ones (open squares). The impedance spectrum at –0.5 V was obtained starting from a bias potential of –0.30 V and shifting it gradually by –50 mV increments up to the attainment of –0.50 V.

Fig. 7 - Plots of capacitance C (circles) and conductance G (squares) against the applied potential for the RC mesh ascribed to the polar head region, at a DPTL/DOPS tBLM in a buffer solution of 0.1 M KCl, pH 6.8, in the absence (solid symbols) and in the presence of 0.4 μg/mL SP25A (open symbols). The impedance spectra were recorded proceeding toward progressively more negative bias potentials, starting from a value of –0.30 V.

Fig. 8 - Charge transients at a DPTL/DOPS tBLM in a buffer solution of 0.1 M KCl, pH 6.8, and 0.4 μg/mL SP25A, obtained by jumping from E_i = –0.30 V to final potential values varying from –0.50 to –0.80 V by –50 mV increments.

Fig. 9 - CV at a DPTL/DOPS tBLM in a buffer solution of 0.1 M KCl, pH 6.8, and 1 μg/mL SP25A, recorded between –0.20 and –0.90 V (solid curve), and between –0.20 and –1.20 V (dashed curve). The gray curve corresponds to the CV in the absence of SP25A. Scan rate = 50 mV/s.

Fig. 10 - CV at a DPTL/DOPS tBLM in a buffer solution of 0.1 M KCl, pH 6.8, and 1 μg/mL SP25A, before (dash-dotted curve) and after addition of 1×10^{-4} M $TlNO_3$ (dashed curve). The gray curve corresponds to the CV at bare mercury in 0.1 M KCl and 1×10^{-4} M $TlNO_3$. Scan rate = 50 mV/s.

Fig. 11 - CVs at a DPTL/DOPS tBLM in unbuffered solutions of 0.1 M KCl and 0.4 μg/mL SP25A at pH pH 5.4 (solid curve) and pH 3 (grey curve). The dashed curve corresponds to the CV at pH 3 after addition of 1×10^{-4} M $TlNO_3$. Scan rate = 50 mV/s.

Fig. 12 - Charge transients at a DPTL/DOPS tBLM in an unbuffered solution of 0.1 M KCl and 0.4 μg/mL SP25A, pH 5.4, obtained by jumping from E_i = –0.30 V to final potentials varying from –0.55 to –0.80 V by –50 mV increments.

Fig. 13 - CV at a DPTL/DOPS tBLM in a solution of 0.04 M Na_2H_2ATP and 0.4 μg/mL SP25A, pH 3.3, before (dashed curve) and after the addition of 0.2 M KCl (solid curve). The grey curve corresponds to the CV in the absence of SP25A.

Fig. 14 - CVs at a DPTL/DOPA tBLM in 0.1 M KCl and 0.4 μg/mL SP25A, recorded between –0.20 and –0.90 V at pH 5.4 (dashed curve) and pH 6.8 (dotted curve), and recorded between –0.20 and –1.20 V at pH 5.4 (solid curve).

Fig. 15 - Peptidoglycan synthesis catalyzed by a Class A PBP and tentative intervention of SP25A octadepsipeptide before the start of this synthesis. The functional groups of some residues, which are possibly relevant to such an intervention, have been evidenced. The glycan strand is elongated by transglycosylation (TG) with lipid II and forms cross-links by transpeptidation (TP), via release of D-Ala^5. Gray bars, MurNAc linked to pentapeptides represented either in detail or as arrows, for simplicity; white bars, GlcNAc; zigzag line, undecaprenyl residue; black circles, phosphate groups; gray octahedron, SP25A octadepsipeptide.